INFORMATION TO USERS

This manuscript has been reproduced from the microfilm master. UMI films the text directly from the original or copy submitted. Thus, some thesis and dissertation copies are in typewriter face, while others may be from any type of computer printer.

The quality of this reproduction is dependent upon the quality of the copy submitted. Broken or indistinct print, colored or poor quality illustrations and photographs, print bleedthrough, substandard margins, and improper alignment can adversely affect reproduction.

In the unlikely event that the author did not send UMI a complete manuscript and there are missing pages, these will be noted. Also, if unauthorized copyright material had to be removed, a note will indicate the deletion.

Oversize materials (e.g., maps, drawings, charts) are reproduced by sectioning the original, beginning at the upper left-hand corner and continuing from left to right in equal sections with small overlaps. Each original is also photographed in one exposure and is included in reduced form at the back of the book.

Photographs included in the original manuscript have been reproduced xerographically in this copy. Higher quality 6" x 9" black and white photographic prints are available for any photographs or illustrations appearing in this copy for an additional charge. Contact UMI directly to order.

Numerical modeling study of the circulation of the Greenland Sea

Masłowski, Wiesław, Ph.D.

University of Alaska Fairbanks, 1994

U·M·I

300 N. Zeeb Rd.
Ann Arbor, MI 48106

NUMERICAL MODELING STUDY OF

THE CIRCULATION OF THE GREENLAND SEA

A

THESIS

Presented to the Faculty

of the University of Alaska Fairbanks

in Partial Fulfillment of the Requirements

for the degree of

DOCTOR OF PHILOSOPHY
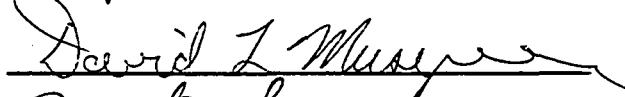
By

Wiesław Masłowski, M.S.

Fairbanks, Alaska

May 1994

NUMERICAL MODELING STUDY OF

THE CIRCULATION OF THE GREENLAND SEA

By

Wieslaw Maslowski

RECOMENDED:

Co-Chairman, Advisory Committee
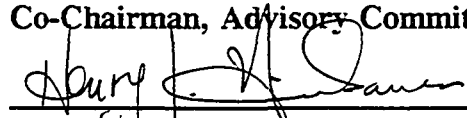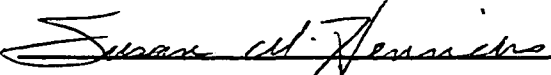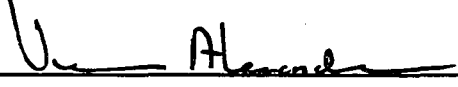
Co-Chairman, Advisory Committee

Program Head

APPROVED:

Dean, School of Fisheries and Ocean Sciences

Dean of the Graduate School

May 5, 1994

Date

Abstract

This study is a simulation of the circulation of the Greenland Sea aimed at modeling some of the issues related to the Great Salinity Anomaly (GSA) and deep water formation using a primitive equation ocean general circulation model (Semmer, 1974). The features of the model include: 1) a high resolution, 2) real topography, 3) open boundaries at the south and north, and 4) temporally variable wind and thermohaline forcing. The model is used to study: 1) the spreading of a fresh water anomaly 2) the mechanisms of cross frontal mixing that lead to deep water formation 3) the general circulation of the deep and upper layers of the ocean and their dependence on wind and thermohaline forcing, and 4) the possible implications of meso-scale and large-scale variability on climate change.

One of the major results of this work is the simulation of continental shelf waves propagating along the shelf slope of Greenland between 77°N and 72°N. Waves with a subinertial period of 17.2 hrs, a wavelength of 363 km, a phase speed of 586 cm/s and a group velocity of 409 cm/s, are found. Possible mechanism for generation of shelf waves is presented. It is suggested that some energy related with wave activity may support cross-frontal mixing in the East Greenland Current (EGC), where formation of the two main sources of North Atlantic Deep Water (e.g. Norwegian Sea Deep Water and Denmark Strait Overflow Water) have been reported.

The results from the GSA simulation suggest that during the early stage of the GSA (e.g. during its propagation with the EGC to the south, in the late 1960s) when no

observations are available, the fresh water signal is not being mixed into the interior circulation of the Greenland Sea gyre. The second experiment, representing recirculation of the GSA from the North Atlantic back into the Greenland Sea, in the late 1970s, shows freshening in the Greenland Sea gyre of comparable magnitudes (-0.05 to –0.1 psu) to the observed ones. These results agree with the earlier indirect measurements (Rhein, 1991; Schlosser et al., 1991) indicating dramatic reduction of deep water renewal in the Greenland Sea in the late 1970s and early 1980s.

From the general circulation experiments it has been found that the ocean response to seasonal forcing is mainly barotropic. This implies a strong topographic control in the distribution of currents and hydrographic variables. Most of the areas of topographic steering which are simulated in the region have been reported in the literature. The so-called Molloy Deep eddy shows its direct dependence on the large scale dynamics affecting the northward flow of the West Spitsbergen Current (WSC), controlling this way a net mass transport into the Arctic Ocean. Simulations with different wind forcing suggest dependence of the Greenland Sea gyre circulation on the variations with time of the local wind forcing. Results indicate that monthly mean wind stress forcing probably underestimate wind forcing in the model. Analysis of surface, intermediate and deep ocean velocity fields compare reasonably well with observations

Table of Contents

List of Figures

List of Tables

List of abbreviations

AIW — Arctic Intermediate Water

AODW — Arctic Ocean Deep Water

ASW — Arctic Surface Water

AW — Atlantic Water

CBDW — Canadian Basin Deep Water

CI — contour interval

dof — degrees of freedom

DSOW — Denmark Strait Overflow Water

EGC — East Greenland Current

EGF — East Greenland Front

EOF — Empirical Orthogonal Function

GFZ — Greenland Fracture Zone

GIN Sea — Greenland, Island, and Norwegian Seas

GSA — Great Salinity Anomaly

GSDW — Greenland Sea Deep Water

JMC — Jan Mayen Current

MIZ — Marginal Ice Zone

NADW — North Atlantic Deep Water

NSDW — Norwegian Sea Deep Water

OB — open boundary

OGCM — ocean general circulation model

PF — Polar Front

PIW — Polar Intermediate Water

PSD — power spectrum density

psu — practical salinity units

PW — Polar Water

rAtIW — return Atlantic Intermediate Water

TAF — time amplitude function

TKE — total kinetic energy

WSC — West Spitsbergen Current

Dedication

To my mother

Acknowledgments

I would like to take this opportunity to thank my two advisors, Dr. Joe Niebauer and Dr. Zygmunt Kowalik, for their support, guidance and friendship through the study. I wish to extend this special thanks to Dr. Mark Johnson for his help and support during most recent years of this work. I thank Dr. Vera Alexander, Dr. Dave Musgrave, and Dr. Weely Weeks for their critical reading of this manuscript. I would like to thank my colleagues Dr. Steve Okkonen, Dr. Dave Salmon, and Dr. Tom Weingartner for taking an active interest in this work. Finally I would like to thank my wife Agata and daughters Justyna and Malwina, whose love, encouragement, and patience helped me successfully finish this study.

Chapter 1 INTRODUCTION

Deep water formation is the most important climatic feature of the Arctic Ocean and its adjacent seas (Broecker, 1991). It is generally accepted that relatively warm and saline deep water (Arctic Ocean Deep Water (AODW)) formed on the Arctic shelves (Aagaard, 1981; Aagaard et al., 1985) flows through Fram Strait, where it is mixed with the much colder and fresher deep water that is formed by convection in the Greenland Sea (Greenland Sea Deep Water (GSDW)) (Aagaard et al., 1991). As a result of this mixing, Norwegian Sea Deep Water (NSDW) forms and overflows the Iceland-Scotland Ridge system becoming one of the two major sources of North Atlantic Deep Water (NADW). Denmark Strait Overflow Water (DSOW), is formed in the Iceland Sea (Swift et al., 1980; Swift and Aagaard, 1981) and at intermediate depths of the East Greenland Current (EGC) by mixing of fresh and cold Polar Water (PW) of the Arctic origin with recirculating in the central Greenland Sea warm and saline Atlantic Water (AW) (Strass et al., 1993). It becomes the other source of NADW.

It is commonly accepted that the Greenland Sea and the Weddell Sea are the most important areas where convective renewal of intermediate and deep waters contribute to world ocean ventilation. These waters start the so-called "conveyor-belt" circulation in the global ocean, which drives a global-scale transport of heat and fresh water between the high-latitude North Atlantic and the Pacific Ocean, helps maintain the Arctic sea ice cover and affects the atmospheric radiation balance through the ice albedo. Any

variability in these water characteristics is of great importance not only to local but also global circulation.

The northern North Atlantic "Great Salinity Anomaly" (GSA) of the late 1960s and 1970s, is regarded as an ocean climate event of considerable importance, being only second to El Nino in its global impact (Mysak, 1991). The GSA is considered to be a small scale analog of the halocline catastrophes in the past, i.e., a temporary shut down of the conveyor, resulting in a rapid global reorganization of the climate system to a glacial mode of operation. The GSA, an event resulting from an anomalous sea ice and fresh water outflow from the Arctic Ocean (Aagaard et al., 1989), significantly altered the properties of waters feeding the Greenland-Iceland-Scotland Ridge overflow (Aagaard et al., 1991; Clarke et al., 1990; Meincke et al., 1990; Rhein, 1991; Schlosser et al., 1991). As a result of freshening in the upper layers, deep convection in the Greenland Sea dramatically decreased during 1980s. Since some studies (Aagaard and Carmack, 1989) indicated that the present mode of global ocean circulation might be very sensitive to such variations in fresh water flux from the Arctic, a modeling approach was used here to study the influence of the GSA on the dynamics of the Greenland Sea. The following major aspects of the Greenland Sea dynamics are addressed in this study:

1) Spreading of fresh water anomaly as it enters from the Arctic Ocean and later as it recirculates from the North Atlantic back into the Greenland, Iceland and Norwegian (GIN) Seas.

2) Mechanisms of cross frontal mixing allowing for mixing of waters with different characteristics, and leading to deep water formation.

3) General deep and upper layer circulations.

4) Possible implications of meso-scale and large-scale variability on climate change.

Studies of global climate change clearly require a significantly improved understanding of the circulation of all the Arctic Ocean and its adjacent seas. Modeling experiments using data from field measurements save money, time, and equipment, and can greatly enhance our knowledge of the dynamics of these poorly studied regions. With the quickly increasing power of computational resources becoming available for scientific use, it will soon be possible to develop an eddy-resolving model of the Arctic Ocean that can be incorporated in eddy-resolving global ocean models, which have, to date, omitted high latitude regions. A limited-area model of the Greenland Sea proposed here may be viewed as a case study and a forerunner of future large-scale experiments.

In the first chapter, the general oceanography, including bathymetry, major water masses, circulation and atmospheric forcing, is presented. Chapter 2 describes the numerical model and input data.

General circulation experiments designed to study the dynamics of the Greenland Sea are discussed in Chapter 3. In this chapter continental shelf waves are simulated. These waves have a period of 17.2 hrs, a wavelength of 363 km, a phase speed of 586 cm/s, and a group velocity of 409 cm/s. A disturbance produced by the Greenland Fracture

Zone (GFZ) in the southward flow of the EGC is suggested as a generation mechanism for such waves. The cross-frontal component of group velocity may provide energy for water mass mixing across the East Greenland Front (EGF). The location of maximum wave activity between 76°N and 73°N coincides with the reported observations of cross frontal mixing, where formation of NSDW (Aagaard et al., 1991) and DSOW (Strass et al., 1993) has been reported.

As expected, the ocean response to seasonal forcing is mainly barotropic, what implies topographic steering of the currents in the Greenland Sea. A typical example of topographic steering is the so-called Molloy Deep eddy (Wadhams and Squire, 1983; Smith et al., 1984; Bourke et al., 1987). This cyclonic eddy, that is trapped on the depression depicted by the 3000 m isobath between 79°N and 80°N in Fram Strait, is simulated to be directly dependent on the strength of the northward mass transport of the WSC. The eddy accounting for as much as 2–3 Sv of northward flow, may be viewed as a mechanism controlling heat, salt and mass transport into the Arctic Ocean. It may also provide a good explanation of discrepancies in estimates of inflow of the WSC into the Arctic Ocean. Results supporting separation of the Greenland Sea gyre into two smaller gyres along the GFZ, as reported in literature (Kolterman and Machoczek, 1985; Quadfasel and Meincke, 1987), are presented in this chapter. Also westward turning branch of the WSC in the northern Boreas Basin, and the flow of the EGC with the Jan Mayen Current (JMC) branching of to the east at about 73°N (Bourke et al., 1992), are closely correlated to local topography. Experiments indicate that circulation in the region

and especially in the Greenland Sea gyre is strongly influenced but is not directly related to wind forcing. It is rather controlled by basin-wide and regional scale qusigeostrphic normal modes, that are excited by variable winds but undergo their own dynamics.

Simulations of fresh water signal propagation from both the north and the south are modeled in Chapter 4. Two experiments are designed to study the GSA propagation in the Greenland Sea, one for the early stage of the GSA propagation to the south, when there is no observation and second representing recirculation of the GSA from the North Atlantic into the Greenland Sea for verification with available data (Dickson et al., 1988) and for comparison with other model results (Legutke, 1991b; Hakkinen, 1993). Results obtained in this chapter agree with the earlier indirect measurements (Rhein, 1991; Schlosser et al., 1991) suggesting that the fresh water signal was not mixed into the interior circulation of the Greenland Sea gyre. hence formation of GSDW was not altered at the early stage of the anomaly spreading, in the late 1960s through mid 1970s. The process of deep convective overturn was dramatically reduced later, when the GSA recirculated back into the Greenland Sea gyre in the late 1970s and early 1980s, what has been suggested by both observations (Clarke et al., 1990; Meincke et al., 1990) and numerical experiments (Legutke, 1991b).

Finally in Chapter 5 a summary and discussion is presented. Possible linkage of the dynamics and low frequency variabilities in the Greenland Sea with large scale ocean circulation and the atmosphere-sea ice-ocean system is suggested.

Section 1.1 <u>Bathymetry</u>

The bathymetry of the Greenland Sea is complicated (Fig.1.1) and imposes major constraints on the dynamics of the circulation as it sets the geometry of the basin, its inner subdivisions, and its connections with other oceans. From a dynamical point of view it directs the flow, since geostrophic currents follow lines of the constant ambient potential vorticity (f/H), where f is the Coriolis parameter and H is the water depth (Pedlosky, 1987). Since changes of f are small compared to changes in bottom topography in the Greenland Sea , hence contours of constant H (Fig.1.1) are also representative of contours of f/H. The geographic position of the Greenland Sea, between the Arctic and the North Atlantic Oceans, together with the above mentioned conditions determines its thermohaline characteristics.

To the south, the Greenland Sea is limited by the Iceland Plateau, Jan Mayen Island and Mohns Ridge, all being extensions of Mid-Atlantic Ridge system (Fig.1.1). The Greenland, Iceland and Norwegian Seas are commonly referred to as the GIN Sea (also Nordic Seas), which is about one third the volume of the main Arctic Ocean (e.g. Canadian and Eurasian Basins). Fram Strait, the passage between Greenland and Spitsbergen, separates the Greenland Sea from the Arctic Eurasian Basin. It is the only deep (2600 m) connection between the Arctic Ocean and the rest of the world ocean. Greenland, with its wide (~250 km) shelf sloping rapidly into abyssal plains is a natural boundary of the basin to the west. The Knipovich Ridge, which is the northward extension
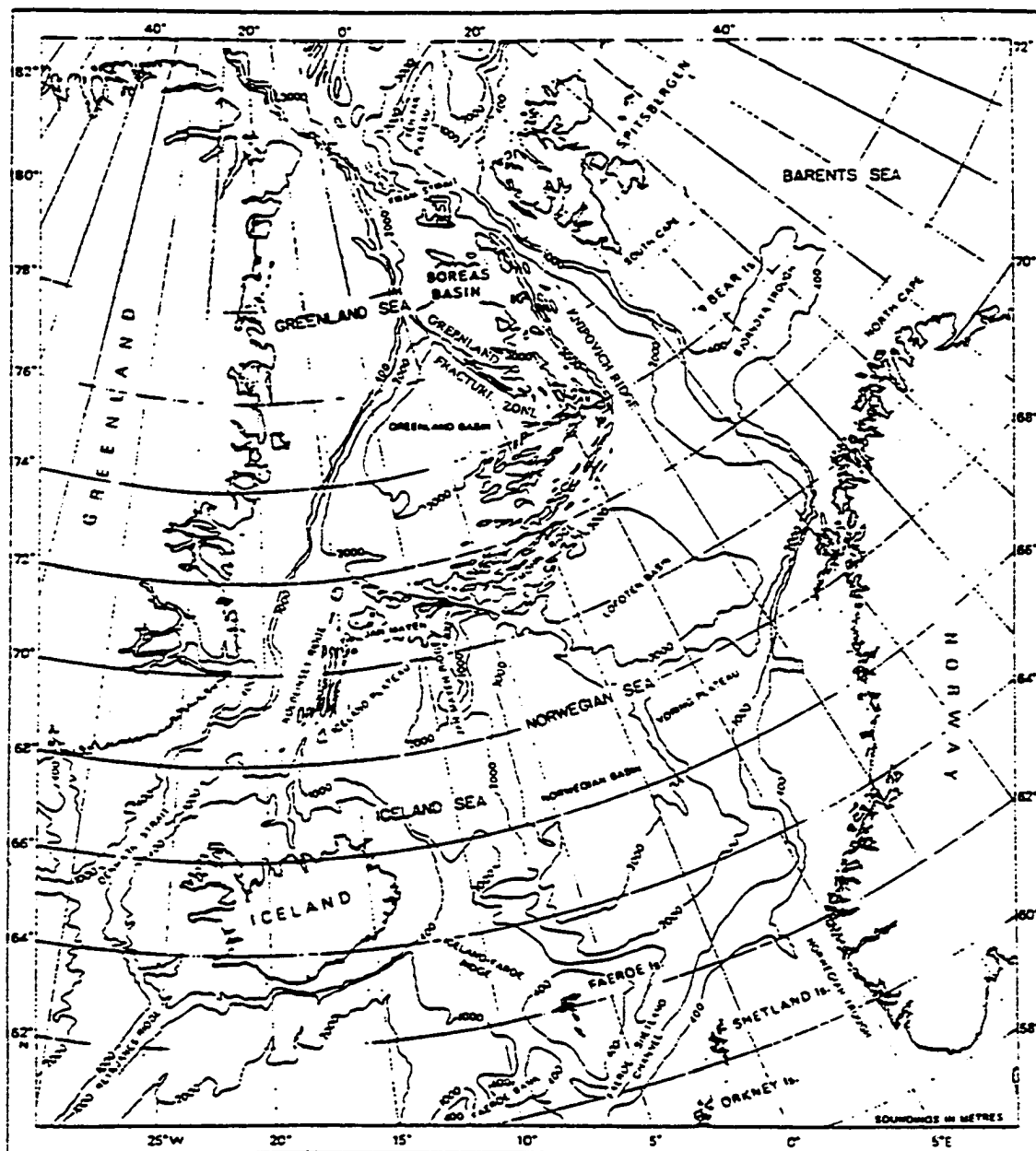
Figure 1.1 The bathymetry and major named topographic features of the Nordic Seas on a polar stereographic projection. Depth contours are in meters (from Jonsson, 1989).

of the Mohns Ridge. backed by the narrow shelves of Spitsbergen and Bear Island, sets the

eastern boundary. There are two abyssal plains separated by the Greenland Fracture Zone,

of which the northern (Boreas) is smaller and shallower at ~3200 m than the southern

(Greenland) at ~3600 m. North of the Boreas Abyssal Plain there is the Hovgard Fracture

Zone, with a minimum depth of ~1300 m. Finally, just south of Fram Strait there is

the Arctic's greatest depth, the Molloy Deep with a maximum depth reaching ~5600
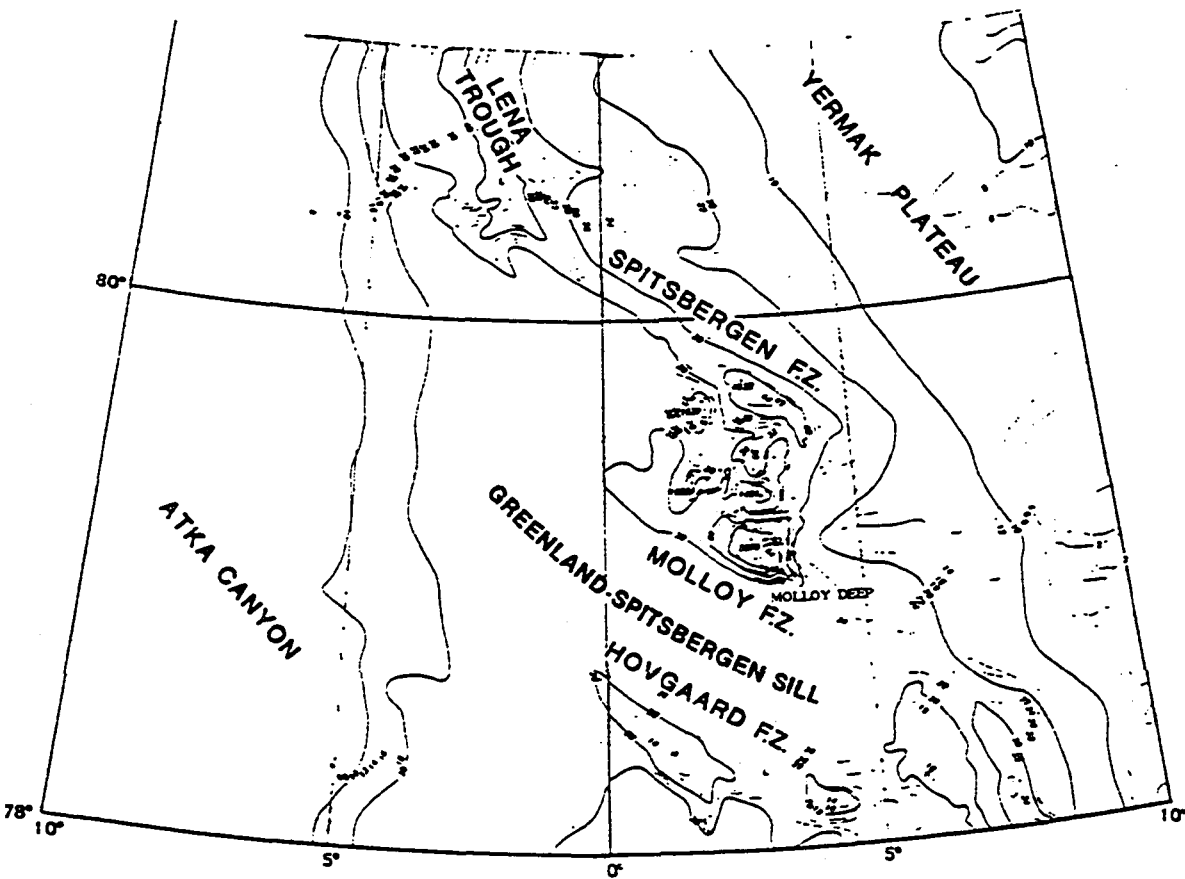
Figure 1.2 Details of the bathymetry in the Fram Strait area. Contour values are
in hundreds of meters. and point values are depths in meters (from Perry, 1986)

about 1500 m (Fig.1.2).

The Greenland Sea, and in general the whole GIN Sea, is in both geomorphological and hydrological sense, a continuation of the Arctic Ocean rather than the North Atlantic. The Greenland-Scotland Ridge that separates the North Atlantic from the GIN allows only overflows of deep dense water formed to the north, whereas there is continuous deep flow through Fram Strait out of and into the Arctic Ocean.

Section 1.2 Major water masses of the GIN Sea

Through this work, many different water masses will be mentioned, some of them of local origin, others of remote origin but all important to the processes discussed here. To make this discussion clear the major water masses will be described below. Others not mentioned in this section will be defined later in the text.

Starting from the surface and then going down, the following major water masses are recognized in the Nordic Seas (as defined by Swift (1986) and also Johannessen (1986) and Hopkins (1991)):

— Atlantic Water (AW) is traditionally defined to be any water with salinity greater than 35.0 psu (practical salinity units). It has profound influence on the northern polar region. It enters the GIN Sea over the Greenland Scotland ridge with a water temperature of 6 to 8°C and salinity of about 35.1 to 35.3 psu. It exits through Fram Strait with salinity close to 35.0 psu. Its temperature decreases between the Greenland Scotland ridge and Fram Strait, by about 5°C in both

winter and summer. It is carried north by the Norwegian Atlantic Current and by its branches (Fig.1.3): the North Cape Current entering the Barents Sea, and the West Spitsbergen Current flowing north. AW enters the GIN Sea as a wide core of warm water, reaching from the surface down to about 800m and part of it leaves through Fram Strait beneath the fresher and colder Arctic Surface Water. The rest recirculates back into the Greenland Sea to become intermediate water with a salinity of about 34.9 to 35.0 psu and temperature of about 0 to 2°C. This branching and recirculation is why it is called return Atlantic Intermediate Water (rAtIW)

— Polar Water (PW) is formed in the Arctic Ocean and exits through Fram Strait and is transported by the East Greenland Current into the Greenland Sea. Its depth range is from the surface to about 150 m. Over that depth, its temperature changes during winter from the freezing point (approximately −1.5°C) to 0°C and salinity changes from 30 psu to 34 psu.

— Arctic Surface Water (ASW) refers to surface water coming in or going out of the GIN Sea with a temperature greater than 0°C for the salinity range 34.4 to 34.7 psu and greater than 2°C for the range 34.7 to 34.9 psu.

Upper Arctic Intermediate Water (upper AIW) is the next layer of water in order of increasing density. Its θ-S limits are less than 2°C and in the range of 34.7 to 34.9 psu

Polar Intermediate Water (PIW) is found near the East Greenland Current as far south as

the Denmark Strait with temperatures below 0°C and salinities between 34.4

psu and 34.7 psu.

Lower Arctic Intermediate Water (lower AIW) is the layer above the deep water domain.

It shows temperature and salinity maxima at depths of about 250 to 400 m or

deeper. Its temperature range is 0 to 3°C and the salinity is greater than 34.9

psu. The temperature and salinity maxima are clear signs that this water mass

is produced by the cooling and sinking of AW.

— Greenland Sea Deep Water (GSDW) originates from the process of deep water

formation in the Greenland Sea. It extends from about 500 m down to the

bottom with temperatures falling to between −1.1 to −1.3°C and salinities

34.88 to 34.90 psu. It is believed to be denser (in situ) than Arctic Ocean

Deep Water (AODW).

— Norwegian Sea Deep Water (NSDW) similar to GSDW but it is slightly warmer at

about −0.5 to −1.1°C and salinity of 34.92 psu occupying depths below 2500 m.

— Canadian Basin Deep Water (CBDW) is characterized by temperature around −0.5°C,

salinity 34.95 psu. Within the GIN Sea it is also called Arctic Ocean Deep

Water (AODW).

Section 1.3 Hydrology and circulation

The major features of the circulation in the GIN Sea have been qualitatively known since the pioneering work by Helland-Hansen and Nansen (1909). General circulation in the Greenland Sea and Fram Strait region is dominated by two opposite flowing boundary currents that link the Arctic Ocean to the North Atlantic (Fig. 1.3).

The WSC, which is really the northernmost extension of the Gulf Stream-North Atlantic-Norwegian Atlantic Current system, carries relatively warm and salty water northward with a velocity generally less than 10 cm/s (Hanzlick, 1983). Some water from the Norwegian Atlantic Current forms the North Cape Current as it turns to the east into the Barents Sea, but the major part of it is transported north bringing significant amounts of heat and salt into the polar region. Part of the WSC enters the Arctic Ocean through Fram Strait submerging under the sea ice and the cold and less saline Arctic Surface Water, and follows the continental slope east. North of Spitsbergen it spreads as a counterclockwise current in the Arctic to recirculate back toward Fram Strait. The rest of the WSC water does not enter the Arctic Ocean but branches off westward, to submerge under the Polar Water carried south within the EGC (Johannessen, 1986). It is believed that heat released into the atmosphere along the path of the Norwegian Atlantic Current maintains anomalously warm winters in northern Europe (Broecker, 1991). It also accounts for the relatively steady southern limit of sea ice advected out from the Arctic Ocean. Winter temperature and salinity characteristics of the core of the Norwegian
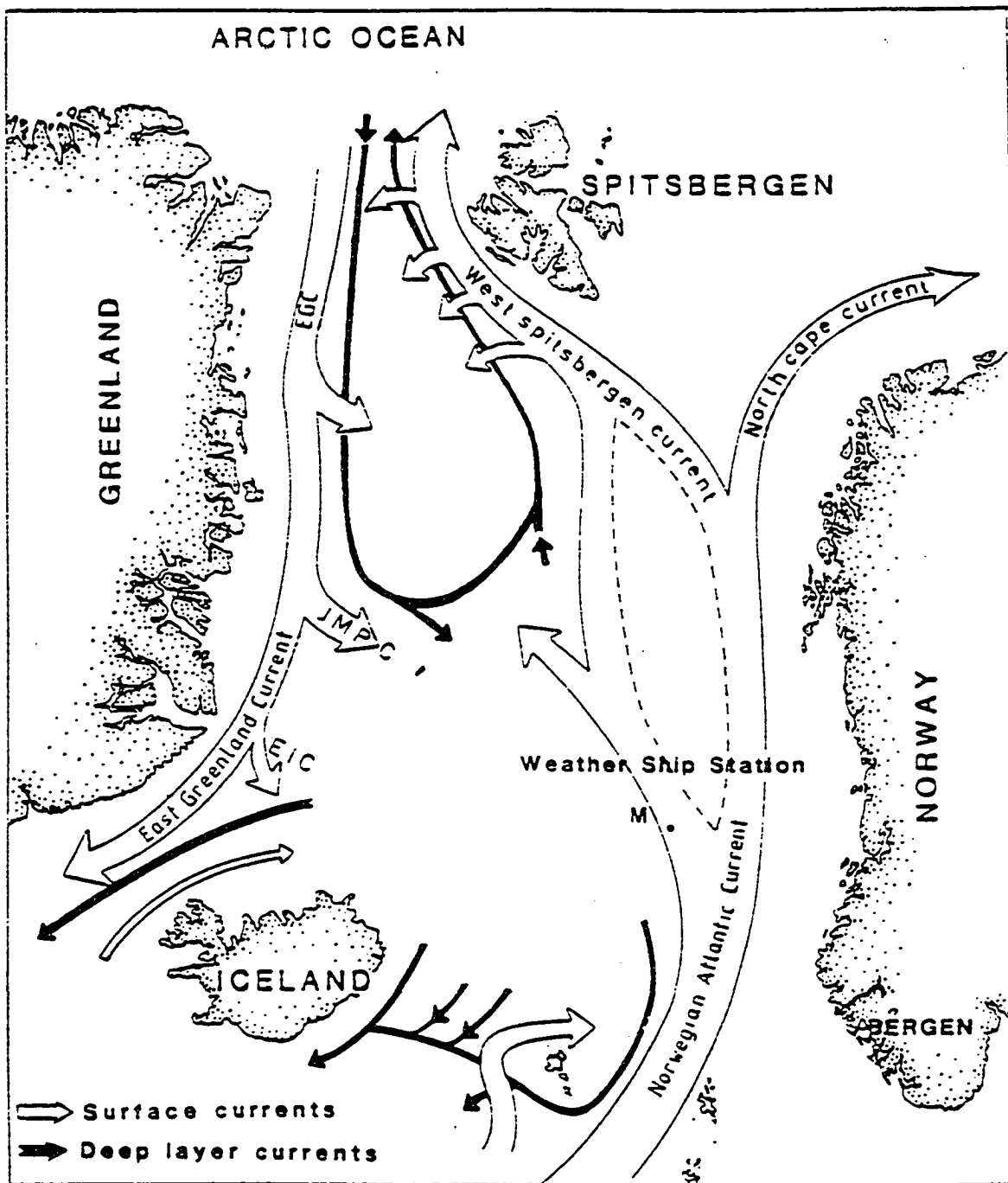
Figure 1.3 The surface and subsurface circulation in the Nordic
Seas. The names of major currents are shown (from Jonsson, 1989)

Atlantic Current at 69°N, just before it divides into two separate currents. are >+6°C and 35.1 psu respectively. In Fram Strait. at 80°30'N where the WSC converges with the colder and fresher water and sea ice. these characteristics are close to +2.0°C and 34.97 psu.

Hanzlick (1983) found from current-meter measurements that the heat transport by the WSC in Fram Strait during 1976–77 was about 46×10^{12}W (1 Watt=$1m^2kg/s^3$), and the mass transport about 5.6 Sv (1 Sv=$10^6 m^3/s$). Mass transport through Fram Strait at 79°N was suggested by Jonsson (1989) to be 3±1 Sv. which is closer to the previous estimate given by Timofeyev (1962). and also more recently by Stigebrandt (1981), Ostlund and Hut (1984) and Rudels (1987). Table 1.1 lists the WSC transport estimates by some researchers.

The situation in the Fram Strait area is complicated by the presence of the Hovgard Fracture Zone that may cause the mean current to flow northwestward on the southern side and southeastward on the northern side due to topographic steering (Jonsson. 1989). Another degree of complexity is added due to the existence of a semi-permanent cyclonic eddy, the Molloy Deep eddy, just north of 79°N that is believed to be a feature related to abrupt changes of depth around the Molloy Deep and neighboring seamounts (Wadhams and Squire, 1983; Smith et al., 1984; Bourke et al., 1987b; Johannessen et al., 1987).

The WSC is generally agreed to have maximum transport in late fall and winter. which then decreases through the spring into a summer minimum (Timofeyev. 1962; Hanzlick. 1983; Jonsson. 1989). Annual mean transport may vary by more then 30% (Timofeyev.

Table 1.1 WSC transport estimates by various researchers.

Author	Transport (Sv)	Remarks
Leonov(1947)	2.5	78°N section (dynamic method)
Hill and Lee (1957)	1.1 (3.2 max)	74°30'N section (upper 400m with 750db reference (1949-1956))
Kislyakov (1962)	3.2 ±1.5 (0.5 min summer; 5.5 max. winter)	74°30'N section with 1000db reference
Timofeyev (1962)	3.1±0.6	78°N section with 1000db reference. From annual estimates 1933-1960
Aagaard et al. (1973)	8.0	79°N unsing current-meter data 1971-1972
Greisman (1976)	7.0 (11 max. Sep.: 3 min Feb)	79°N using current meter data 1971-1972 and hydrogralhy
Hanzlick (1983)	5.6 (11.9 max Dec.: 1.4 min. Mar)	79°N section using current-meter data 1976-1977 and hydrography
Jonsson (1989)	3 ±1 (max late fall. winter)	79°N section using current-meter data 1984-1985 and 1985-1986

1962), over different time scales ranging from three to over 30 years (Mandel, 1979). However as existing time series are not as long as desired this is still a matter of some speculation. Such interannual changes in volume transport are of great importance since they could cause significant perturbations in the Arctic Ocean heat budget.

On the western side of the Greenland Sea, the EGC, carries ice and cold, low-salinity waters southward, with a surface velocity greater than 25 cm/s. Thus, in some sense, it provides a simple symmetry to the Greenland Sea circulation with the north flowing

WSC balanced by the south flowing EGC. In contrast to the northward transport of the Atlantic Water, the EGC follows the continental slope off Greenland and exits the GIN Sea through the Denmark Strait (Fig.1.3). It is estimated that about $4-5 \times 10^3$ km^3 /year of ice (Vinje and Finnekasa, 1986) and about 3 Sv of water (Foldvik et al., 1988) flow through Fram Strait via the EGC. Although the estimates of the EGC mass transport in Fram Strait have varied over the years (see Table 1.2), the estimate of 3 Sv by Foldvik et al. (1988), is quite close to the most recent estimates for the WSC. setting a reasonable balance of no net mass flow through Fram Strait on an annual basis. In contrast to oceanic flow. the export of ice is closely coupled to the local meridional component of

Table 1.2 EGC transport estimates by various researchers.

Researcher	Transport (Sv)	Remarks
Jakhelin (1936)	1.3	72°30'-75°N. dynamic method
Timofeyev (1963)	4.9	Total deduced from water balance
Vovinckel and Orwig (1970)	3.4	From total mass balance
Aagaard and Coachman (1968a)	31.5	Total (69-82°N), winter 1965
	7.7	PW (<0°C, <150 m)
	21.3	rAtIW (>0°C. 200-800 m)
	2.5	Deep Water (<0°C. >800 m)
Worthington (1970)	4.0	PW. from mass balance
Mosby (1962)	2.0	From total mass balance
Aagaard and Greisman (1975)	7.1	Total equated to WSC
	1.8	Deep Water component
	5.3	rAtW component
	0.1	Ice component
Foldvik et al. (1988)	3.0	<700 m. current measurements

wind stress (Hibler and Walsh, 1982). There is no obvious known seasonal or interannual variability in the volume flux of the EGC through Fram Strait (Foldvik et al., 1988).

The circulation in the Greenland Sea consists of a large cyclonic gyre, the Greenland Sea gyre. It is closed to the east and west by the EGC and the WSC respectively, to the south by the eastward moving branch of the EGC, the Jan Mayen Polar Current, and at the north by the westward moving branch of the WSC (Fig.1.3). This picture of generally cyclonic circulation has some modifications to it, just to recall the already mentioned topographic steering effect over the Hovgard Fracture Zone and Molloy Deep area, or over the Greenland Fracture Zone (Quadfasel and Meincke, 1987).

Within the domain of Fram Strait, steep bottom topography acts as a local guiding agent to the flow since the topographic β effect, dominates the planetary β by orders of magnitude. However, in the mesoscale range the currents are strongly influenced by local baroclinic instabilities (Johannessen et al., 1987). Topographic steering suggests the existence of a strong barotropic mode of the fluid. From the conservation of potential vorticity, the barotropic flow tends to follow lines of constant (f/H). This condition is largely fulfilled by the WSC but in the EGC the situation is not as clear (Quadfasel et al., 1987). Barotropic motions may be important in the EGC because significant currents there have been measured over the slope (more than 2 cm/s below 1000 m) extending to near-bottom (Foldvik et al., 1988). Hence the EGC can not be simply a buoyancy-driven outflow from the Arctic Ocean but must have one or more other driving mechanisms. The

motion of deep water was suggested to be small (Coachman and Aagaard, 1974), but the

body of available information to date is far too small to construct their circulation patterns.

Figure 1.4 is adopted from Hopkins (1991) to show the large scale horizontal

distribution of water properties at the surface in the Greenland Sea. The major oceanic

fronts (see Fig.1.5) can be located in both winter and summer tracer fields. The East

Greenland Front (EGF) positioned mostly above the Greenland shelf slope has the best

signature in winter surface salinity distribution (Fig.1.4b) and it is represented by a sharp

salinity gradient between 34.0 and 34.3 psu. It separates fresh Polar Water to the west

from the more saline waters of the Greenland Sea gyre. In summer the EGF is strongly
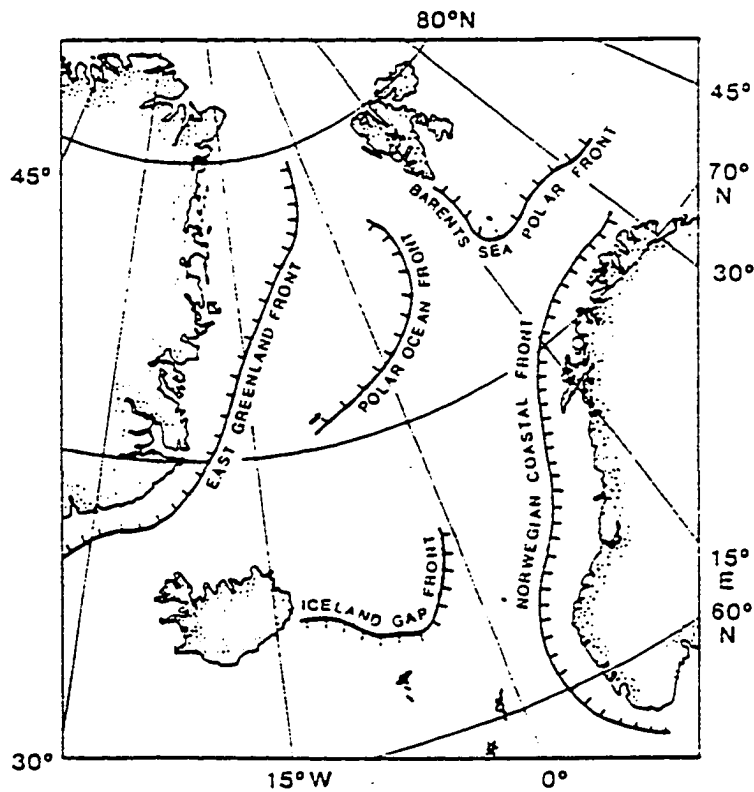
Figure 1.4 Fronts of the Nordic Seas (from Johannessen, 1986)

correlated with an increase of temperature from 0 to 3°C (Fig. 1.4d) and with the summer

position of the ice edge. Also the Polar Oceanic Front (PF) can be recognized by the

surface distribution of tracers. In winter it is depicted by a jump in temperature from 0

to 3°C, and salinity from 34.9 to 35.0 psu, and in summer by an increase of temperature

from 4 to 6°C with a salinity about the same as during the winter.

Between the two fronts (Fig.1.5) very dense surface waters are found in the Greenland

Sea in winter, with $\sigma_t > 28.00$ which indicate a very good potential location for deep water

formation. Most observations of deep open ocean convection come from the central

Greenland and Boreas Basins (Bogorodskii et al., 1987; Johannessen et al., 1991; Roach

et al., 1993; Rudels et al., 1989) where the winter surface density is at the maximum.

The horizontal distribution of tracers at the surface clearly shows that the GIN Sea is

a region where the two major water masses the Atlantic Water and the Polar Water,

converge, a process which has a great influence on the complex dynamics of the ocean-

sea ice-atmosphere system there.
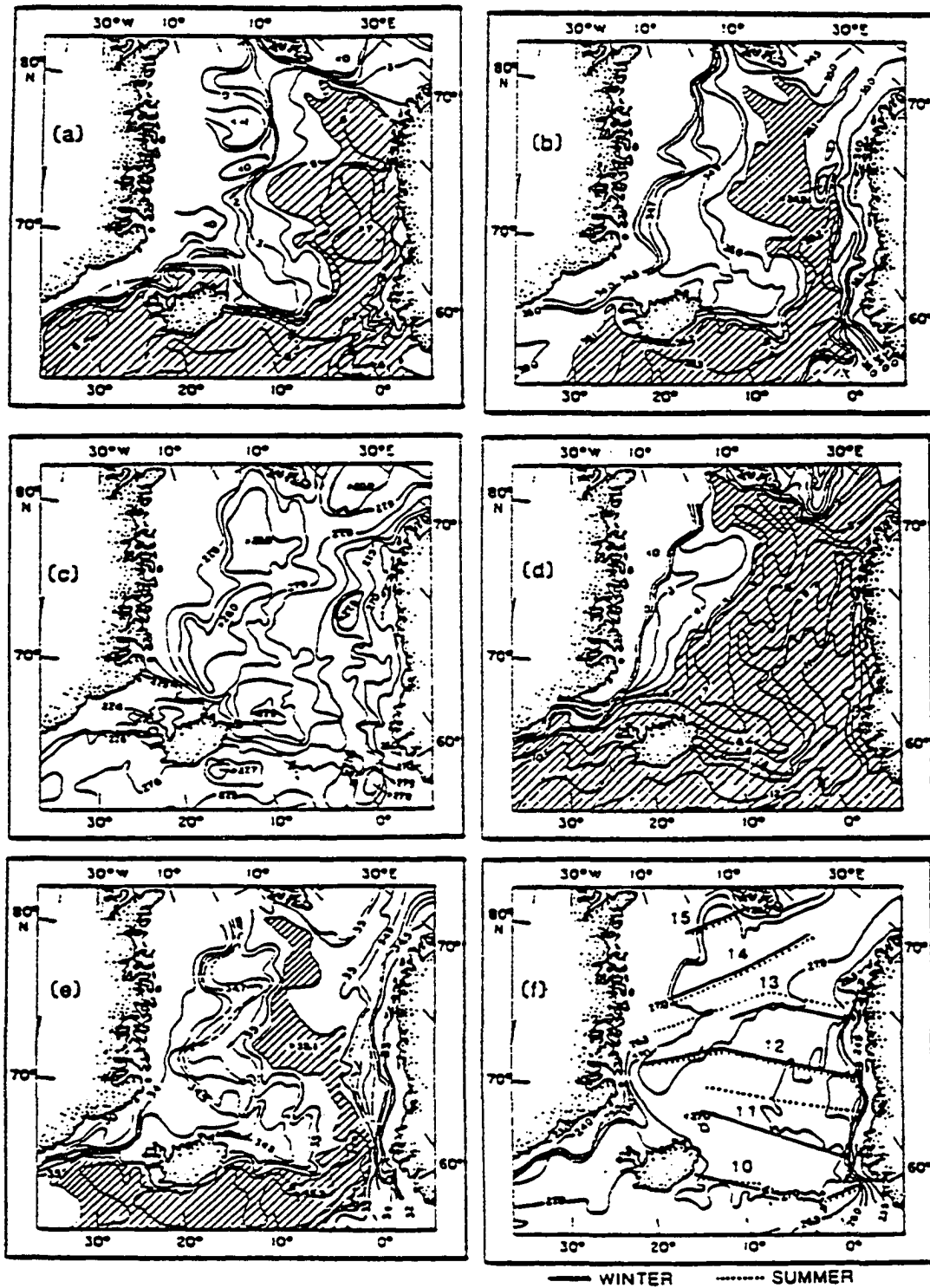
Figure 1.5 Surface contours of T, S, and σ_t for the GIN Sea: (a) winter temperature, (b) winter salinity, (c) winter σ_t, (d) summer temperature, (e) summer salinity, and (f) summer σ_t. Data are from the "Polar Front" surveys 1957–1958 (Dietrich, 1969) (adopted from Hopkins, 1991).

Section 1.4 Major dynamical processes

The GIN Sea ice cover plays an important role in the complex dynamics of the region, such as in air-sea interaction including exchange of momentum heat and mass, in surface buoyancy flux through the melting/freezing cycle, and also in reflection and scattering of energy. These are the general reasons to start this section with some discussion of ice, although due to complexity of the numerical approach, it has not been explicitly modeled here. The numerical approach to account for some of the most important processes influenced by the presence of sea ice will be addressed later in sections discussing modeling.

In the Nordic Seas, sea ice is the major source of fresh water. Its volume in advection, melting and freezing in the area is crucial to water column stability and hence to establishing the potential for open ocean convection, as well as the distribution of oceanic fronts (Fig.1.4).

Ocean fronts in the Nordic Seas are convergence zones between cold, less saline water and warm, saline water where the strong changes in temperature and salinity compensate each other in such a way as to reduce the density gradients (Johannessen, 1986). Mesoscale and short time variability of the frontal wave structure and eddies may be of great significance to convection by allowing cross frontal turbulent fluxes. These fluxes, for example, would be an important way of exchange of water properties across the Polar Front between the East Greenland Current and the Greenland Sea gyre (Foldvik

et al., 1988). The Polar Front, which separates the cold, low salinity polar waters west

of the front from warmer and more saline water with an Atlantic component to the east,

extends north from Jan Mayen to the area between Spitsbergen and Greenland. The PF

is generally in the same region both winter and summer with its location well correlated

with the position of the Mohns Ridge. This supports the idea that topography is dominant

in influencing the limit of the ice cover during winter. If the wind, for example, forces

ice across the frontal boundary, the ice melts rapidly in the warmer Atlantic Water.

The Polar Front defines the open ocean limit of the marginal ice zone (MIZ) which is

generally defined as the transition region from the open ocean to the pack ice, where

strong air-ice-ocean interactive processes occur (Johannessen et al., 1987).

In the MIZ region north of Svalbard, Johannessen et al. (1983) observed current

meanders with horizontal scales of 20–30 km which shed off eddies of around 10 km

scale, i.e. approximately the internal radius of deformation. The size of these eddies

increases downstream in the EGC up to 40 km and their observed lifetime is between

20–30 days. Their generation is attributed to local horizontal shear instabilities of jet-like

currents along the ice edge (Johannessen et al., 1987).

Another type of mesoscale variability in the WSC away from fronts has been reported

by Hanzlick (1983) who interpreted the abundance of mesoscale activity in his current

meter records as evidence for baroclinic instabilities in the sheared boundary current.

These instabilities were observed to have spatial and temporal scales of 30–40 km and

3–5 days, respectively. A third important class of eddies are the topographically trapped ones, the most prominent being the cyclonic "Molloy Deep Eddy" (Smith et al., 1984; Bourke et al., 1987).

In their year-long moored current meter measurements from the EGC near 79° N, Foldvik et al., (1988), observed many so-called trains of eddies and eddy-pairs with cross-stream scales of about 10 km. Their results suggest that the role of eddies in the cross-frontal heat transport in the area is small, at least below about 100 m. If the lateral turbulent heat flux is small, it implies that local baroclinic instability is not a major source of the eddies. It also implies that the EGC does not interact significantly with the interior of the Greenland Sea gyre. The exchange processes between the EGC and the gyre can result via cross-frontal eddies further south, downstream in the Jan Mayen Current, or as episodic events in the Ekman layer.

The details of deep water formation are only speculative. The leading candidates are intense small scale convection (20–50 km), the so-called chimneys occurring in regions of cyclonic mean circulation involving more then one water mass (Killworth, 1979), and subsurface formation which involves both convergence of water masses and double diffusive mixing (Carmack and Aagaard, 1973). It is commonly accepted that the Greenland Sea and the Weddell Sea are the most important areas where convective renewal of intermediate and deep waters contribute to world ocean ventilation (GSP Group, 1990).

Deep water formation is the most important climatic feature of the Arctic Ocean and its adjacent seas (Broecker, 1991). As indicated by Aagaard and Carmack (1989), the GIN Sea is delicately poised with its ability to sustain convection. Thus even relatively small variations (6%) in the fresh water outflow from the Arctic Ocean via the EGC are able to alter or even to stop the convection in the GIN Sea. The northern North Atlantic "Great Salinity Anomaly" (GSA) of the late 1960s and 1970s, which was mainly manifested by an anomalously large outflow of sea ice from the Arctic Ocean (Figures 1.6, 1.7) changed the upper ocean salinity characteristics by 0.1–0.2 psu, was suggested (Schlosser et al., 1991; Rhein. 1991) as the cause of ~80% reduction in the formation of the Greenland Sea Deep Water in the 1980s.
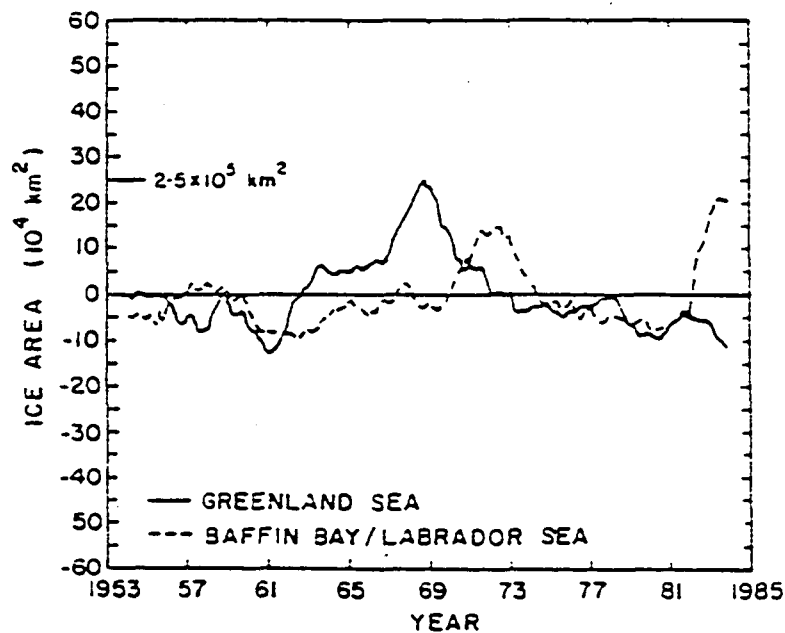
Figure 1.6 Superposition of the 25–month smoothed anomalies of areal sea-ice extent in the Greenland Sea and Baffin Bay/Labrador. (From Mysak and Manak, 1989)
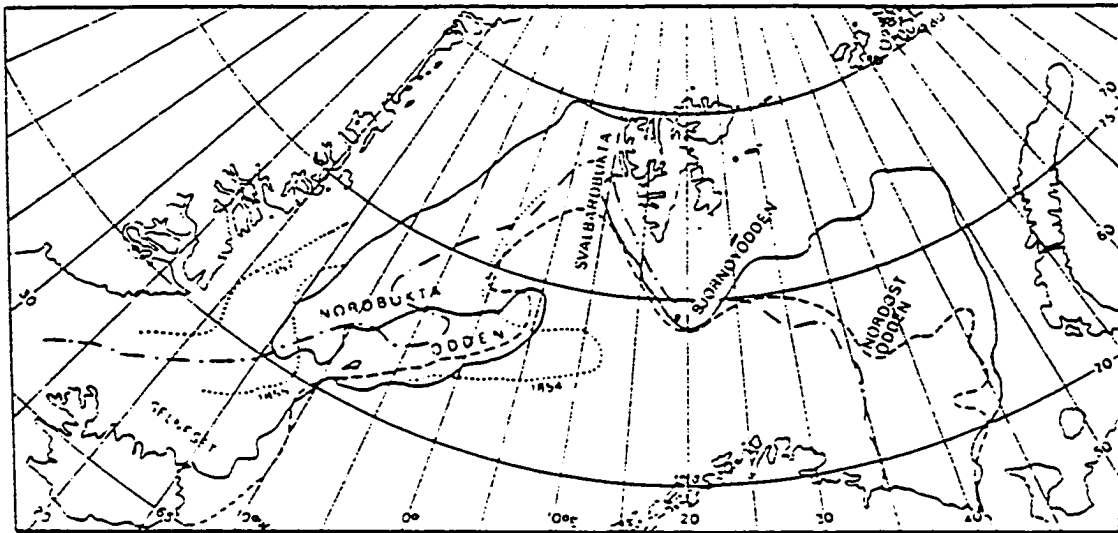
Figure 1.7 Extreme developments of the ice-edge position. The dashed-and-dotted line is for April 1966, the dashed line is for 10–20 April 1968, and the continuous line is for 1–10 April 1970. The dotted lines are ship observations in April 1854, 1855, and 1957. (From Wadhams, 1986)

Deep waters formed in the polar latitudes, overflow Denmark Strait and other passages in the Greenland Scotland Ridge to start the so-called "conveyor-belt" circulation (Broecker, 1987) (Fig. 1.8), that is believed to be driven by the salt left behind at low (tropical and subtropical) latitudes as the result of atmosphere water-vapor transport from the Atlantic to the Pacific Ocean. Some very cold periods in the past might be the result of a temporary shutdown of the conveyor. This is known as the halocline catastrophe, and it was proposed for past deglaciations (Broecker, 1991). The GSA is considered to be a small analog of the halocline catastrophes (Mysak, 1991). A major difference is that it did not require dramatic increases in fresh water flux to effect a capping of the convection. nor did it depend on deglaciation.

Anomalies such as the GSA could be critical to the nature of the global thermohaline circulation. According to Mysak (1991) the GSA should be regarded as an ocean climate event of considerable importance, second only to El Nino in its global impact.

Great Ocean Conveyor Belt

ATLANTIC OCEAN

PACIFIC OCEAN

INDIAN OCEAN
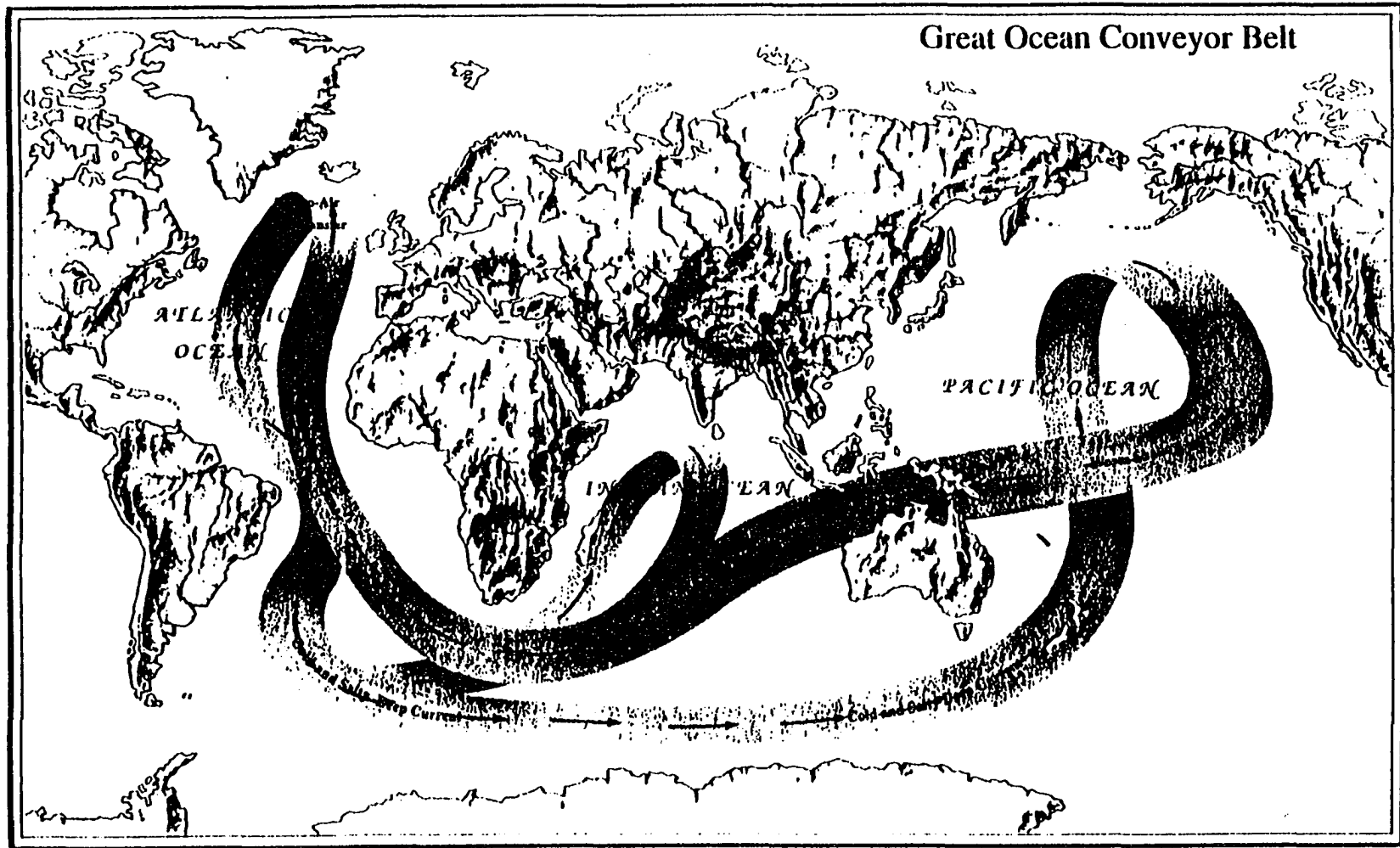
Figure 1.8 The great ocean conveyor logo (from Broecker, 1987).

Section 1.5 <u>Atmospheric forcing</u>

The annual mean distribution of atmospheric surface pressure (Fig.1.9a) shows that the GIN Sea is greatly influenced by the Icelandic low pressure system, but somewhat less by the high-pressure cells, over Greenland and the Canadian Basin. The low pressure trough, as illustrated by the mean position of the Arctic Front extending from Iceland into the Barents Sea, is not a synoptic feature over one month. As shown in Fig.1.9b it is due to higher frequency cyclonic oscillations passing along the mean direction of the Arctic Front. North of the front winds are easterly and south of the front they are westerly.

The Icelandic low is most intense during winter months and it is mainly a result of significant heat and moisture loss from the ocean surface into the atmosphere (Fig.1.10a). In spring the intensity of the Icelandic low rapidly diminishes (Fig.1.10b), and the incidence of cyclones becomes smaller with their main track shifted to the southeast (Fig.1.9). Through the summer, atmospheric pressure gradients are minimal, winds are weak, and overall atmospheric forcing is small (Fig.1.10c). During the fall, the major pressure systems of the Polar high and the Icelandic low continue to build and move toward their respective winter maximum and minimum positions (Fig.1.10d). The mean wind speed closely follows variability of the atmospheric pressure over an annual cycle, ranging from 5 to more that 10 m/s. More discussion on the atmospheric forcing will follow in the section on input data for the model.
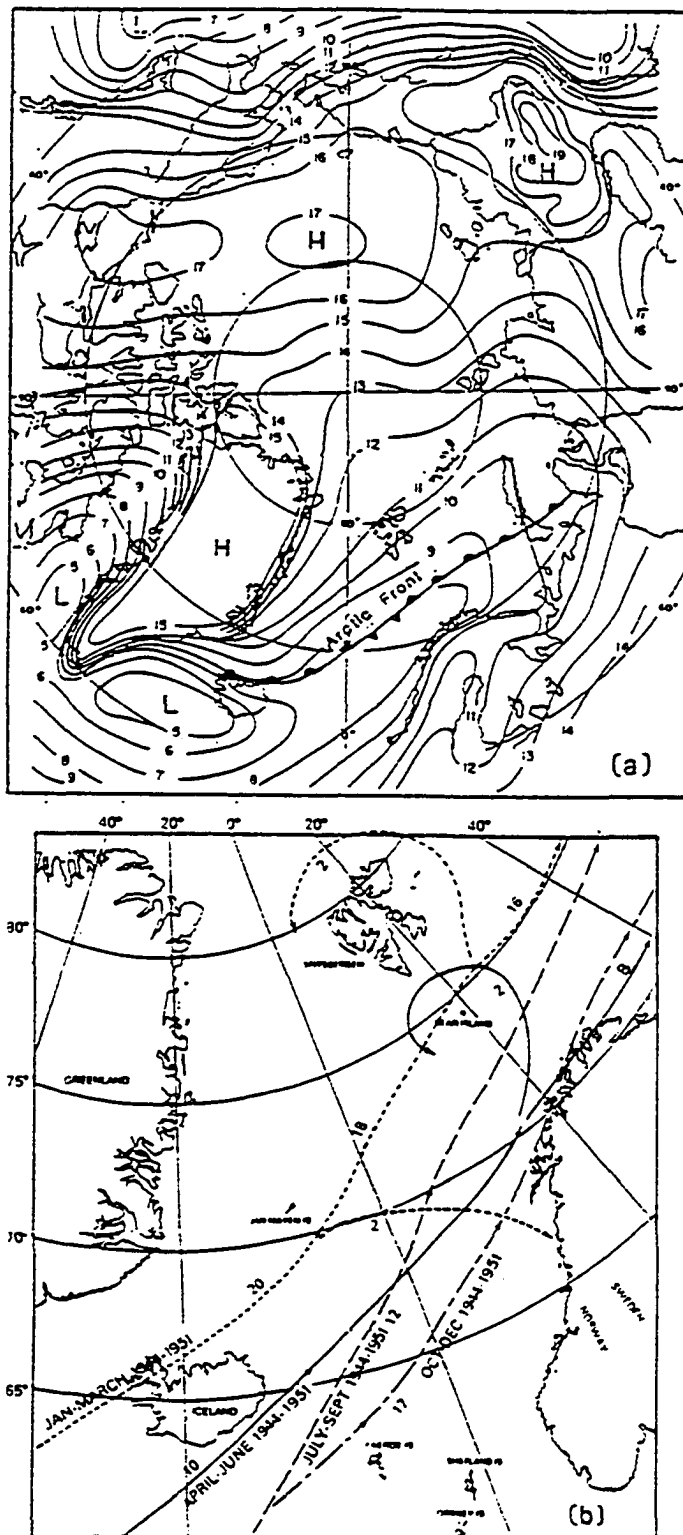
Figure 1.9 a) Annual mean sea level air pressure (mbar) (from Vowinckel and Orvig,
    1970), b) The mean tracks of low-pressure centres (severe storms). The numbers
along the tracks indicate the relative frequency of the storms. (From Gathman, 1986)
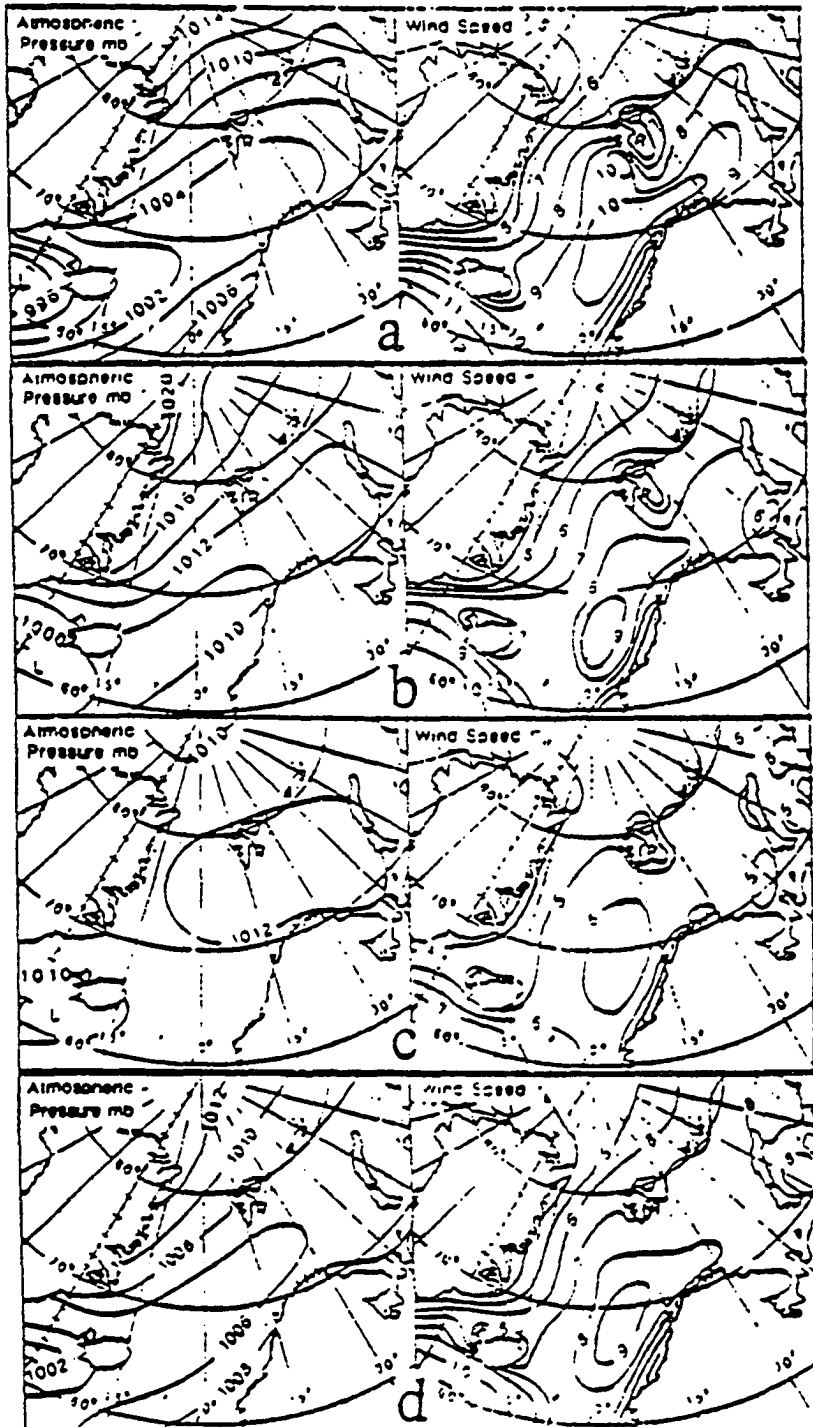
Figure 1.10 Mean sea level pressure and mean wind speed variations for (a) January, (b) April, (c) July (d) October (from Hopkins, 1991)

Chapter 2 THE MODEL AND INPUT DATA

In this chapter, a three-dimensional primitive equation prognostic model of the Greenland Sea and input data are presented. The model allows prediction of three-dimensional and time dependent distributions of velocity, density, temperature and salinity in an ocean of arbitrary geometry and bottom topography. After major reconstruction of Semtner's (1974) version, the general circulation ocean model used here allows for incorporation of open boundaries at the south and north as it is necessary to simulate dynamics defined by two major currents in the region. the EGC and the WSC. To decrease the effects of lateral viscosity, which can significantly limit realistic energy levels in mesoscale and large scale circulation. a scale selective biharmonic mixing operator is used for horizontal sub-grid scale parametrization of momentum. heat. and salt transfers.

In the first section previous modeling studies in the polar regions are discussed. Then the ocean model is introduced in next section. followed by short discussion on the input data and parameters used in the simulations.

Section 2.1 <u>Previous</u> <u>modeling</u> <u>studies</u>

There have been many attempts to numerically model the dynamics of the polar regions, prescribing artificial data for stratification, bathymetry, and forcing (Hakkinen, 1986, 1987; Hakkinen et al., 1992; Niebauer and Smith, 1989; Smith et al., 1988; Roed and O'Brien, 1983). The previous efforts in modeling the GIN Sea with realistic data are limited. The major problem a modeler faces in this region is lack of good, ready to use, realistic data that would present satisfactory coverage in space and time. However, even with presently available sparse measurements some dynamical processes can be modeled and understood better now.

Another difficult issue related to limited-area models, as already mentioned, is the need to provide the open boundary (OB) conditions that would allow for undisturbed propagation of perturbations out of the region as well as variable forcing in time and space at the OB using data from observations, if such data exist and are available.

The simple solution to this problem is to increase the domain of the model sacrificing resolution, and to enclose the region with solid walls so no mass transport occurs through the boundary, assuming that the boundaries are away from the region of interest so they have little or no effect on interior solutions. An example of this approach is Hibler and Bryan's (1984, 1987) coupled ice-ocean model of the Arctic Ocean including the Norwegian and Greenland Seas. Horizontal resolution of their model was of about 160 km x 160 km, much too low to resolve details of the circulation. A similar model was

also developed more recently by Riedlinger and Preller (1991) with resolution of about 127 km x 127 km. Semtner (1976, 1987) also studied the Arctic Ocean with its adjacent seas using a coupled ice-ocean model. However on the open boundaries he prescribed steady mean values of mass transport and temperature and salinity from observations. Although the horizontal resolution of 110 km in his model was higher than in the two previous models, he was still not able to resolve details of the bathymetry and currents in the GIN Sea. The predicted currents in the above three models are rather low, probably because of the fact that excessively large eddy viscosities were used for computational stability.

As for modeling the Nordic Sea region only, the first attempt was done by Creagan (1976) using a two layer model. She neglected the EGC and prescribed an inflow of total 30 km^3/hr (~8.3 Sv) through the Faeroe-Shetland Channel and a corresponding outflow through Fram Strait, values which are much higher than most recent estimates. In spite of these deficiencies, the model quite well predicted quantitatively the gross features of the wind driven circulation, including the occurrence of cyclonic gyres over each deep basin.

A big step forward in modeling the GIN Sea circulation was done by Legutke (1987, 1991a) who used a primitive equation ocean model with horizontal resolution of about 20 km. For horizontal diffusion she used a Laplacian coefficient of 10^7 cm^2/s or 5x10^7 cm^2/s (depending on experiment). At the open boundaries she prescribed mass transport from observations. The total inflow through the Faeroe-Shetland Channel was taken to

be 5.3 Sv and the outflow of 5.9 Sv, and the inflow of 0.6 Sv was used through Denmark Strait, and 7 Sv of the inflow (i.e., EGC) and the outflow (i.e., WSC) through Fram Strait was prescribed. which is probably too large by a factor of 2. All the other openings were assumed as closed boundaries. Vertical shear of velocities on the OB was calculated from hydrographic sections using the thermal wind relation. Legutke (1987) ran a series of experiments lasting one month each and using different stratification and wind forcing (annual or seasonal means) for each experiment. In most cases OBs were prescribed from annual mean Levitus (1982) data. The current fields produced by these simulations in general are in agreement with existing observations. The bottom pressure torque was generally found to be the dominant term in the vertically integrated vorticity equation.

In more recent work. Legutke (1991a), started with adjusted to topography climatological annual mean Levitus (1982) temperature and salinity data. investigated the GIN Sea current fluctuations as forced by historical 6-hourly wind-stress data of 2.5-year period. In this study, predominantly barotropic wave-like motions on the shelves and the trapping of the fluctuations by closed (f/H)—contours were simulated and seemed to be important. The simulated. fluctuating kinetic energy was between 2 to 4 orders of magnitude below the observed level. mainly due to high viscosity, missing eddy activities and poor resolution of density fronts. Simulated and observed transport time series showed reasonable agreement.

Using the same model. Legutke (1991b) also studied some aspects of the Great

Salinity Anomaly of the 1970s. She found that a variability in wind forcing, as observed in the 1970s could provide a good explanation of the fresh water anomaly persistence in the Greenland and Norwegian Seas.

Stevens (1991) investigated the general circulation in the Nordic Sea using a three-dimensional primitive equation ocean general circulation model. Although the resolution of his model was relatively low, about 55 km, and the momentum Laplacian viscosity coefficient was high. 10^8 cm^2/cm, he used the OB conditions described in his earlier paper (Stevens. 1990). The stream function of 3 Sv for the inflow (EGC) and outflow (WSC) through the northern OB (83°N) was prescribed. On the southern OB (56°30'N) stream function ·data' were generated using a separate closed boundary model stretching 7°30' on either side of the southern OB. Temperature and salinity from Levitus (1982) annual mean data were prescribed on the OBs. Stevens run a seasonal experiment continuously for fifteen years. forcing the model with surface seasonal fields of temperature. salinity and wind stresses. while fixing the stream function and temperature and salinity at the OBs at the annual mean values. The simulated mass transport variability in the Greenland Sea gyre ranged between 16 Sv in summer to 30 Sv in winter.

Section 2.2 The numerical model

To study the three dimensional circulation of the Greenland Sea area, a primitive

equation general circulation ocean model (OGCM) is used, specifically Semtner's version

(1974) of Bryan's (1969) original code. The model allows prediction of three-dimensional

and time dependent distributions of velocity, density, temperature and salinity in an

ocean of arbitrary geometry and bottom topography. Since an OGCM treats the ocean
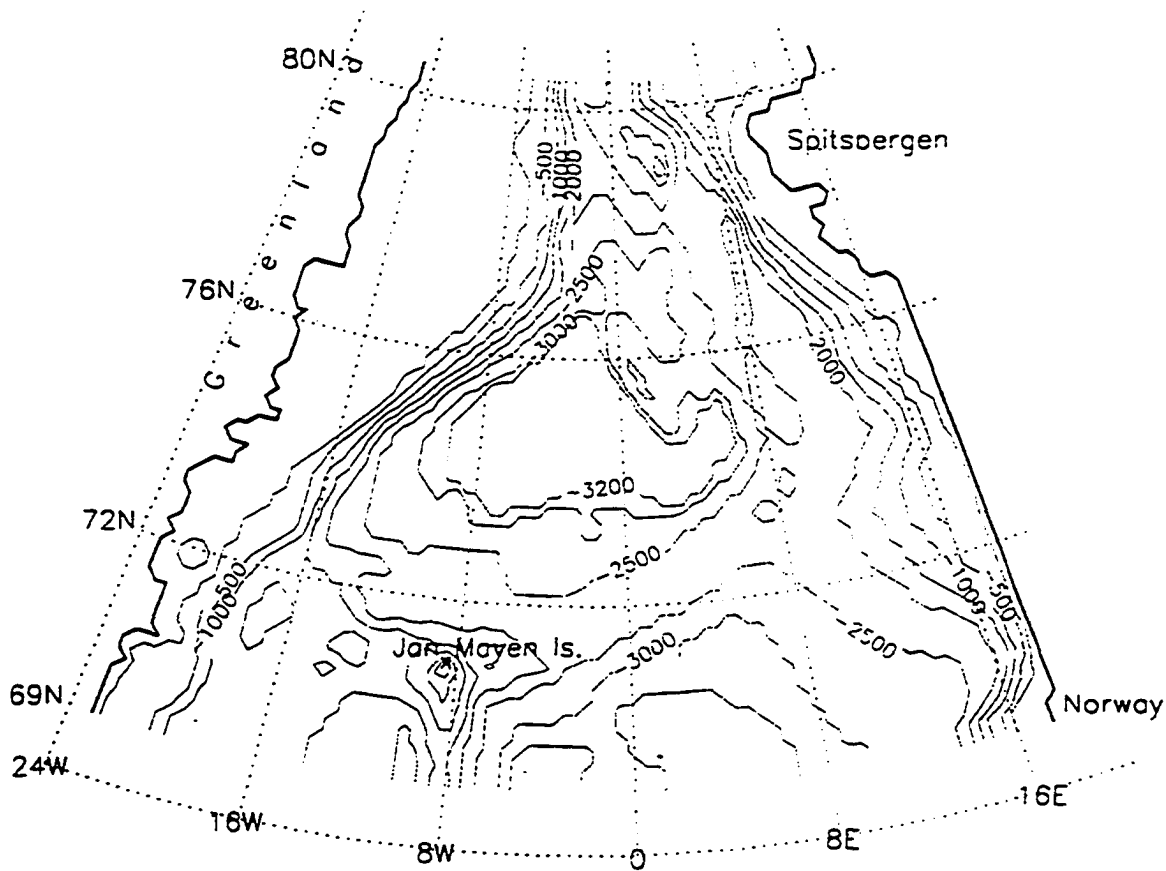
Figure 2.1 The model domain and bathymetry. Contour interval (CI) is 250 m.

as a closed basin, the code has been reconstructed to allow the incorporation of open

boundaries at the north and south, as required to model the area shown in Fig.2.1.

(boundary conditions are discussed in the next section). The earth is taken to be a sphere

of radius a, rotating with angular velocity Ω. A spherical coordinate system is used with

λ, $\dot{o}$, and z representing longitude, latitude, and height. The model adopts hydrostatic,

Boussinesq, and rigid-lid approximations. It assumes that the ocean is incompressible,

and, based on scale analysis, neglects the Coriolis terms and viscous terms involving w

in the horizontal momentum equations. The sea surface is assumed to be a horizontal

rigid lid to prohibit high frequency external gravity waves, without seriously affecting

the lower frequency motions in which most of the energy is concentrated, and to allow

longer time steps. The horizontal momentum equations for the zonal (λ) and meridional

(φ) directions, respectively are

$$\frac{\partial u}{\partial t} + Lu - \frac{uv \tan o}{a} - fv =$$

$$-\frac{1}{\rho_0 a \cos o}\frac{\partial p}{\partial \lambda} + \kappa \frac{\partial^2 u}{\partial z^2} + \left\{ \begin{array}{l} A_M\left\{ \nabla^2 u + \frac{(1-\tan^2 o)u}{a} - \frac{2\sin o}{a^2 \cos^2 o}\frac{\partial v}{\partial \lambda} \right\} \\ B_M \nabla^4 u \end{array} \right. \tag{1.1}$$

$$\frac{\partial v}{\partial \lambda} + Lv + \frac{u^2 \tan \dot{o}}{a} + fu =$$

$$-\frac{1}{\rho_0 a}\frac{\partial p}{\partial o} + \kappa \frac{\partial^2 v}{\partial z^2} + \left\{ \begin{array}{l} A_M\left\{ \nabla^2 v + \frac{(1-\tan^2 o)v}{a} + \frac{2\sin o}{a^2 \cos^2 o}\frac{\partial u}{\partial \lambda} \right\} \\ B_M \nabla^4 v \end{array} \right. \tag{1.2}$$

The hydrostatic approximation is

$$\frac{\partial p}{\partial z} = -\rho g \tag{1.3}$$

As convective mixing can not occur in a hydrostatic model some form of parametrization

must be used to take it into account. The 'convective adjustment' algorithm used in the

model checks water column stability and if the water column becomes statically unstable it is instantaneously mixed to produce a stable water column. The continuity equation (assuming incompressibility: $\frac{1}{\rho}\frac{D\rho}{Dt} = 0$) is

$$\frac{1}{a\cos o}\frac{\partial u}{\partial\lambda} + \frac{1}{a\cos o}\frac{\partial}{\partial o}(v\cos o) + \frac{\partial w}{\partial z} = 0 \tag{1.4}$$

The conservation equations of potential temperature T and salinity S are

$$\frac{\partial T}{\partial t} + LT = \kappa\frac{\partial^2 T}{\partial z^2} + \begin{cases} A_H\nabla^2 T \\ B_H\nabla^4 T \end{cases} + \gamma(T^* - T) \tag{1.5}$$

$$\frac{\partial S}{\partial t} + LS = \kappa\frac{\partial^2 S}{\partial z^2} + \begin{cases} A_H\nabla^2 S \\ B_H\nabla^4 S \end{cases} + \gamma(S^* - S) \tag{1.6}$$

The last term on the RHS of equation (1.5) and (1.6) is the Newtonian damping term of the robust diagnostic model (Sarmiento and Bryan. 1982). Coefficient γ is an inverse time constant. and T^* and S^* are input data based on interpolated observations in the Greenland Sea. A simple explanation of the robust diagnostic technique follows. For very large γ equations (1.5) and (1.6) reduce to

$$T = T^*$$

$$S = S^*$$

For γ to be very large. a time constant must decrease to 0. and the model reduces essentially to the diagnostic model (e.g. T and S vary in space but are constant in time). In the other limit. when γ is very small the last term in equations (1.5) and (1.6) is negligible and the model becomes fully prognostic. The damping terms create artificial sources and sinks of heat and salinity which push the predicted fields toward observed

values. A time constant governs the rate of damping. The robust diagnostic model partially conserves water mass properties along trajectories, but still does not depart far from observations. Finally, probably the most important feature of this approach is that it dramatically reduces the time of spin-up to the observed density field when compared with the spin-up time of a fully prognostic model.

The equation of state is

$$\rho = \rho(T, S, p) \tag{1.7}$$

The density is calculated with a nonlinear polynomial function of potential temperature T, salinity S, and pressure p, as given by UNESCO (1983). The ocean is contained between the surface $z=0$ and the bottom $z=-H(\lambda, \phi)$, with z being positive upwards. Components of the velocity vector are u, v, and w in the λ, ϕ, and z directions, respectively. The Coriolis parameter is $f = 2\Omega \sin \phi$, g is acceleration due to gravity and ρ_0 is mean water density. The advection operator is defined as

$$L(\sigma) = \frac{1}{a \cos \phi} \frac{\partial}{\partial \lambda}(u\sigma) + \frac{1}{a \cos \phi} \frac{\partial}{\partial \phi}(v\sigma \cos \phi) + \frac{\partial}{\partial z}(w\sigma) \tag{1.8}$$

The horizontal Laplacian operator is

$$\nabla^2 \sigma = \frac{1}{a^2 \cos^2 \phi} \frac{\partial^2 \sigma}{\partial \lambda^2} + \frac{1}{a^2 \cos \phi} \frac{\partial}{\partial \phi}\left(\cos \phi \frac{\partial \sigma}{\phi}\right) \tag{1.9}$$

and the horizontal biharmonic operator is

$$\nabla^4 \sigma = \frac{1}{a^2 \cos^2 \phi} \frac{\partial^2}{\partial \lambda^2}\nabla^2 \sigma + \frac{1}{a^2 \cos \phi} \frac{\partial}{\partial \phi}\left(\cos \phi \frac{\partial}{\partial \phi}\nabla^2 \sigma\right) \tag{1.10}$$

The vertical eddy coefficient κ is used both in the momentum and the diffusion equations. A and B are the horizontal eddy coefficients for the Laplacian and biharmonic diffusions, respectively. Their subscripts H and M are respectively, for diffusion and momentum.

Biharmonic friction (following A. Semtner. personal communication, 1992) rather than standard Laplacian friction is used for the horizontal sub-grid scale parametrization of momentum. heat. and salt transfers. The biharmonic friction operator is scale selective. meaning that it dissipates small scale motions more quickly than large scale motions. whereas Laplacian operator dissipates all scale motions evenly. Such an arrangement allows realistic energy levels in both mesoscale eddies and the large scale circulation. while eliminating short wave disturbances to that could produce computational instabilities (Pond and Pickard. 1983). Figure 2.2 (Bang, 1991) shows that decay rates of biharmonic diffusion decrease more rapidly with wavelength than those of the Laplacian diffusion. For example. a Laplacian coefficient of 2.5×10^7 will have the same decay rate for wavelengths of about 70 km as the biharmonic coefficient of -8×10^{19}, but at larger wavelengths (≥ 400 km) the Laplacian damping is more than an order of magnitude larger. It also shows that for wavelengths between 200 and 300 km the biharmonic coefficient of -8×10^{19} is equivalent to the Laplacian coefficient of 5×10^6.

The Semtner and Mintz (1977) formula to compare the biharmonic coefficient to the Laplacian coefficient. which can be derived from dissipation rates of the smallest scale
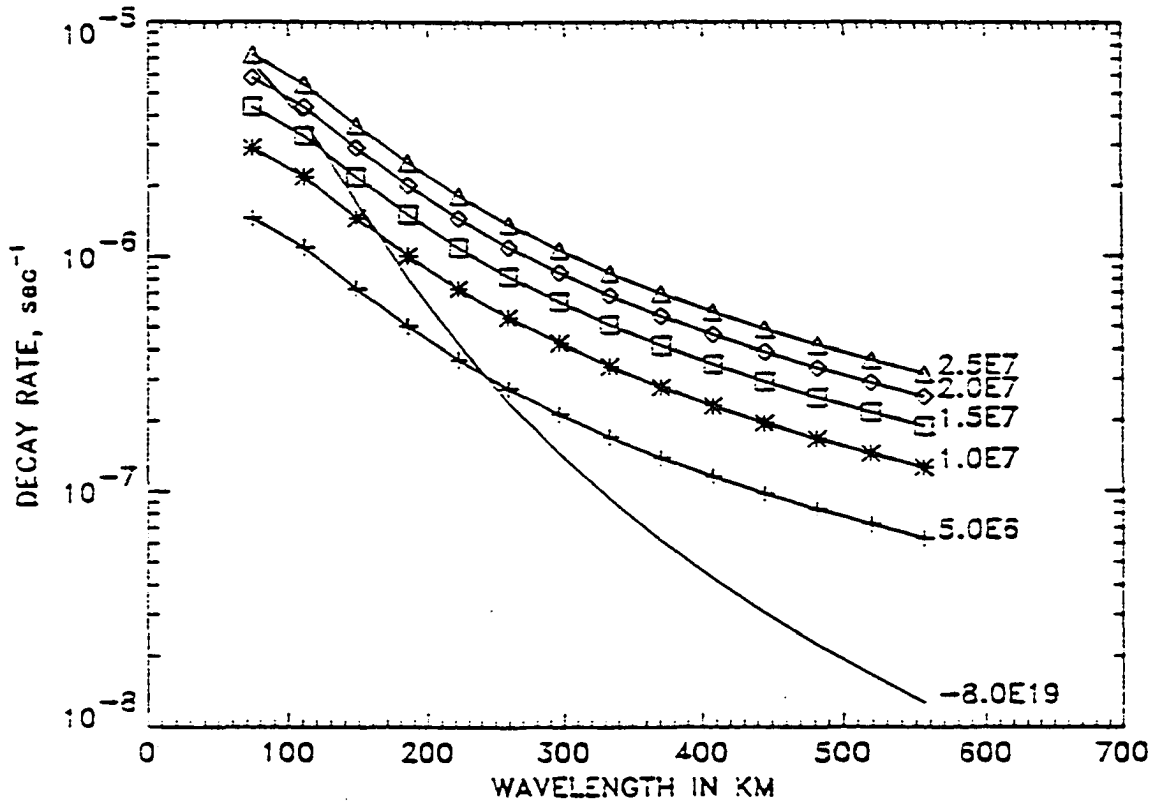
Figure 2.2 Decay rates of the two grid-size motion by biharmonic (solid) and
Laplacian (with marks) diffusion as function of wavelength (from Bang, 1991).

motion by two formulations, is

$$B_M = -\frac{A_M \delta x^2}{4}$$

(1.11)

where δx is the grid size. A value of $1/6°$ (18.52km) is used. For the biharmonic

coefficient of momentum diffusion a value of -1×10^{18} is used. An equivalent Laplacian

coefficient would be of about 1.2×10^6.

Another comparison of the biharmonic coefficient versus Laplacian coefficient for-

mulae for the thickness of Munk's boundary layer (Pedlosky, 1987) can be used, since

the dynamics of the layer strongly depends on friction. For Laplacian-type horizontal friction parametrization, the width of the Munk layer is defined as $(A_M/\beta)^{\frac{1}{3}}$, and for biharmonic-type it is modified to $(-B_M/\beta)^{\frac{1}{5}}$, where $\beta = \frac{\partial f}{\partial o}$. A value of β of 5.9×10^{-14} 1/(cms) is used here. For quantitative comparison it is reasonable to assume that the two types of horizontal friction parametrization would have similar effects within the Munk's boundary if its estimated thickness is the same. Hence, we get the biharmonic coefficient in terms of the Laplacian coefficient to be

$$B_M = -A_M^{\frac{5}{3}}\beta^{-\frac{2}{3}}$$ (1.12)

and for a biharmonic coefficient of -1×10^{18}, an equivalent Laplacian coefficient would be of about 3.2×10^5, which is about a quarter of the value obtained by (1.11). This means that (1.11) possibly overestimates the effect of the Laplacian diffusion for a given value of biharmonic coefficient.

The equations describing motion, temperature and salinity are solved using a finite difference formulation. The finite difference grid is a Arakawa "B" type grid (Arakawa, 1972), in which tracer points T, S and stream function points ψ are placed in the center of cells and the horizontal velocity components u, v are situated at the corners. In the vertical T, S, w, u, v are located in the center of the cell. More details on the numerical formulation and on methods for finding solutions may be found in Semtner (1974).

Section 2.3 <u>Boundary conditions</u>

The boundary condition of momentum flux through the surface

$$\vec{\tau}_s = \rho_0 \kappa \frac{\partial \vec{u}}{\partial z} \quad at \quad z = 0 \tag{1.11}$$

is derived from observed data (Hellerman and Rosenstein. 1983) that are discussed in section 2.4. The ocean surface is assumed to be a horizontal rigid lid. so that

$$w = 0 \quad at \quad z = 0 \tag{1.12}$$

A no flux boundary condition is used at the ocean surface and bottom for temperature and salinity. The thermohaline forcing is incorperated by the use of the robust diagnostic method. hence

$$\rho_0 \kappa \frac{\partial (T.S)}{\partial z} = 0 \quad at \quad z = 0 . \ and \quad z = -H(\lambda. \dot{\phi}) \tag{1.13}$$

Since sea ice is not modeled. an extra algorithm is added to ensure that surface temperatures do not fall below the freezing point at a given surface salinity.

The bottom friction is computed using a linear formula (Heaps. 1973)

$$\vec{\tau}_b = \rho_0 \left(\kappa \frac{\partial \vec{u}}{\partial z} \right)_h = -k \vec{u}_h \quad at \quad z = -H(\lambda. \varphi) \tag{1.14}$$

where the subscript h indicates the bottom layer velocity, and the linear coefficient k has dimensions of distance over time. A 4 day e-folding time scale for damping is used here. Linear bottom friction was added to the lowest layer of the model to provide a realistic

sink of energy for expected mesoscale variability (Semtner and Chervin. 1988). Velocity

at the ocean bottom is required to parallel the slope. i.e.,

$$w = -\frac{u}{a\cos\phi}\frac{\partial H}{\partial\lambda} - \frac{v}{a}\frac{\partial H}{\partial\phi} \quad at \quad z = -H(\lambda,\phi) \qquad (1.15)$$

Local limited-area models have great and important advantages over large scale

OGCM models in that they are able to resolve horizontal scales within a range of the

local radius of deformation. Simulations by such models can be viewed as valuable

forerunners of large scale OGCM experiments in the sense that they indicate the effects

of higher resolution on key processes and regions. thus guiding the parametrization of

these processes and regions in OGCMs (Walsh. 1992). Their major disadvantage is the

necessity to prescribe boundary conditions along open peripheries of a modeled region.

Before introducing an approach for open boundary conditions. boundaries which have

to unconditionally remain open in order to simulate the most important dynamics of the

Greenland Sea. must be defined. The modeled region was chosen to extend from 69°N

to 80°30'N. and from 23°W to 18°E. This locates the Greenland Sea in the center of

the domain (Fig. 2.1). Greenland at the west constitutes a natural closed boundary of

the domain. To the east. a closed boundary is assumed. since Spitsbergen, Bear Island.

and the Norwegian shelves provide partial closing. Because the Barents Sea is relatively

shallow. about 250–350 m. any transport across it is likely to be small, a view which

is supported by Aagaard and Greisman (1975). More recently, Druet and Jankowski

(1991) estimated the net eastward mass transport across 17°E. between Spitsbergen and

Norway, to be less than 2 Sv, based on the CTD survey in summer 1988. The two other

boundaries, Fram Strait and the parallel 69°N between Greenland and Norway have to

remain open since the major currents (i.e. WSC and EGC) transport water meridionally

there. In this study, volume fluxes of 4.2 Sv (outflow of the WSC and inflow of the ECG)

at the northern boundary and 8.2 Sv (inflow and outflow) at the southern boundaries are

prescribed, respectively.

On solid lateral walls the advective and no-slip boundary conditions for temperature

and salinity is used for biharmonic diffusion

$$\frac{\partial \sigma}{\partial n} = 0 \quad and \quad \frac{\partial}{\partial n} \nabla^2 \sigma = 0 \qquad (1.16)$$

where σ is either temperature or salinity, and n is the direction normal to the boundary.

The no-slip and one additional boundary condition for numerical closure on solid

walls is used here for the momentum so that

$$\vec{u} = 0 \quad . \quad \nabla^2 \vec{u} = 0 \qquad (1.18)$$

More discussion on boundary conditions on solid lateral walls for use with biharmonic

diffusion is provided by Bang (1991).

Open boundary (OB) conditions used here are mainly those described by Stevens

(1990), with some modifications for the use of biharmonic instead of Laplacian horizontal

diffusion. This approach can be viewed as another modification of the Sommerfeld

radiation condition (Sommerfeld, 1949), which states that

$$\sigma_t + c_\sigma \sigma_n = 0 \quad at \quad the \quad OB \qquad (1.19)$$

where σ is any of the model's dependent variables. c_σ is the propagation speed of disturbances, t time, and n the coordinate normal to the OB. Subscripts t and n denote differentiation with respect to the subscript. This type of OB condition is defined by Stevens as a passive OB condition. because it does not allow forcing at the OB. It only needs to let phenomena that are generated within the domain of interest propagate out without reflecting or distorting. The second type of the OB conditions is an active one in which the boundary condition actively forces the interior solution. However, disturbances must still be able to leave the region of interest without distorting its interior or creating problems near the OB.

On the OB. the fields of velocity u and v, and tracers T and S must be internally continuous with the density field. In the model. total velocities are computed as a sum of external and internal modes. External mode velocities are defined, in terms of the stream function as

$$\bar{u} = \frac{1}{H} \int_{-H}^{0} u \, dz = -\frac{1}{Ha} \frac{\partial w}{\partial \varphi}$$

$$\bar{v} = \frac{1}{H} \int_{-H}^{0} v \, dz = \frac{1}{Ha \cos \varphi} \frac{\partial w}{\partial \lambda}$$

(1.20a)

and the existence of w is guaranteed by the non-divergent nature of the vertically integrated flow. i.e.,

$$\frac{1}{a \cos \varphi} \frac{\partial}{\partial \lambda} \left(\int_{-H}^{0} u \, dz \right) + \frac{1}{a \cos \varphi} \frac{\partial}{\partial \varphi} \left(\cos \varphi \int_{-H}^{0} v \, dz \right) = 0$$

(1.20b)

Use of stream function w and T and S for the OB conditions by no means simplifies the problem. but at least it is consistent with the model calculation of the interior points. In

the case of the stream function, any cross-boundary volume transport produced by effects outside the modeled region must be prescribed from observations or from an exterior model covering a larger domain. The WSC and the EGC are doubtlessly not only the result of wind forcing within the GIN basin, so their transports at the boundaries must be specified.

The internal mode velocities are calculated in the model from the equations of motion (1.1 and 1.2). At the OB they are calculated from the linearized equations of motion. i.e.,

$$\frac{\partial u}{\partial t} - fv = -\frac{1}{\rho_0 a \cos o}\frac{\partial p}{\partial \lambda} + F^u$$
$$\frac{\partial v}{\partial t} + fu = -\frac{1}{\rho_0 a}\frac{\partial p}{\partial o} + F^v$$

(1.21)

where F^u and F^v describe the frictional terms in x and y, respectively. This almost eliminates the requirement for using velocity points outside the domain. The only exception exists in the diffusion terms, which have to be retained for stability. For Laplacian diffusion Stevens (1990) simply assumes that points outside the domain have the same value as adjacent points on the OB. In the case of biharmonic diffusion, the same assumption has been made both to $\vec{u}$ and $\nabla^2\vec{u}$.

To calculate pressure gradients in (1.21), the distribution of density, or rather of temperature and salinity, on the OB has to be determined. The passive OB condition can be described by the conservation equation of tracers (temperature and salinity) simplified so that only outward advection or diffusion is allowed. For simplicity, only the advective term perpendicular to the boundary is retained. The equation in such a form for the

zonal OB is

$$\frac{\partial(T.S)}{\partial t} + \frac{v}{a}\frac{\partial(T.S)}{\partial\phi} = F^{T.S} \tag{1.22}$$

where $F^{T.S}$ describes the frictional terms in tracer equations. If the advective velocity at a particular point on the OB is directed out of the region, then the values of tracers at this point will be determined from the interior. It may happen though that the advective velocity will be directed inside the region while the internal wave propagation will be directed out of the region through the OB. In such case a piling up of wave energy at the boundary may occur. Therefore the correcting phase speed c_T must be calculated from the finite difference form of the equation

$$\frac{\partial(T.S)}{\partial t} = -\frac{c_T}{a}\frac{\partial(T.S)}{\partial\phi} \tag{1.23}$$

at points adjacent to the boundary at the previous time step for each level in the vertical. If the sum of the advective velocity v and the phase speed c_T is directed out of the region, the following equation to calculate tracers is used

$$\frac{\partial(T.S)}{\partial t} + \frac{(v+c_T)}{a}\frac{\partial(T.S)}{\partial\phi} = F^{T.S} \tag{1.24}$$

It is worth noticing that by setting v and $F^{T.S}$ to zero, the original Sommerfeld radiation condition (1.19) is obtained.

If the direction of the resultant velocity is into the modeled region, the tracer may either remain at its previous value or be set to some prescribed value. The first option is a passive-type one, while the second option is just the active OB condition. To eliminate

possibilities of discontinuity in the vicinity of the boundary, especially where the resultant velocity in (1.24) changes sign, the tracer is smoothly forced towards its prescribed value when the velocity is into the region, by using the following equation

$$\frac{\partial(T,S)}{\partial t} = \gamma((T^*, S^*) - (T,S)) \tag{1.25}$$

where the term on the RHS is similar to Newtonian damping term in (1.5 and 1.6), i.e. T^*, S^* are values prescribed from observation and γ is a constant with units $[s^{-1}]$.

The finite difference formulation of the southern OB condition is described in detail by Stevens (1990). Treatment of the northern OB is the same with only a few details changing, mainly the direction of the outward resultant velocity. The same scheme could be used for any boundary orientation.

Section 2.4 Input data

The area to be modeled extends between 69°N and 80°30'N, and between 23°W and 18°E. As explained earlier the western and eastern boundaries are closed and the northern and southern boundaries remain open. The depth distribution in the GIN Sea is shown in Figure 1.1. The topographic gradients as calculated in this work and also by Legutke (1991a) are up to 4×10^{-2}. Such abrupt changes in depth can cause numerical instabilities in a primitive equation model (Killworth, 1987; Ramming and Kowalik, 1980; Kowalik and Murty, 1993). To ensure numerical stability, smoothing was applied to the original 1/12° resolution depth data (Sloss, 1986) to get the model bathymetry of resolution 1/2°x1/6°. The depth distribution after smoothing is shown in Figure 2.1. The

Greenland and Boreas Basins, and the Greenland Fracture Zone are still well resolved. Even the Molloy Deep, although modified, can still be distinguished to the north. The $1/6°$ of model meridional resolution used here is equal to about 18.5 km. and $1/2°$ of zonal spacing increases resolution from about 20 km at 69°N, and 14 km at 75°N, to about 9 km at 80°30'N. Since the major direction of water transport in the Nordic Seas is meridional. increasing zonal resolution with latitude is desired. In the vertical, depth is resolved by 21 layers. where the following numbers indicate the mid-depths of sequence of layers (10. 50. 120, 200. 300. 430. 600. 800. 1000, 1200. 1400, 1600. 1800, 2000, 2200. 2400. 2600. 2800. 3000. 3200. 3400 m). The 200 m resolution in the deep ocean is mainly to resolve variability in bottom topography.

For wind forcing. the monthly mean wind stress data of Hellerman and Rosenstein (1983) were used. Over large scales, away from lateral boundaries. and in the absence of gradients in topography. the meridional transport is described by the Sverdrup balance. $\beta M_y = curl_z \tau_\eta$, where β is latitudinal variation of the Coriolis parameter f, M_y, M_x are the total meridional and zonal mass transports in the wind influenced layer. and $curl\tau_\eta = \partial\tau_y/\partial x - \partial\tau_x/\partial y$ is the vertical component of the curl of the wind stress (Pedlosky, 1987). The wind stress curl annual mean and the monthly means of February and August representative for winter and summer months are shown in Figure 2.3. These were calculated by the central finite difference formulation from the wind stress. The annual mean field is characterized by positive values over most of the area. only close to the Greenland coast are negative values observed. Two separate maxima are situated
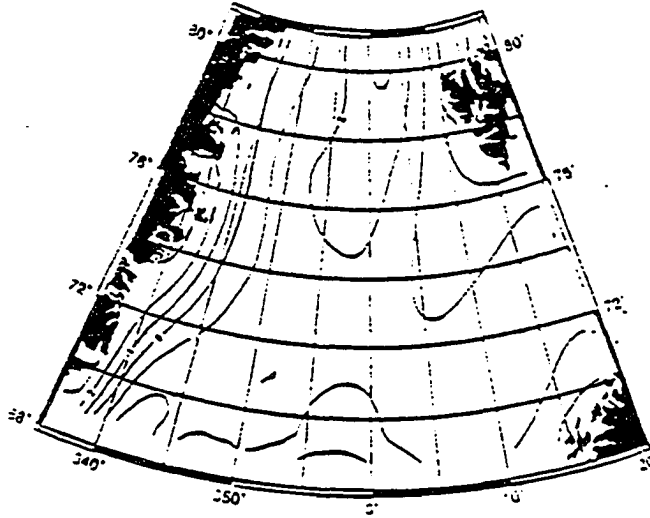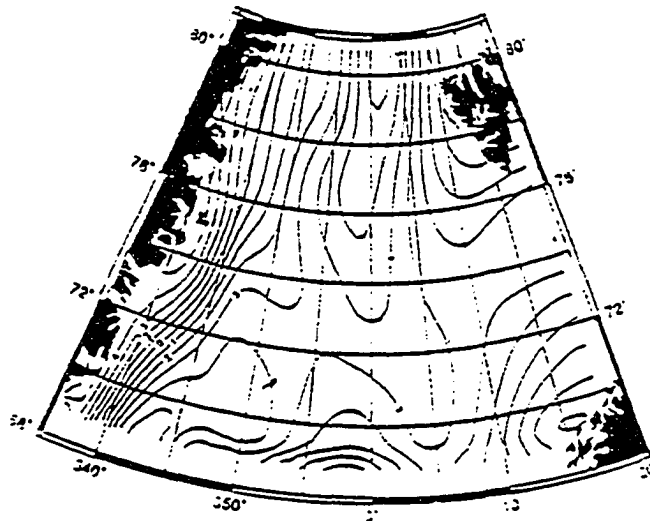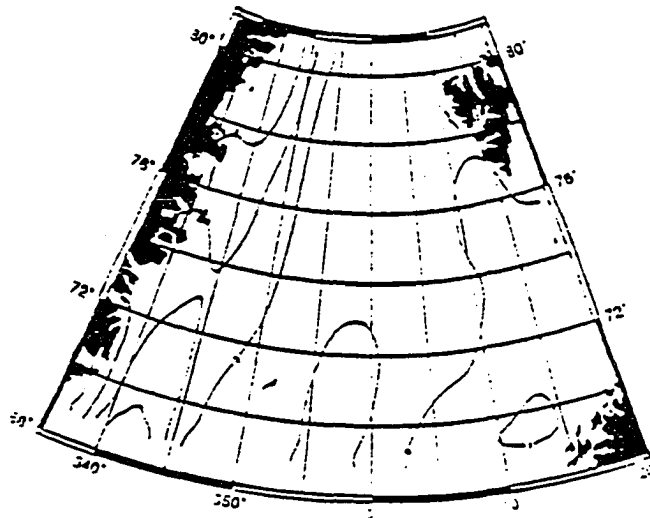
Figure 2.3 Mean wind stress curl distribution as calculated from the wind stress data of Hellerman and Rosenstein (1983): (a) annual. (b) February. (c) August. Unit is $1 \times 10^{-8} dyn/cm^3$.

somewhere in the center of the northern and southern boundaries, both with a maximum of

$3x10^{-8}$ dyn/cm^3. To the west the wind stress curl decreases rapidly to eventually become

negative close to the Greenland coast. The strong seasonal cycle as already shown in the

sea level pressure fields also exists in the wind stress curl data. The mean distribution

in August which is typical of the summer months between May and September shows

practically zero wind stress curl over the whole area with some weak positive values at the

south. During September and October wind stress curl starts to build up reaching its full

winter strength by November. This pattern then lasts through March. The winter mean

distribution is similar to the annual mean pattern, only much stronger, with a maximum

up to $6x10^{-8}$ dyn/cm^3. This seasonal pattern reflects the strength of the Icelandic low,

that was discussed earlier. Finally it is worth noting that instantaneous wind stress curl

values had to be much higher to yield strong monthly mean values for winter months

(Bakun, 1973).

The temperature and salinity data of Levitus (1982) were used for initialization and

forcing of the general circulation baroclinic model. In the GIN Sea, climatological data

are sparse and highly smoothed in time and in space without taking into account the large

influence of the topographic structures. In addition, as mentioned earlier, topographic

gradients are large. Density data that are badly adjusted to the topography, can induce

unrealistic strong currents near steep topographic features. These can exist even in a

steady state. To avoid shocking the model by initialization with such data (Semtner

and Chervin, 1988), the following approach is taken. The original Levitus data were

compiled with 1° resolution at 33 standard oceanographic depths from the sea surface

to 6000 m for the annual mean data, at 24 standard depths from the surface to 1500 m

for the monthly mean salinity data, and at 19 standard depths from the surface to 1000

m for monthly mean temperature data. These data were interpolated in horizontal to

1/2°x1/6° resolution using cubic spline interpolation, and then were linearly interpolated

in the vertical to obtain values at the model depths. The model was initialized with

these data, running for 5 months with static stability adjustment and diffusion as the only

operating terms (J. Wilkin, personal communication, 1993). This allowed the model to

adjust the temperature and salinity fields to static stability. These data were then saved

and used as the climatology for the experiments. The resultant surface distribution of

temperature, salinity and σ_t for the annual, winter and summer month means is shown

in Figures 2.4–2.7.

a)

b)

c)
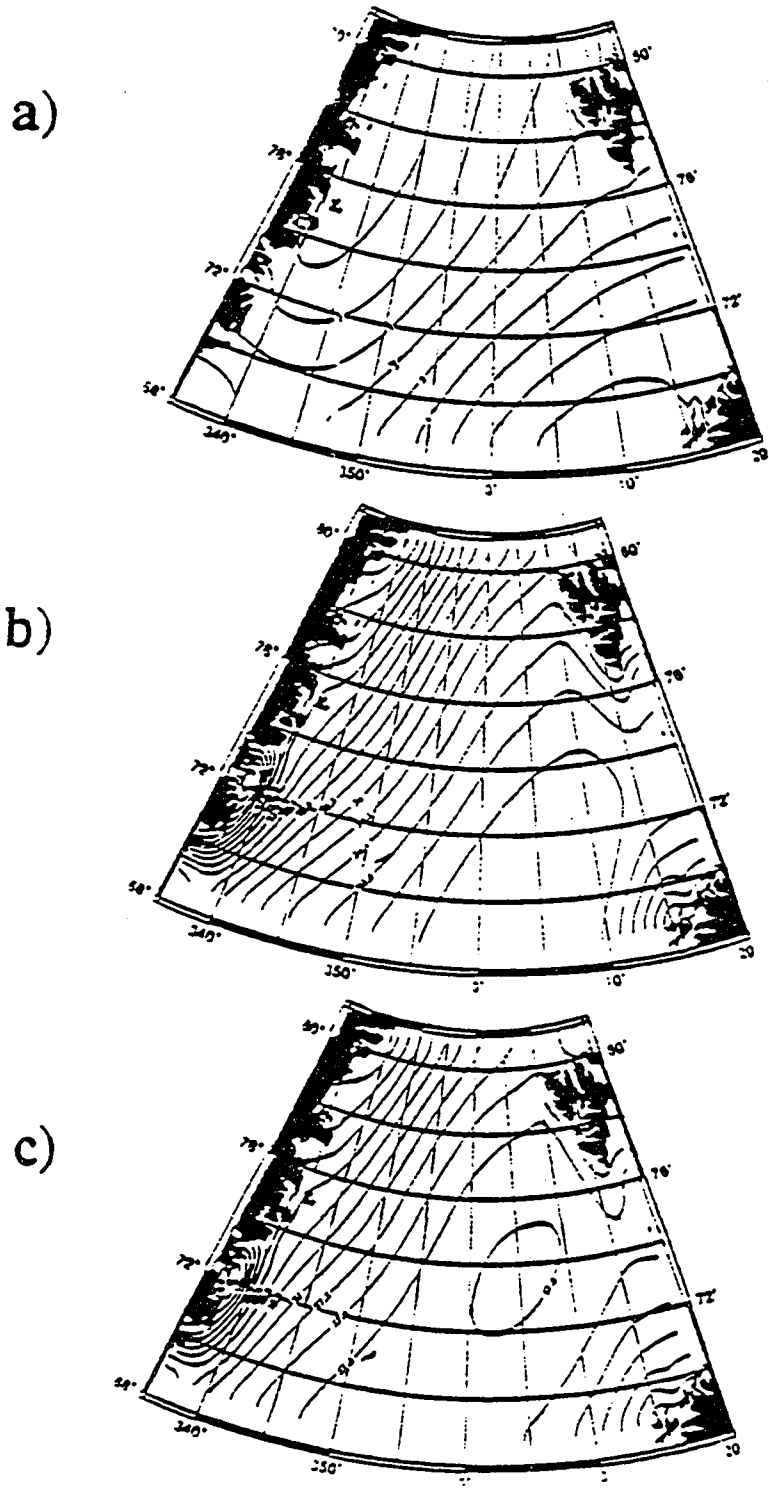
Figure 2.4 The surface annual mean distribution of (a) temperature. (b) salinity. and (c) σ_t used in the model.
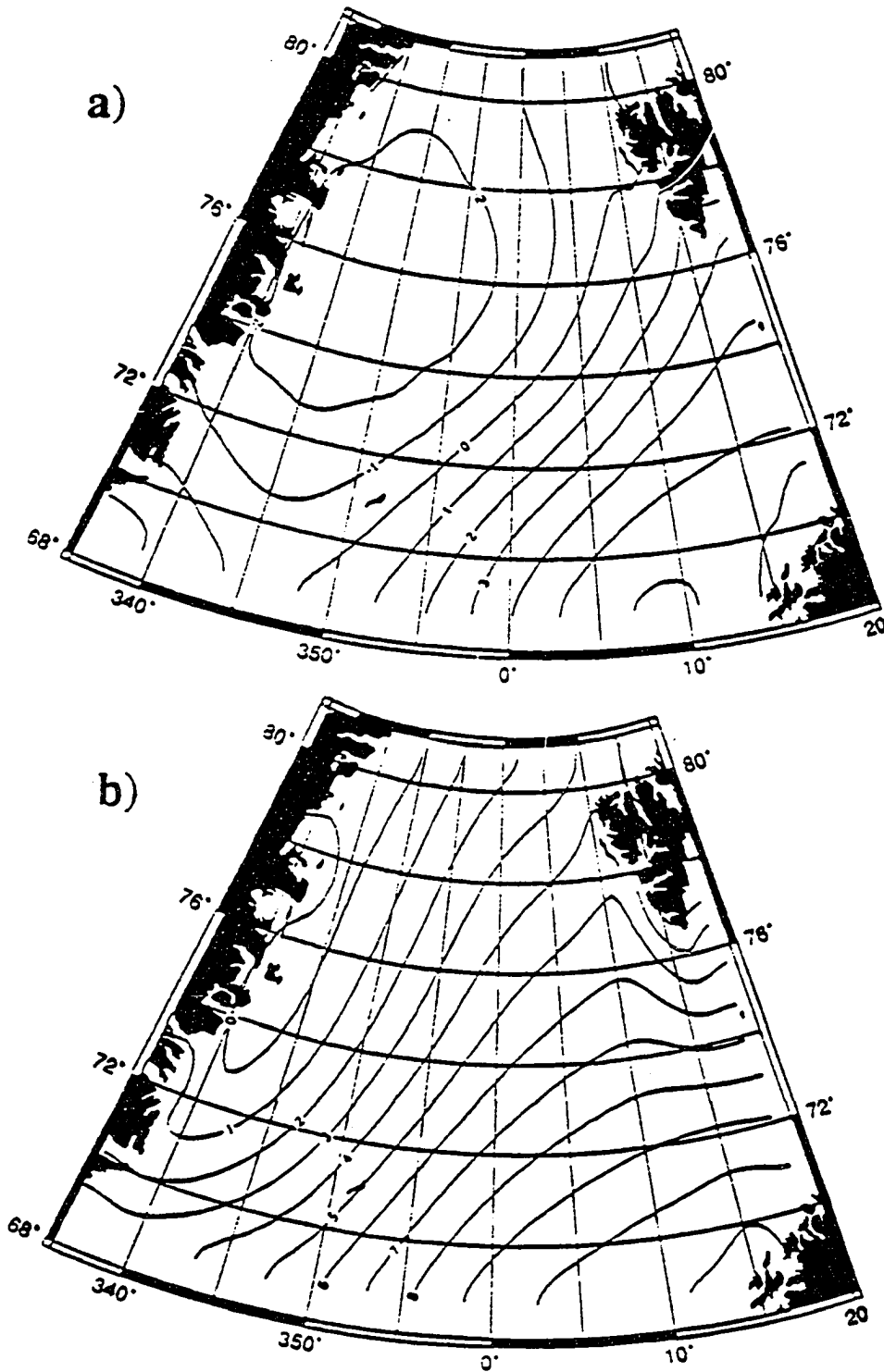
Figure 2.5 The monthly mean surface temperature
of (a) February, and (b) August used in the model.
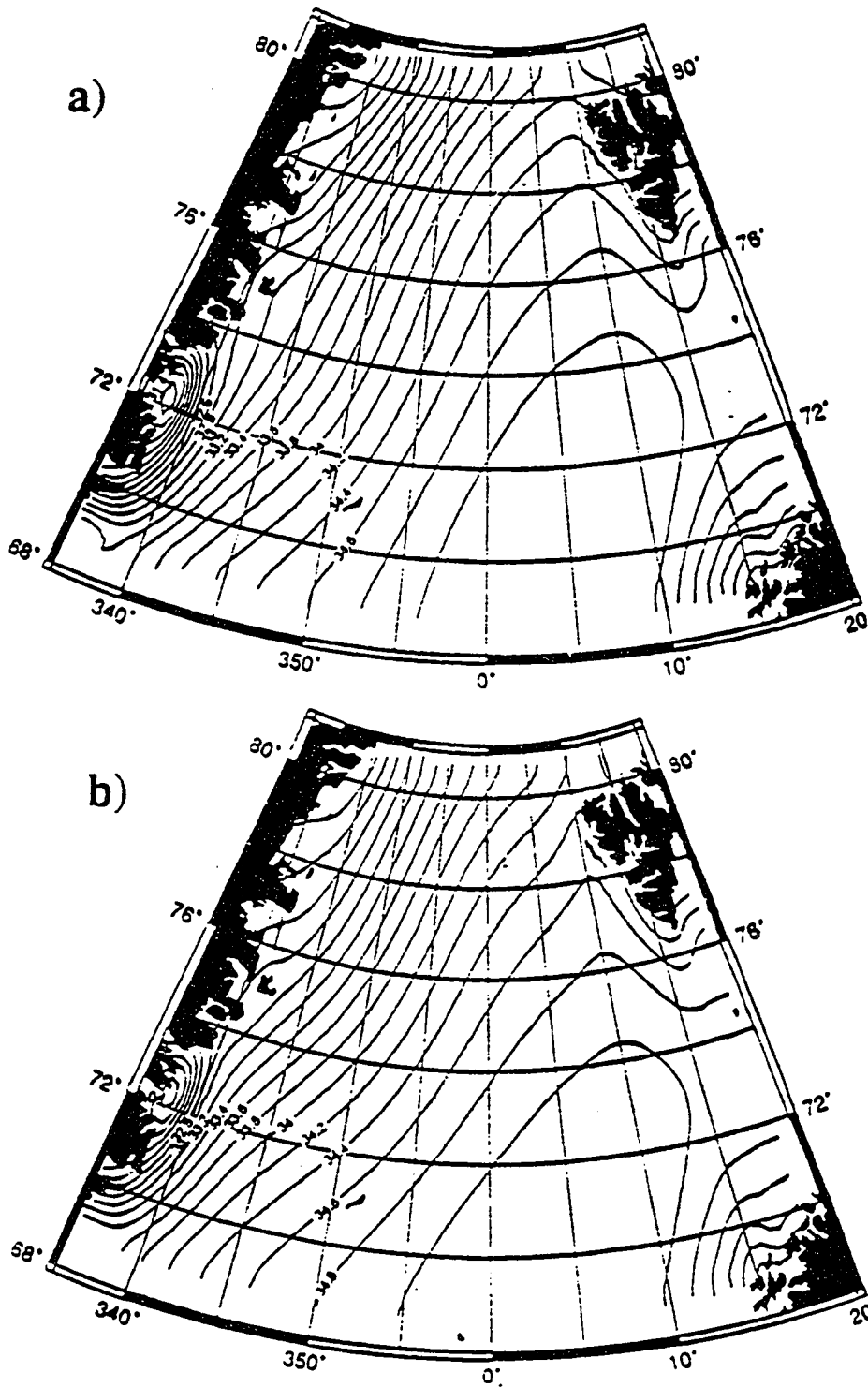
Figure 2.6 As Fig. 2.5 but salinity.

a)

b)
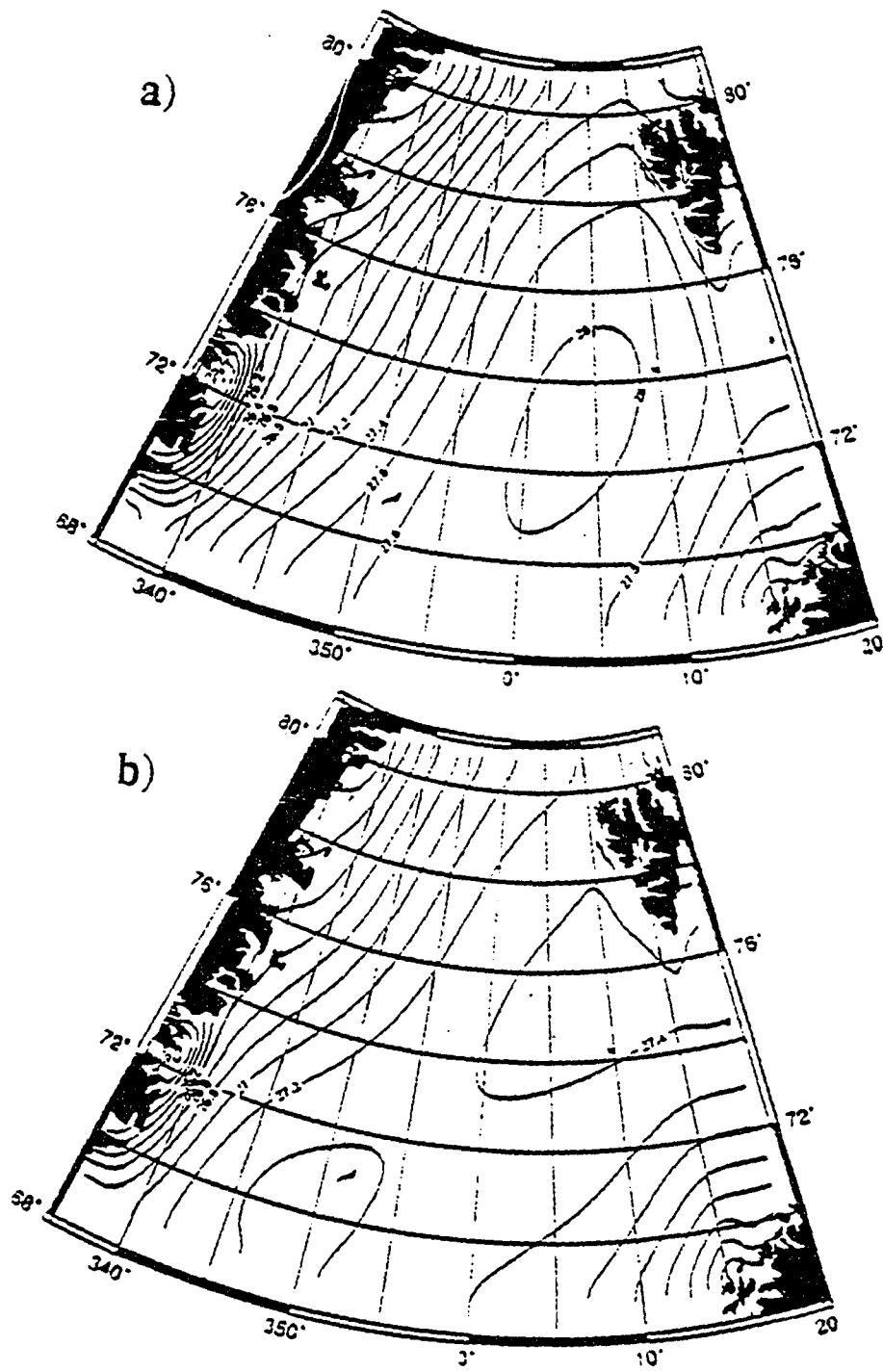
Figure 2.7 As Fig. 2.5 but σ_t.

Chapter 3 GENERAL CIRCULATION

Section 3.1 Introduction

To study the general circulation of the Greenland Sea, a series of experiments has been performed starting from the simple, barotropic case forced by constant winds and topography, to a fully prognostic baroclinic seasonal experiment. By increasing the complexity of forcing in each experiment, the influence of each component of forcing on the basin dynamics may be studied almost separately, providing improved understanding of the relative importance of wind and thermohaline forcing on the general circulation in the Greenland Sea. The methods used in each experiment will be explained first and then the results and their analysis will be presented.

Section 3.2 Barotropic, constant winds, and topography experiment

Since it is well acknowledged that topographic steering is one of the major mechanisms effecting the circulation in the Nordic Seas (Bourke et al., 1987; Johannessen et al., 1987; Quadfasel and Meincke, 1987; Jonsson, 1989; Legutke, 1991a) this study starts with an experiment examining its importance on the overall circulation of the region.

3.2.1 Methods

The modeled area along with the resolved topography is illustrated in Fig.2.1. Jan Mayen Island remains in the region as the only island. As described in section 2.4, the domain extends from 69°N to 80.5°N and from 23°W to 18°E, placing the Greenland Sea

58

in the central position of the modeled region. A timestep of $\Delta t=2400$ seconds is used. Simple vertical mixing parametrization with constant eddy and diffusivity coefficients of 1 cm^2/s is used. In the horizontal, Semtner's (1974) original code is modified to use scale selective, biharmonic sub-grid mixing parametrization. Boning and Budich (1992) in their study of an idealized eddy resolving ocean basin (between $0°$ and $65°N$) by a primitive equation model use biharmonic coefficient of $-1x10^{18}$ cm^4/s for horizontal viscosity and $-4x10^{18}$ cm^4/s for horizontal diffusivity. Their meridional grid spacing is $1/6°$ or ~18.5 km and $1/5°$ in zonal spacing, which varies from ~22 km at the equator to ~9.4 km at $65°N$. Since that is almost the same resolution as in this study, the values of biharmonic coefficients of horizontal viscosity and diffusivity used by Boning and Budich (1992) are adopted for this study.

The open boundary conditions required for this experiment are only those for stream function, i.e., volume transport. In the barotropic model temperature and salinity are held constant in space and time. To provide a condition for volume flow through an open boundary, one must prescribe the stream function either from observations or from the results of a coarse grid model covering a larger domain.

In the case of Fram Strait, there are measurements of currents and water mass characteristics (Aagaard et al., 1973, 1985b, 1988; Hanzlick, 1983; Foldvik et al., 1988). The steep bottom topography of the strait induces topographic steering which suggests the existence of a strong barotropic mode of the flow. Tables 1.1–1.2 of chapter 1 list

most of the recent information available from different studies on mass transport through

Fram Strait. From these tables, it looks like volume flow of about 3±1 Sv to the north

and to the south is a reasonable estimate. In searching for a way to account for seasonal

variability, which is known to exist at least in the WSC (Hanzlick, 1983, Jonsson, 1989),

a slightly overprescribed volume transport of ∼4.2 Sv in both directions through Fram

Strait is adopted here. As will be shown later, this overprescribed stream function will

allow for undisturbed exchange of volume through the northern open boundary during

maximum current flow, and overprescribed inflow of the EGC will recirculate back to

the north during weak current flow. The distribution of stream function prescribed on

the relatively narrow northern boundary is shown in Fig.3.1a. It is quite simple and

almost symmetric about 2°W. This flow distribution, i.e., to the north on the eastern side

and to the south on the western side of Fram Strait, is also consistent with baroclinic

flow, as deduced from the thermal wind relationship. This will be discussed later in the

baroclinic experiments.

As can be seen in Fig.3.1b the distribution of the stream function on the southern

open boundary is not simple. First of all, there is much less information available

on the circulation patterns and water mass characteristics along 69°N, more then 1600

km in distance between Greenland and Norway. The outflow through Denmark Strait

is quite well documented (Ross, 1984: Swift et al., 1980: Swift, 1984: Dickson et

al., 1990), and the Iceland Sea circulation is believed to be rather weak (Stefansson,

1962: Malmberg, 1972: Swift and Aagaard, 1981), and there is some information on
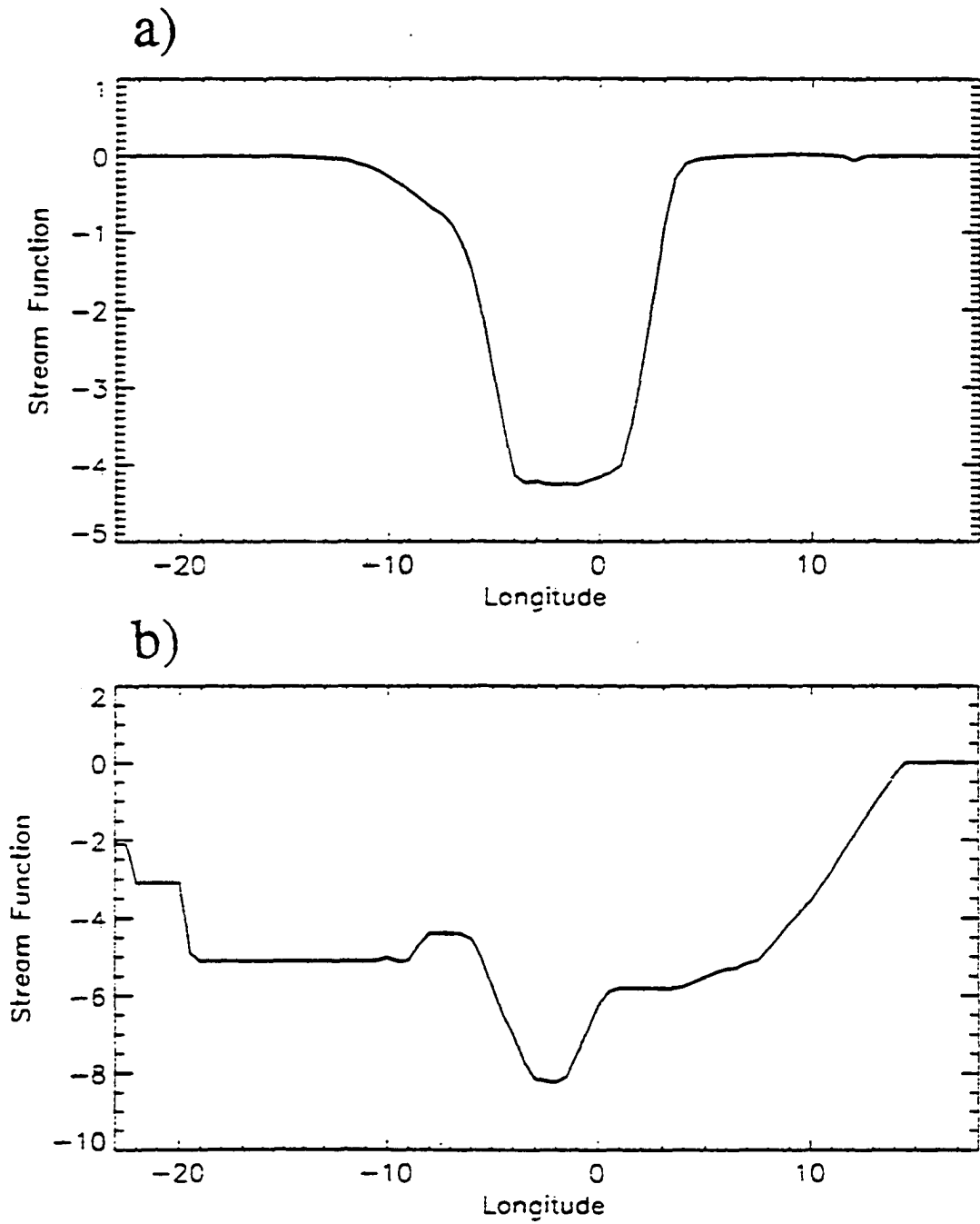
Figure 3.1 The distribution of the stream function
on the open boundaries: a) northern. b) southern

the circulation in the Lofoten Basin. Some studies imply the existence of a cyclonic gyre over all the Norwegian Sea (Helland-Hansen and Nansen, 1909; Creagan, 1976; Stevens, 1991). Others (Hermann and Thomsen, 1946; Dickson, 1972, Johannessen, 1986) suggest a separation of the Norwegian Atlantic Current with the main branch following the Norwegian shelf slope and a minor branch flowing in direction of Jan Mayen Island. The latter circulation scheme is used in this study. A difficult issue in estimating mass transport at this boundary is the complexity of the vertical structure of the currents flowing through the boundary. This is the area where deep dense waters overflow from the Greenland Sea and the Arctic Ocean (Worthington, 1970; Peterson and Rooth, 1976; Hansen and Meincke 1979; Aagaard et al., 1991), and continue their way south to form the North Atlantic Deep Water (NADW), which is the major component of conveyor-belt circulation of the global ocean (Fig.1.8).

Local topographic steering implies strong barotropic flow. the wind stress curl distribution sets the conditions for interior geostrophic flow. and the Ekman transport distributes water masses at the surface. All this suggests that the line along 69°N is not the best choice for an open boundary. but early experiments with other domains proved to be worse. Extending the domain farther south to Iceland and the Faroe-Shetland Channel does not improve data availability, and also brings about a question of computational resource limitations. Decreasing the domain by moving the open boundary to the north would make the circulation in the Greenland Sea too much influenced by boundary conditions.

Based on the above discussion, the distribution of stream function along the southern open boundary was deduced as follows. Ross (1984) estimated cold and dense water overflow south through Denmark Strait to be ∼2.9 Sv. Upper layer waters of the EGC together with the circulation within the Iceland Sea are estimated to account for as much as 2.2 Sv. To support cyclonic circulation in the Iceland Sea (Stefansson, 1962: Malmberg, 1972), there should be some northward flow on the western side of the Jan Mayen Ridge. In the northernmost part of the Norwegian Basin, the branch of the Norwegian Atlantic Current that flows northwest toward Jan Mayen Island should at least in part recirculate south along the eastern side of the Jan Mayen Ridge. Farther to the east the Atlantic Water moves mainly northward. On both the open boundaries no net mass flux balance is assumed. Total mass transport of ∼8.2 Sv south and north through 69°N is prescribed.

This total mass transport is still just a "guess", but a reasonable one based on the available field information and model results of a larger domain extending further south to include latitude 69°N. Problems arise on the southern open boundary because the prescribed mass transport can not account for local space and time variabilities. At a wide open boundary such as the southern boundary of this model it is natural to expect some current discontinuity due to mismatch between the prescribed boundary stream function and the interior solutions. Steady flow through the boundary will prevent such local instabilities from propagating out of the domain or dissipating. Stevens (1990) suggests increasing the diffusion in the region close to open boundary if such problems occur. However this may give rise to unreasonable circulation in some areas of variable viscosity,

which could influence interior results (J. Wilkin, personal communication, 1993).

A different approach has been introduced in this study. A set of carefully designed short experiments with both barotropic and baroclinic oceans proved that by increasing bottom friction coefficients next to the open boundary, most of the problems due to the mismatch between prescribed flow through open boundary and interior circulation disappeared. Increased friction in the bottom layer efficiently dissipates eventual numerical instabilities that usually occur where sharp changes in the bottom topography on open boundary exist, and where it is difficult to account correctly for the barotropic component of currents there. Also such an approach should generate no spurious currents since the linear bottom friction formulation used here for bottom stress calculations works as a simple Newtonian-type damping. This works better than increasing the diffusion on the open boundary which involves terms with the second derivatives in the Laplacian as well as terms with the fourth derivative in the biharmonic sub-grid mixing parametrization, and this is where the unreasonable currents would be expected to originate (D. Chapman, personal communication, 1993).

To solve the problem, a linear increase of bottom friction coefficient is prescribed over 2° of latitude from 71°N to 69°N, where its maximum value of half day e-folding time scale for damping is used. The same linear increase of bottom friction is also used between 13°E and 18°E, just to ensure that no problems occur along the eastern boundary, which is treated in the model as solid wall. High bottom friction close to the southern

open boundary combined with the prescribed locally quite intense currents through the boundary, results in $2\Delta x$ and $2\Delta y$ noise that has been removed at every timestep by a very weak 5–point weighted-average filter (with 0.999 weight in the center) on the stream function between 69°N and 71°N.

Conditions of surface forcing by monthly mean January wind stress (the stronger winter winds) assuming the temperature (T=4°C) and salinity (S=34.9 psu) are constant in time. are used to study the barotropic ocean response to topography.

3.2.2 Results and analysis

The barotropic experiment with constant strong winter winds, has been run for almost five years (1800 days), starting from rest. A time series of the basin-averaged total kinetic energy (TKE) per unit volume. calculated every timestep, is shown in Fig.3.2. It reaches semi-steady state quickly within several days. but full adjustment of the flow to the forcing on the open boundaries takes longer. about 200 days. The time series shows some variable in magnitude and frequency oscillations about semi-steady state position (absolute mean TKE=4.8 erg/cm^3). The bottom plot of Fig.3.2 shows oscillations at time periods as short as several hours.

A one year average distribution of the stream function. which is assumed to be representative of barotropic motions is shown in Fig.3.3a. Maximum strength of the Greenland Sea cyclonic gyre is above 15 Sv. The actual southward total transport in the Greenland Sea gyre is uncertain: determined from measurements. it has been estimated
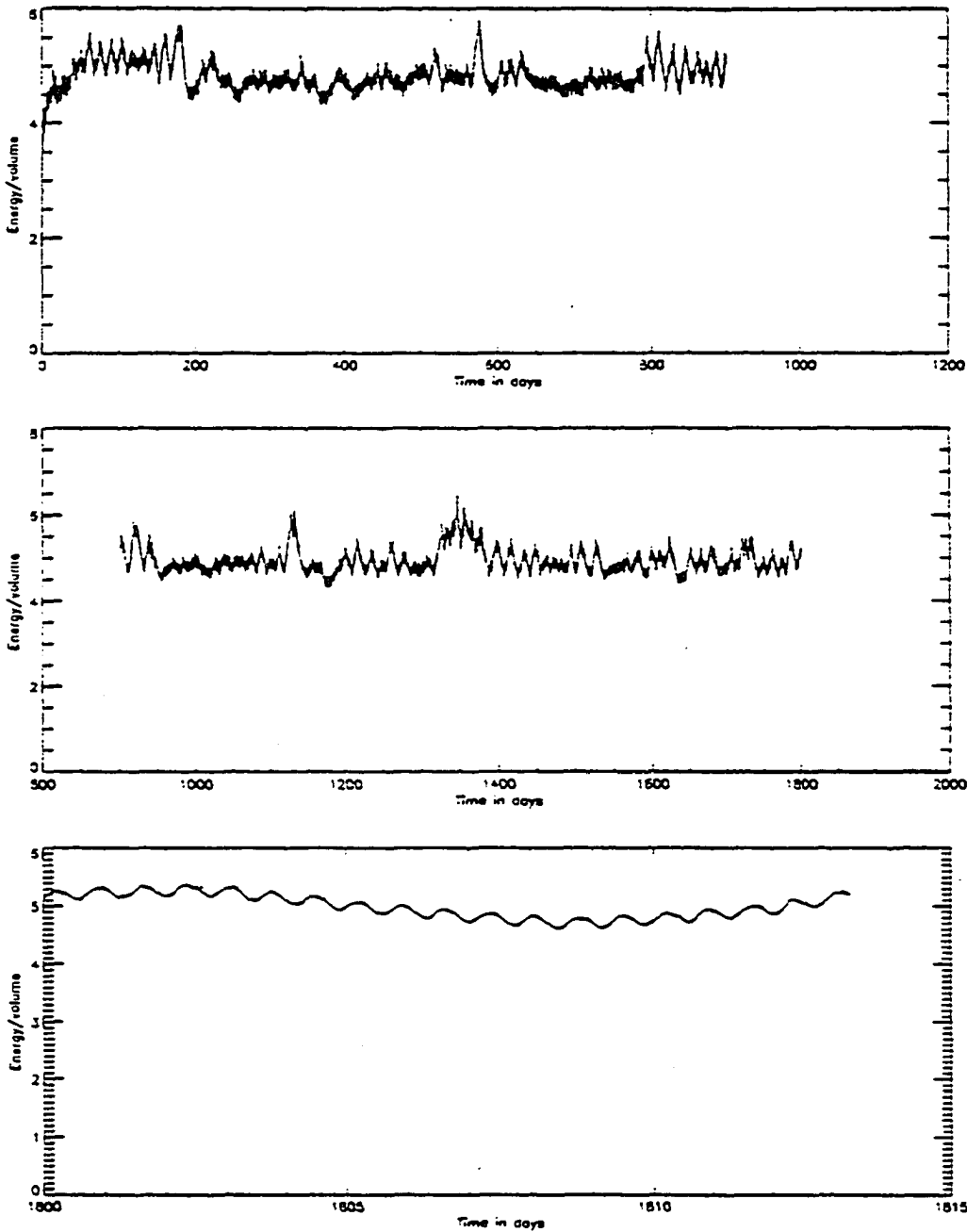
Figure 3.2 Basin-averaged kinetic energy (in erg/cm^3) versus time.
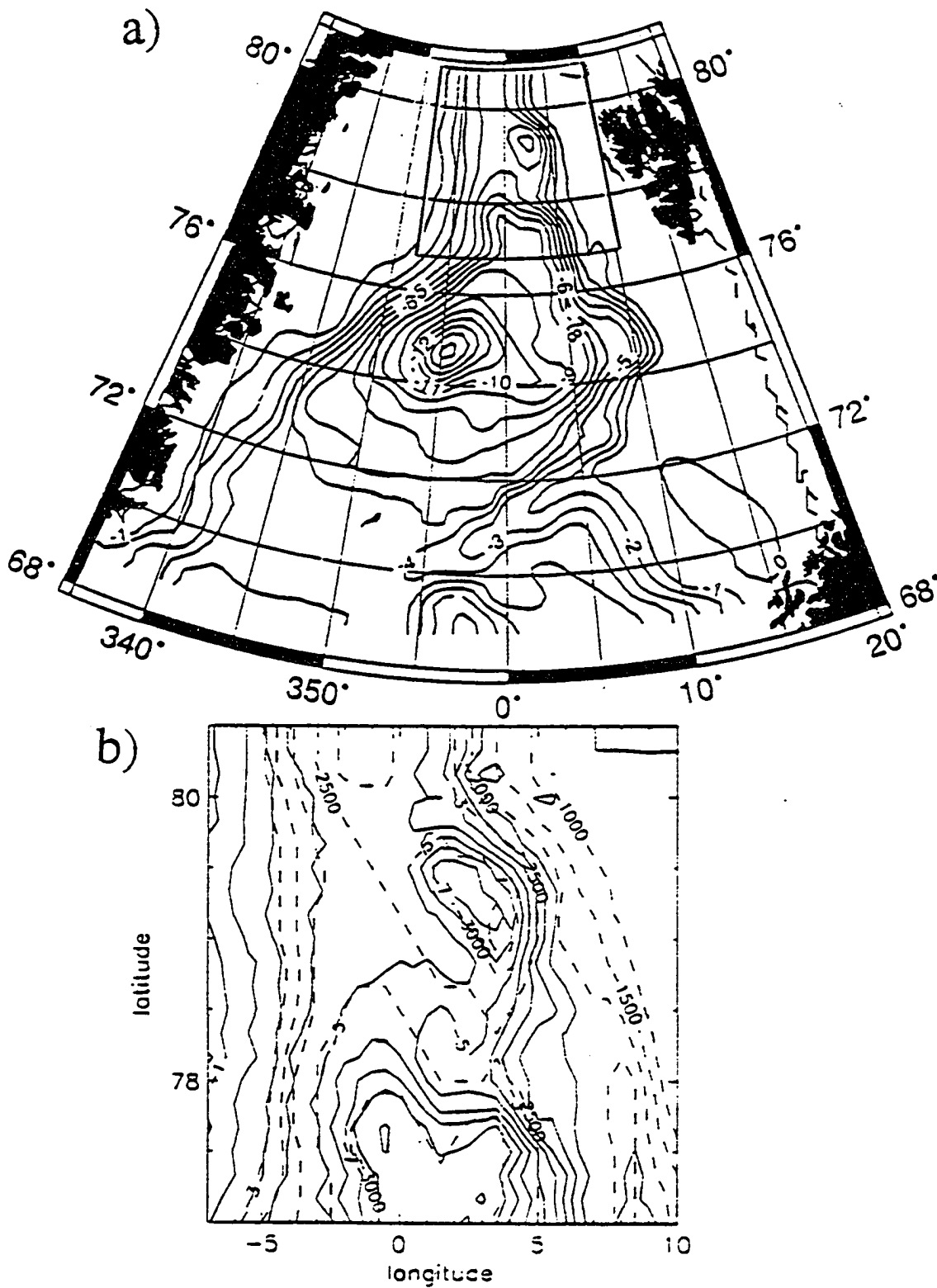
Figure 3.3 a) The year-average stream function distribution (in Sv). b) instantaneous distribution of stream function (solid lines) and isobaths (dashed line) in Fram Strait.

to range from 2 to 35 Sv (Mosby, 1962; Aagaard and Coachman, 1968; Aagaard, 1970; Jonsson, 1989), while a primitive equation model obtained 13.6 Sv (Legutke, 1991a). The EGC is well correlated with the Greenland shelf slope, and the Jan Mayen Current can be recognized as part of the EGC, recirculating east, north of Jan Mayen Island at 71°N. The Norwegian Atlantic Current partly recirculates south within the Norwegian Sea, and the rest of it continues its way to the north to exit through Fram Strait with transport of more than 4 Sv.

Topographically Trapped Eddy

An interesting feature, permanently present in this barotropic experiment, is a stationary eddy, situated near the Molloy Deep, which in this model has a depth of 3300 m. To eliminate an effect of smoothing being automatically introduced by graphic software (GMT) used in Fig.3.3a, another plot, a magnification of the circulation in Fram Strait area at an instantaneous timestep without smoothing is shown in Fig.3.3b. The eddy is elliptic and has dimensions of about 40 and 80 km. Its main axis is in NW-SE direction, and its center is located to the northeast of the Molloy Deep. The permanent eddy encompasses the Molloy Deep and it appears to be trapped on a depression depicted in the model by closed isobath of 3000 m. It is worth noting here that in the real ocean this isobath is not closed around the depression but is open to north into the Arctic Ocean. Due to smoothing of original 1/12° resolution depth data, the bathymetry of Fram Strait is less complicated than in reality (see Fig.1.2 and Fig.2.1).

An eddy like this one has been often reported in literature by Wadhams and Squire (1983), Vinje (1977), Smith et al. (1984), and Bourke et al. (1987). Smith et al. (1984) developed a two-layer ocean model in a 2500 m-deep rectangular basin centered on a 3500 m-deep Gaussian-shaped depression and driven by a 10 cm/s jet from the northeast. The model generated a stationary cyclonic eddy which can be explained strictly in terms of topographic generation without invoking any mean flow baroclinicity or ice dynamics. For a barotropic, inviscid flow, the vorticity equation integrated over the ocean depth H, yields the equation for conservation of potential vorticity Π:

$$\frac{d\Pi}{dt} = \frac{d}{dt}\left(\frac{f + \zeta}{H}\right) = 0 \tag{3.1}$$

where ζ is the vorticity of a column of fluid extending over the full ocean depth

$$\zeta = \frac{\partial v}{\partial x} - \frac{\partial u}{\partial y} \tag{3.2}$$

u and v are perpendicular horizontal barotropic velocity components. f is the planetary vorticity (Coriolis parameter). From conservation of potential vorticity, if the depth of the ocean increases, the vorticity must increase, and if f remains almost constant, the relative vorticity must become more positive (cyclonic). Smith et al. conclude that conservation of potential vorticity and the generally deeper bathymetry of the Molloy Deep area requires that a stationary eddy occur even for pure barotropic flow.

From the CTD measurements in summer of 1984, Bourke et al. (1987) suggest, based on the study of Johannessen et al. (1987), that the eddy may be a part of a larger-scale

(100+ km) cyclonic gyre and its generation may be related to the complex bathymetric province of the region of which the Molloy Deep is only a part.

Based on the results of this model, the simulated eddy can be viewed as an extension of the Greenland Sea gyre, specifically the Boreas Basin flow, that has been disturbed by the presence of the Hovgard fracture zone and the Greenland-Spitsbergen Sill (see Fig.1.2). Part of the northward flow in the Boreas Basin following lines of constant f/H. which coincide here with isobaths. branches of to the west and then to the south as the return Atlantic Water, which submerges under the Polar Water carried within the EGC. On the sill where model depths decrease from more than 3000 m in the Boreas Basin to close to 2000 m. the flow that continues its way north. by conservation of potential vorticity to balance depth decrease. must become more anticyclonic. (see the stream function of 5 Sv and less in Fig.3.3b). The flow that makes it through over the sill "feels" the rapid depth increase in the Molloy Deep and a general depression of ~3000 m. Here. to conserve potential vorticity. the flow now must become more cyclonic. Most of the flow following the shelf slope of Spitsbergen (isobaths 2500 m and less) continues north into the Arctic Ocean. a small part of the flow joins the EGC. and the rest remains trapped generally around the 3000 m isobath as an eddy.

This explanation of the topographic trapping of an eddy over a depression of ~3000 m depths is essentially the same as one given by Smith et al.. (1984). This study though explains generation of the eddy by the northward flow of the WSC, whereas Smith et

al. in their model used a driving flow from the northeast. Such difference probably is not important in explaining the topographic trapping, but the warm core of the eddy (Bourke et al., 1987) suggests its origin from the warm Atlantic Water, brought in from the south. The explanation provided here implies dependence of the eddy on large-scale oceanography in Fram Strait and defines its control on the heat, salt and mass transport into the Arctic Ocean. The results of Quadfasel et al. (1987) obtained during the 1984 Marginal Ice Zone Experiment support the above conclusion. Quadfasel et al. identify two major recirculation branches of the Atlantic Water across the strait to be related: one to the Hovgard fracture zone, and second the Molloy Deep system. The latter recirculation branch may explain the difference between Hanzlick's (1983) estimate of 5.6 Sv flow of the WSC at 79°N and a recent estimate (Jonsson, 1989) of 3 Sv entering the Arctic Ocean. According to simulations presented here (Fig.3.3b), the eddy can account for as much as 2–3 Sv of northward flowing water at 79°N that does not enter the Arctic domain. Results of Quadfasel et al. (1987) indicate the dominating role of the barotropic component of the circulation and relatively small scales of the mean flow, as simulated here, that suggests that results of this barotropic experiment may account for major part of the dynamics there.

Topographic planetary waves

The pattern of circulation in the Greenland Sea presented in Fig.3.3a is based on year-averaged results. Patterns at instantaneous timesteps are different though, especially

within the mid-latitude EGC. In Fig.3.4 a series of 6 stream function distributions, 4 hours apart, is presented. On these plots, waves propagating along the Greenland shelf slope within the EGC may be seen. A perturbation, manifested in on-shelf deflection of the EGC, starts at ~77°N. Perturbations propagating along the shelf slope become much stronger, with maximum amplitude somewhere around 75°N and then completely decay before reaching 72°N. Within about 16 to 20 hours, they make one full cycle (i.e., a new perturbation appears at ~77°N) suggesting a period of waves of several hours, which is similar to the one observed in TKE time series (bottom plot) of Fig.3.2.

In Fig.3.5a, three points were chosen within the EGC along the shelf slope of Greenland, one at 13°W, and 75°N (solid line), second at 7°W, and 77°N (dotted line), and third at 15°W, and 73°N (dashed line), and their stream function magnitudes were plotted against time. Within the sampling period of 320 hours, each point made about 18.5 cycles, giving a time period of oscillations of approximately 17.3 hours. The amplitude of the stream function oscillations at point 1 (located at 13°W and 75°N) is greater than 12 Sv. It is much smaller, about 1 Sv at point 3, located to the south and ~0.5 Sv at point 2, located to the north. To get a better understanding of the horizontal extent of these oscillations, in Fig.3.5b the spatial distribution of stream function amplitude over 20 hours (i.e., greater than period of oscillation) is shown. The variability is confined between ~77°N and 72°N, and between 5°W and Greenland. The main axis of the variability is aligned with the shelf slope, and the maximum amplitude of ~13 Sv is centered at about 13°W and 75°N, in the area where the maximum topographic slopes exist in the
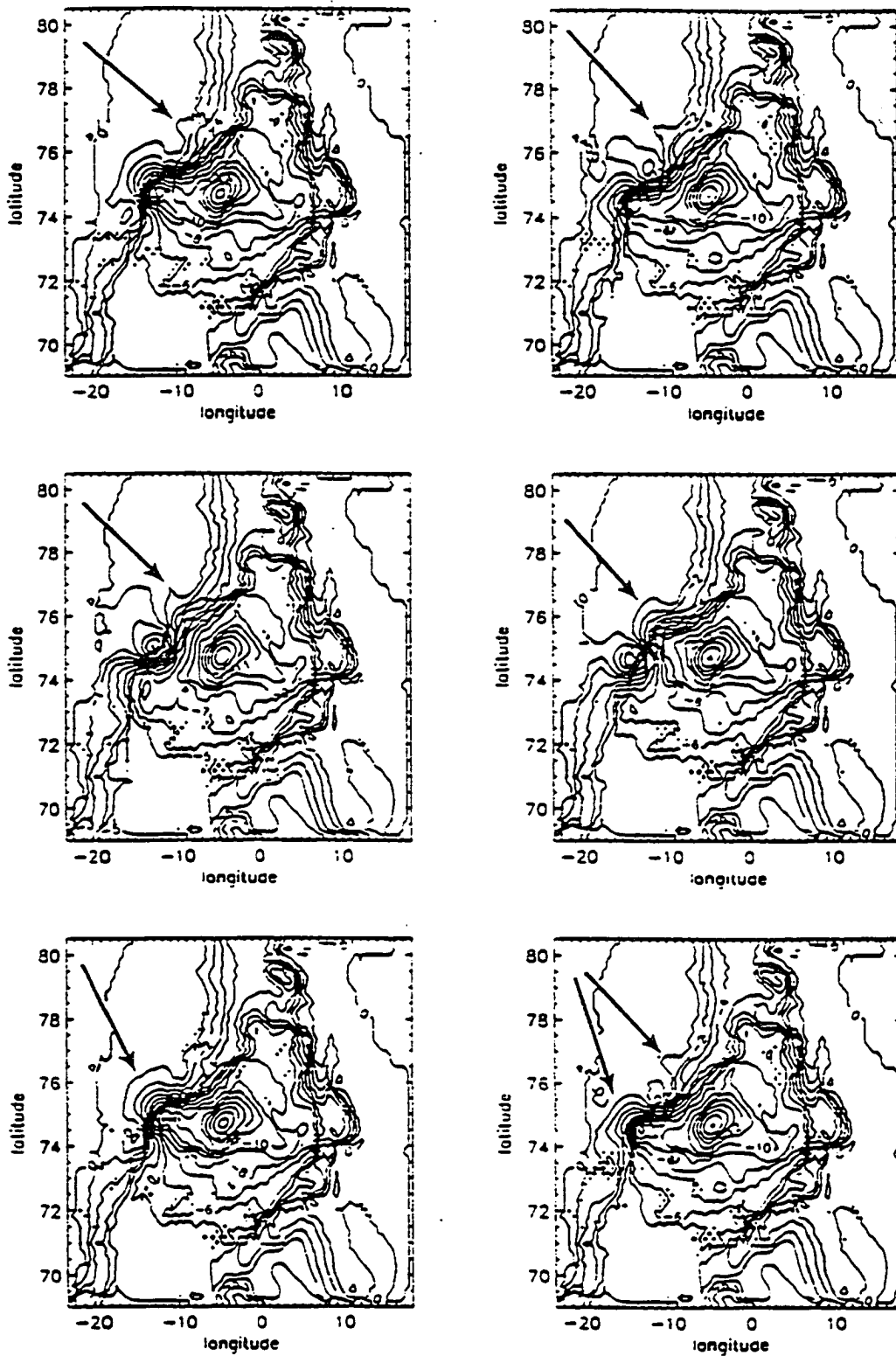
Figure 3.4 Instantaneous stream function distributions (in Sv: the time period of sampling is 4 hrs) showing the wave-like behavior of the mid-latitude EGC.
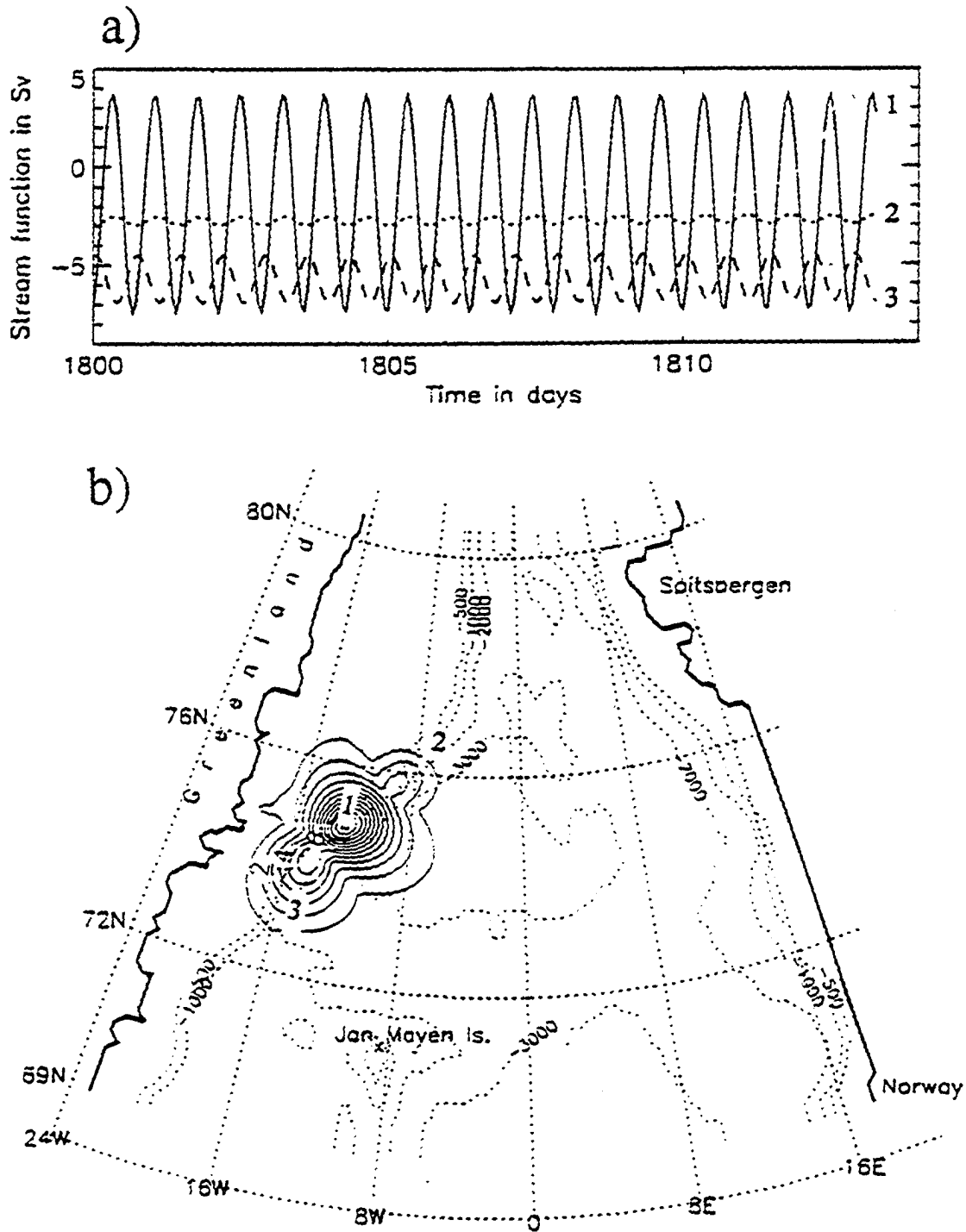
Figure 3.5 a) Stream function timeseries at points shown in lower plot b) spatial distribution of stream function amplitude calculated over 20 hrs.

model. There is no clear signal of oscillation away from this region, suggesting some kind of a standing wave, but a series of plots (Fig.3.4) indicates along-slope, generally southwestward propagation.

To decide about the propagative nature of these oscillations, two plots of the perturbation stream function are presented (Fig.3.6): time-latitude (section along 13°W) and time-longitude (section along 75°N). From the time-latitude plot (Fig.3.6a), southward propagation is deduced with maximum amplitude located at 75°N. and from the time-longitude plot (Fig.3.6b) westward propagation results with maximum amplitude centered at $\sim$12°W. From both plots. a period of $\sim$17 hours. and phase speeds C_x=-1012 cm/s and C_y=-720 cm/s in x (positive to the east) and y (positive to the north) directions. respectively, and a resultant phase speed $|\bar{C}| = \left(\sqrt{\frac{1}{C_x^2} + \frac{1}{C_y^2}}\right)^{-1}$ =586 cm/s. directed to the southwest. are estimated.

Although a wave period of $\sim$17 hours has already been calculated within some degree of certainty, spectral analysis of TKE is presented in Fig.3.7 to precisely define its value. Variance preserving power spectrum density (PSD) of the TKE per unit volume was calculated (Fig.3.7a) from 900–day long timeseries of TKE (middle plot of Fig.3.2). A peak at a frequency of $\sim$1.4 cycle per day (cpd) (i.e.. ω=1.0157x10^{-4} s^{-1}) is clearly dominating in the PSD. and its amplitude is at least about two orders of magnitude greater than any other peak (frequencies f>0.5f$_N$ (8cpd) are not plotted, where f$_N$=1/(2Δ) is the Nyquist frequency). Fig.3.7a was calculated from 900–day long timeseries. Fig.3.7b shows the 'raw' spectrum of Fig.3.7a smoothed by box averaging 51 frequency bands
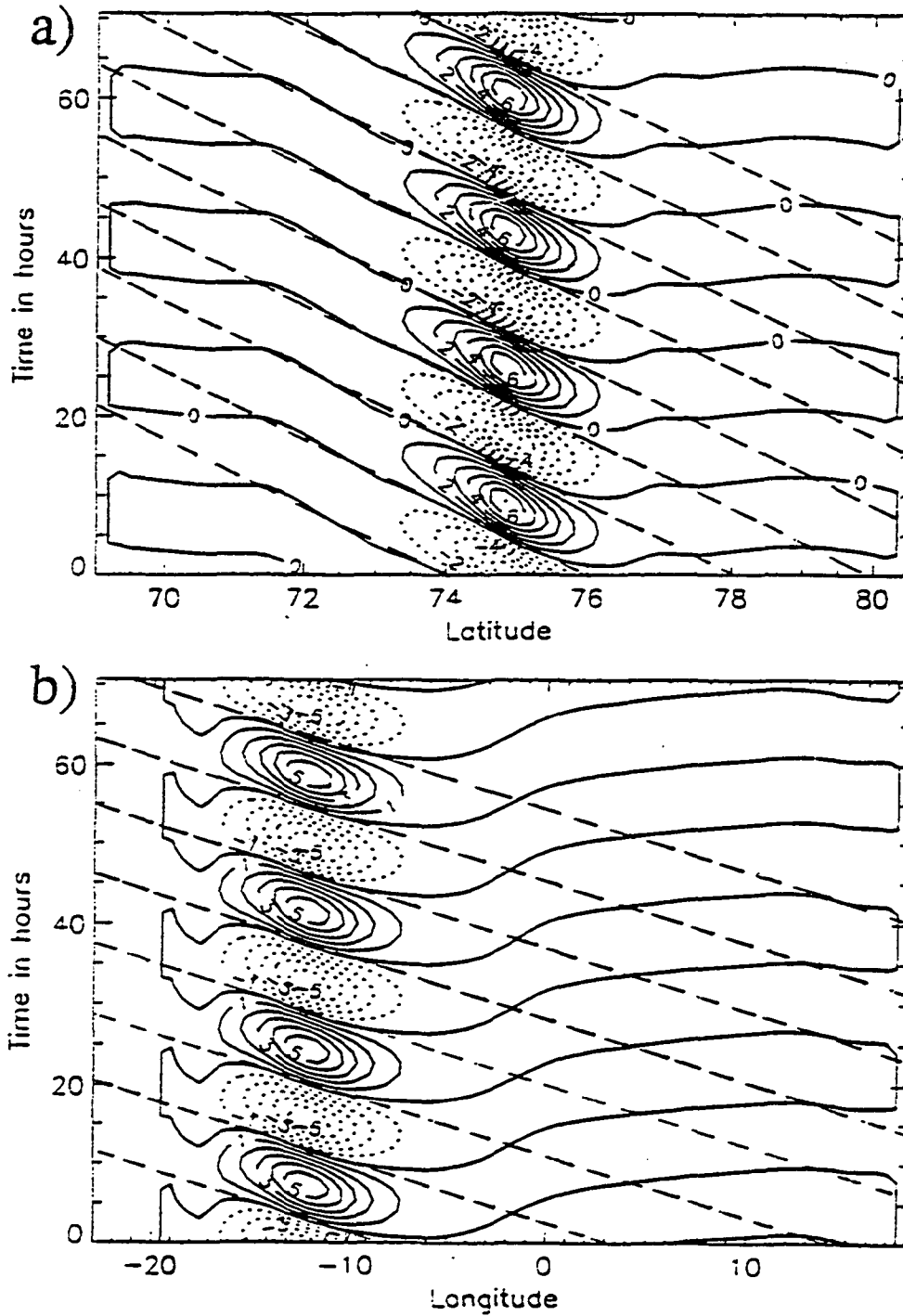
Figure 3.6 a) Time-latitude perturbation stream function (section at 13°W). Superimposed are lines of constant phase speed of 720 cm/s. b) time-longitude perturbation stream function (section at 75°N). Superimposed are lines of constant phase speed of 1012 cm/s

(for 102 degrees of freedom (dof)) and with a 95% confidence interval. The peak at 1.4

cpd is the most important and it translates into a time period of 17.184 hrs.

The first two modes of Empirical Orthogonal Function (EOF) (Fig.3.8– 3.9) represent

a cumulative total of 99.98% of the variance of stream function ~13–day long set

sampled at every third point in both horizontal directions, and every 2 hours. The

spatial distribution of the eigenvector in both EOF modes shows that all of the variability

are concentrated in the area already defined, along the shelf break of Greenland, between

72°N and 77°N. The time periods calculated from the two time amplitude functions (TAF)

are the same and equal to ~17.3 hrs (~18.5 cycle in 13.3 days), in agreement with already

obtained values, (Fig.3.7) and from time series of stream function (Fig.3.5a). A common

weakness of real EOFs, which are used in this study (versus complex EOF), is that

they do not allow for the detection of propagating features. They can be detected using

complex EOF analysis. However, individual real EOF modes of similar variance can be

interpreted as dependent components of a set of EOF modes, that together describe the

same statistical process (North et al., 1982: White and Tabata, 1987). The first two EOF

modes, explain respectively, 53.61% and 46.37% of the total variance in this experiment.

Moreover they both have the same period and their eigenvector distributions have a very

similar pattern, hence even though the two EOF modes are orthogonal to each other

(i.e., linearly independent) they are part of the same propagating process. The two EOF

modes of this experiment are out of phase by roughly ~90° and the two minima and the

maximum of the eigenvector in the second mode, when compared with the first mode, are

a)

b)
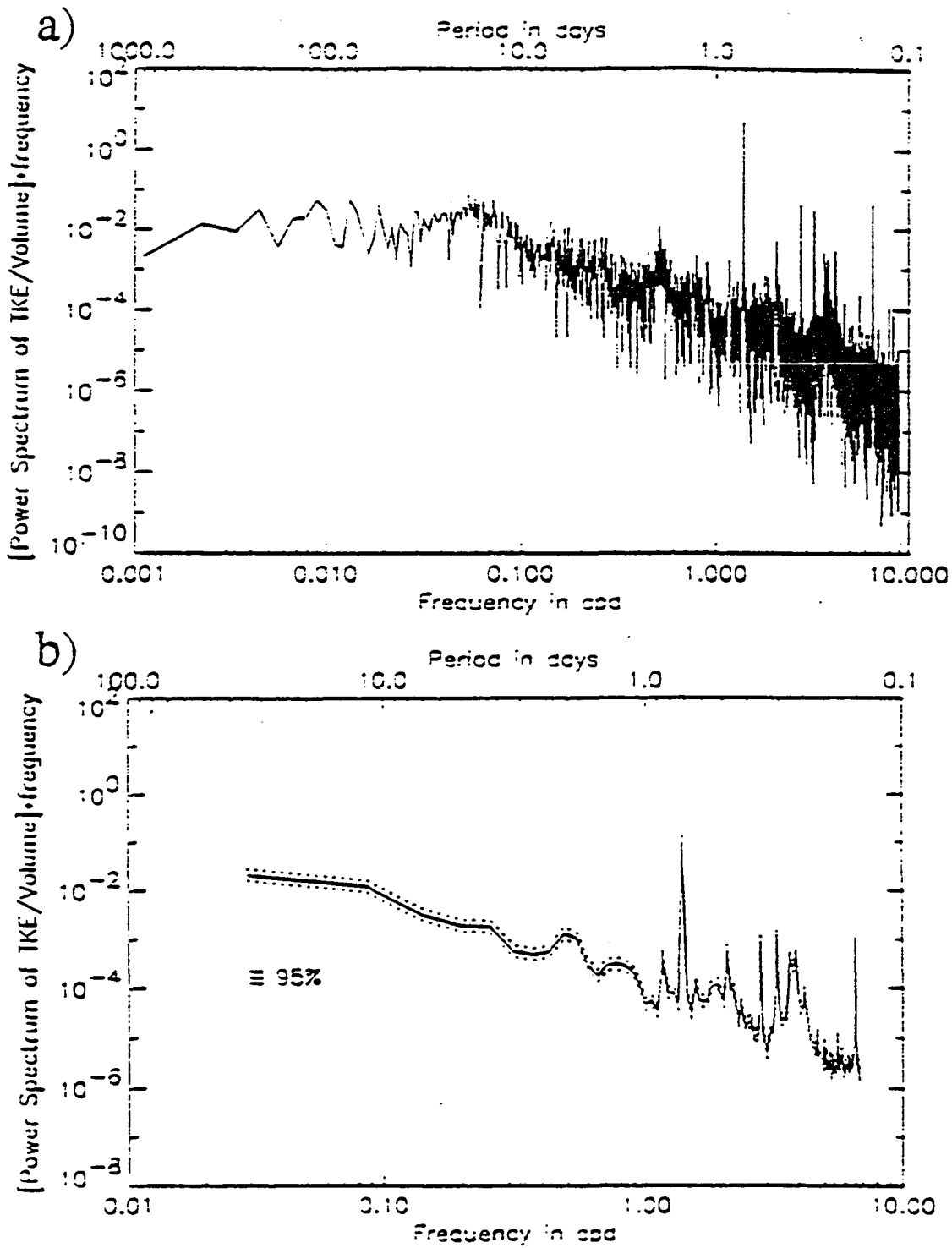
Figure 3.7 The variance preserving power spectrum density of TKE per
unit volume - experiment #1 (f>0.5f_N not plotted): a) "raw" with dof=2.
b) box averaged with dof=102 ("dof" stands for degrees of freedom).
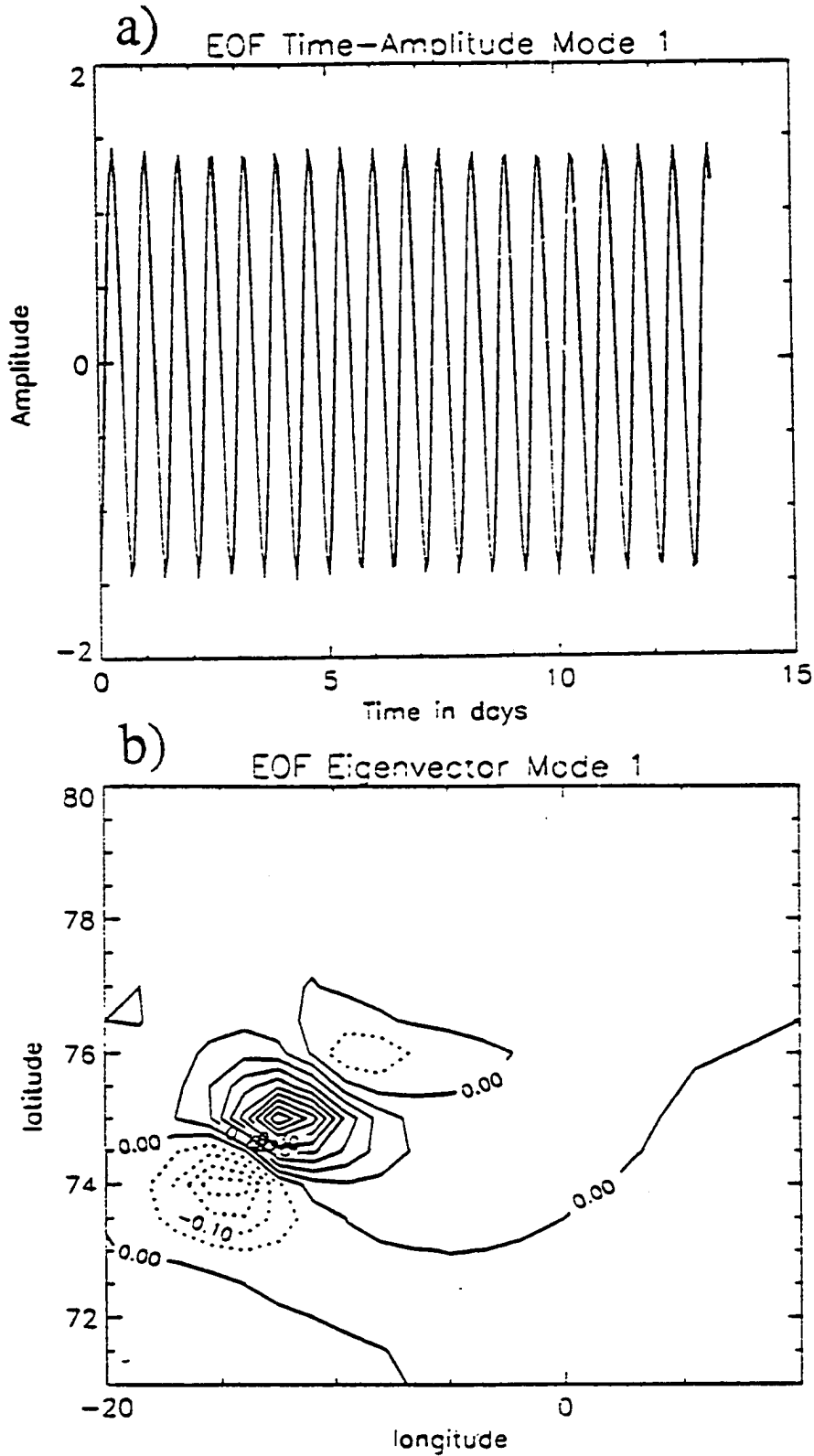
Figure 3.8 EOF mode 1 TAF (top — units are $10^6 m^3/s$) and eigenvector (bottom — CI=0.05 dimensionless units) of stream function - experiment #1.

a)

EOF Time-Amplitude Mode 2

b)

EOF Eigenvector Mode 2
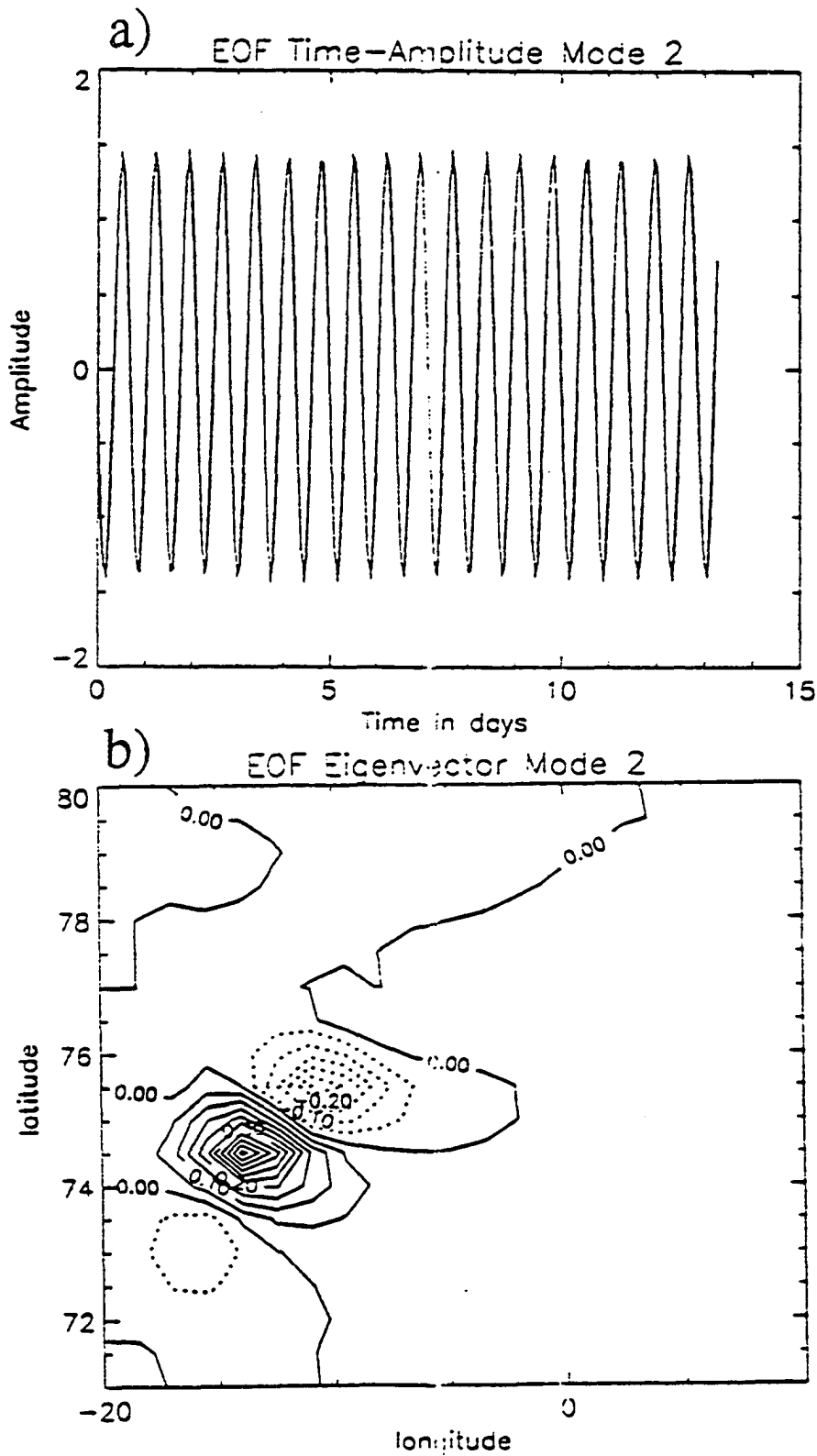
Figure 3.9 As Fig.3.8, but EOF mode 2.

displaced to the south along the slope, suggesting the propagative nature of the feature.

Using values of $T=17.18$ hrs for time period and estimated phase speeds C_x and

C_y, the wavelengths of $\lambda_x=626$ km and $\lambda_y=445$ km are calculated in x and y directions,

respectively. The resultant wavelength is $\lambda=363$ km. The respective wavenumbers are

$k=-1\times10^{-7}$ cm^{-1} and $l=-1.41\times10^{-7}$ cm^{-1}. The resultant magnitude of the wave vector in

x and y coordinate system is $|\bar{\kappa}|=1.73\times10^{-7}$ cm^{-1}. Because the wave field is expected to

be strongly dependent on topography, it is convenient to change to a coordinate system

(x',y') aligned with the topography (Fig.3.10), such that $H=H(y')$. The new coordinate

system is rotated at an angle $\Theta=60°$. The new wavenumber vector components in rotated
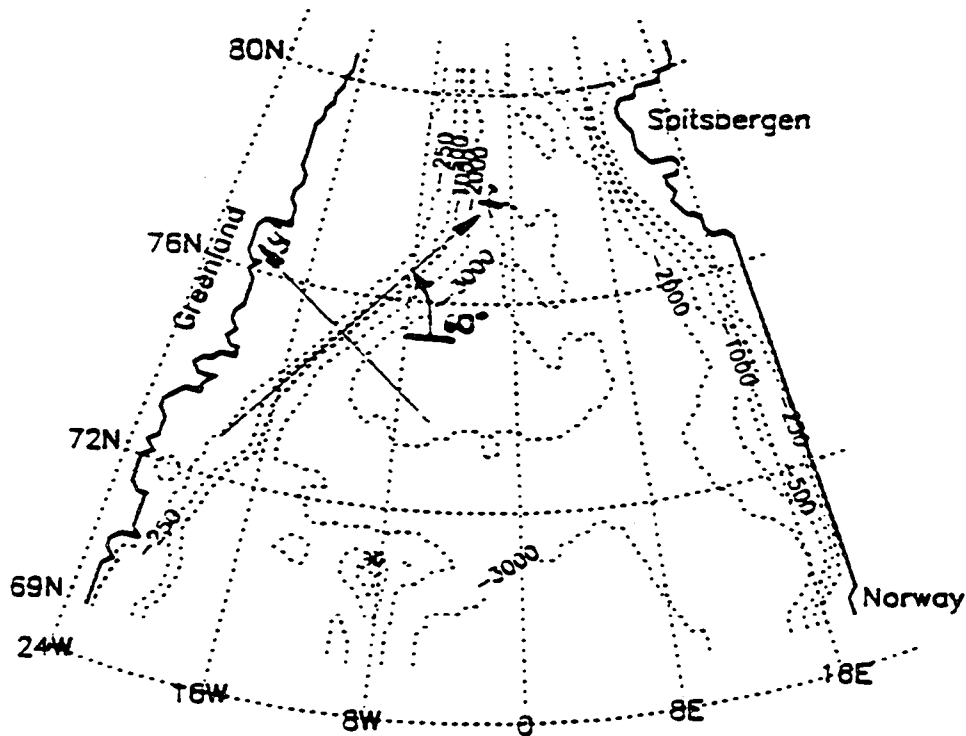
Figure 3.10 The rotated coordinate system, aligned with the topography.

coordinate system (x',y') are $k'=|\bar{\kappa}|\cos\theta=-1.72\times10^{-7}$ cm^{-1} and $l'=|\bar{\kappa}|\sin\theta=0.18\times10^{-7}$ cm^{-1} in x' and y' directions, respectively. From wavenumbers in x' and y' directions their respective wavelengths are $\lambda_{x'}=2\pi/k'=-365$ km and $\lambda_{y'}=3491$ km, and the corresponding phase speed components are $C_{x'}=-5.9$ m/s and $C_{y'}=56.4$ m/s.

Now having calculated all the characteristics, the nature of the waves has to be determined. Since baroclinic effects can not exist in this experiment, only barotropic waves are considered. The observed variabilities are present in the vertically integrated flow, so it is sensible to examine first whether or not a barotropic instability mechanism can account for oscillations at time scales of about 17 hrs. For instability to occur, the gradient of the total vorticity (G) for a flow over sloping topography

$$G = (f - V_x)\left(\frac{H_x}{H}\right) - V_{xx} \tag{3.3}$$

must change sign within the lateral bounds of the flow, i.e., within the flow, G has to be zero at some point (Hanzlick, 1983). Here, f is the Coriolis parameter, V the flow velocity, H the depth, and the subscript x denotes cross-isobath differentiation. Scaling Eq.3.3 by a characteristic velocity V^* and length L^* yields:

$$\left(f^* - \frac{V^*}{L^*}\right)\frac{H}{L^*H} - \frac{V^*}{L^{*2}} = 0 \tag{3.4}$$

After simplifications Eq.3.6 yields the condition that the Rossby number V^*/L^*f^* should be greater than 0.5. For the EGC, $V^* \sim 0.1$ m/s, $L^* \sim 100$ km, and $f^* \sim 10^{-4}$ s^{-1}, so the Rossby number is 0.01 and barotropic instability is unlikely. Even using a large

velocity such as 0.5 m/s. and length scale 50 km only, the corresponding Rossby number is 0.1, so that instability is still only a marginal possibility.

The location of this feature over the shelf slope indicates that topography, i.e., the shelf break, plays an important role in propagation if not generation of the observed waves. Two plane wave types, propagating in generally westward directions, are recognized to depend on the continental slope for their existence, mainly: continental shelf waves and topographic planetary waves. According to Gill (1982), continental shelf waves exist over the sloping boundary at the coast, and they always propagate such that their phase travels with shallow water to the right (in the northern hemisphere). The generation mechanism requires an input of vorticity over the shelf region, and it is usually accomplished by the wind. Other mechanisms, not related to atmospheric forcing such as scattering by coastal or bottom topography irregularities. nonlinear interactions. alongshore variations in topography and variable discharge at the coast may also excite shelf waves (Mysak. 1980).

Based on observations. at mid-latitudes such waves typically have long wavelengths ($\lambda \gg L$, where L is a topographic length scale), low frequencies ($\omega \ll f$), and small amplitudes. In certain coastal regions though. where the shelf is not long and straight. shelf waves of shorter periods (of around 1 day) and wavelengths can be generated (Jida. 1972). Jida found that such waves could be due to resonant response of the ocean to the atmospheric disturbances traveling along the south coast of Japan. He shows

that the parameters of some free wave modes of the system simulating the sea south of Japan and those of the atmospheric disturbance, satisfy the resonance conditions. Also in the WSC at 79°N. Hanzlick (1983) using Brink's (1982) model of free coastal wave propagation. obtained results suggesting that the broad spectral peak at about 6 days observed in the u-component spectra could be due to the existence of shelf waves. However, direct measurements in the WSC do not support the strong, topographically trapped concentration of energetic fluctuations over the shelf break as seen in the model results. A nearly barotropic velocity structure in the model is also different than shown by direct velocity measurements.

It can be easily shown by comparison of their dispersion equations. that continental shelf waves and the topographic Rossby waves are the same type of wave. From Gill (1982). in a case of the exponential depth profile increasing with distance from the coast

$$H = H_o exp(2\lambda y) \tag{3.5}$$

the dispersion relation for continental shelf waves. in a homogeneous ocean with rigid-lid assumption. is

$$\omega = \frac{2fk\lambda}{k^2 + l^2 + \lambda^2} \tag{3.6}$$

where k and l are components of wavenumber in along and cross-shelf directions. respectively, f is the Coriolis parameter. ω is frequency, and λ^{-1} is a characteristic length scale of depth variations.

The Rossby wave, a typical low-frequency motion is to lowest order geostrophic (i.e.. such that the Coriolis term balances the pressure term), but it requires consideration of higher-order dynamical processes for its determination. The geostrophic approximation is a diagnostic relationship and it just says that as the velocity field slowly alters in time, its Coriolis acceleration will continue to balance the evolving pressure gradient. From the potential vorticity equation, changes in total depth of the ocean have similar effects as do changes of f by producing relative motions. There are large regions in the open ocean where mean topographic slopes of the order of $O(10^{-3})$ and larger exist. Although numerically small and generally of little importance. they can significantly affect the propagation of long waves.

Following LeBlond and Mysak (1978), when using the exponential depth profile defined as

$$H = H_o exp\left(\frac{-y}{L}\right) \tag{3.7}$$

where shoaling water is in the positive y-axis direction. and a rigid-lid approximation. the dispersion relation of the barotropic topographic Rossby waves is

$$\omega = \frac{-\left(\beta + \frac{f}{L}\right)k_1}{k_1^2 + k_2^2 + \frac{1}{4L^2}} \tag{3.8}$$

At 75°N. $\beta = \partial f/\partial y = 5.9 \times 10^{-14}$ cm^{-1}s^{-1}. f=1.41×10^{-4} s^{-1}, and assuming a characteristic width of the slope L=100 km gives f/L=1.41×10^{-11} cm^{-1}s^{-1} and f/L>>β. Neglecting β, setting 2λ=-1/L. k_1=k. and k_2=l in Eq.3.8 gives

$$\omega = \frac{2fk\lambda}{k^2 + l^2 + \lambda^2} \tag{3.9}$$

which is the same dispersion relation as given by Eq.3.6. The relation between λ and L can be simply derived from comparison of the depth profiles used in each case.

This shows that continental shelf waves are a type of quasigeostrophic, topographic planetary wave, their motions conserve potential vorticity, and thus their restoring mechanism is due to variations in f/H, as occurs in the topographic Rossby waves (Mysak, 1980). Both wave types are highly rotational: their motion consists of a sequence of eddies of alternating sign, propagating along and confined to the shelf slope region (LeBlond and Mysak, 1978). In quasigeostrophic theory of the Rossby waves, only slight departures of actual depth from the constant value D were allowed. The continental slope invalidates this assumption but major dynamics of continental shelf waves can still be considered on the ground of the quasigeostrophic theory (Pedlosky, 1987), as have been done for example by Rhines (1971), Louis et al. (1982), and Okkonen (1993). Terms of higher order such as the relative accelerations or frictional forces are required for consideration of complete dynamics in the case of topographic Rossby waves. Such terms may become locally even more important in continental shelf waves. Ageostrophic effects, i.e., the cross-isobath flow, may account for a much larger part of the momentum balance. An order of magnitude of the relative acceleration term estimated as Rossby number $\epsilon = \omega / f$, using $\omega = 2\pi / 17 \text{hrs}$ and $f = 1.41 \times 10^{-4} \text{s}^{-1}$ at 75°N, can be as high as 0.72. For constant wind forcing though, the inertial motions can be only feasible during spin up time. PSD of Fig.3.7 shows a peak at ~ 0.5 cpd, which is close to a frequency of inertial motions in the Greenland Sea, however the peak is about three orders of magnitude

smaller then the peak at 17 hrs.

If the simulated waves are in fact topographic planetary waves, then the wave field should lie over topography characterized by a length scale appropriate for the wavelength and the wave period determined from the simulation. Using the wavenumber and frequency from the model results allows the dispersion relation to be solved for a topographic length scale. From Eq.3.8. neglecting β ($\beta \ll f/L$), a formula for L can be derived as

$$L = \frac{-f k_1 \pm \sqrt{k_1^2(f^2 - \omega^2) - k_{2r}^2 \omega^2}}{2\omega(k_1^2 + k_{2r}^2)} \tag{3.10}$$

giving L=67 or 12 km. For comparison. the magnitude of the local topographic length scale is computed as

$$\frac{\frac{\partial H}{\partial y'}}{H} = -\frac{1}{L} \; . \; or \; L = -\frac{H}{\frac{\partial H}{\partial y'}} \tag{3.11}$$

using central differences from the depth data used in the model. The 30 km. 67 km. and 350 km topographic length scale contours are plotted (Fig.3.11a). From Eq.3.11. it follows that for constant slopes ($H_{y'} \sim$ constant). the topographic length scale L is a linear function of depth H. i.e.. an increase in H yields an equivalent increase in L. This also means that for such steep but constant slopes as the continental slope off Greenland. between 73°N and 76°N. lines of constant L have to be parallel to the slope (x'-axis) and to each other. Using the calculated value of slope $H_{y'}=3 \times 10^{-2}$ at 75°N, with L=67 km, gives a depth of approximately 2000m. The main axis of the stream function variability. between 73°N and 76°N over the slope. where all the wave activities are concentrated. as

shown in Fig.3.5b, closely follows the 2000 m isobath, which coincides with the contour line of 67 km of Fig.3.11a. The very basic condition for topographic planetary wave propagation requires slopes to remain constant in the along slope direction (x'-axis), which translates into constant along x'-axis lines of topographic length scale. As seen in Fig.3.11a, parallel to the continental slope lines of constant L exist mainly between 76°N and 73°N, and become variable farther south in this direction. Since phase velocities estimated from Fig.3.6, and wavenumbers, as well as frequency, may vary little around the calculated values, L would change appropriately.

At the low wavenumber limit $(k^2+l^2 << 1/(4L^2))$, continental shelf waves and the topographic Rossby waves are nondispersive, that is the phase speed is independent of wavenumber, and it is equal to the group velocity (Pedlosky, 1987). However the waves estimated in this experiment are not long $(k^2 > 1/(4L^2))$ and wavelengths of the order of ~ 1000 km would still be dispersive for given L=67 km. From the dispersion relation (Eq.3.16), frequency of dispersive waves varies not only through wavenumber $\bar{\kappa}$, but also through variations in the properties of the medium itself, as expressed through the parameter λ (or L). Variable L in the along slope direction changes the wave frequency ω, as defined by ray theory (LeBlond and Mysak, 1978). Variable slopes distribute energy over a wide spectrum of waves in wavenumber and frequency space, whereas constant slopes such as the Greenland shelf slope between 73°N and 76°N (Fig.2.1, 3.11), by defining a value of L along which waves propagate, can accumulate significant amounts of energy in waves of a particular frequency and wavelength. Hence steep but constant

Greenland shelf slopes may act locally as a waveguide for energy transfer.

The slowness curve (a circle of constant wave frequency in wavenumber space), in the rotated coordinate system (x',y'), can be used to illustrate graphically the direction of propagation of energy, i.e., the group velocity, and the phase velocity. From Eq.3.8. neglecting β, the analytical formula for the slowness circle is derived

$$\left(k_1 + \frac{f}{2\omega L}\right)^2 + k_{2r}^2 = \frac{1}{4L^2}\left(\frac{f^2}{\omega^2} - 1\right) \qquad (3.12)$$

with radius $R_0 = \sqrt{\frac{1}{4L^2}\left(\frac{f^2}{\omega^2} - 1\right)}$ and the center at $\left(-\frac{f}{2\omega L}, 0\right)$ (Fig.3.11b). The components of the phase velocity are given by

$$\vec{C}_p = -\frac{\beta}{(k_1^2 + k_2^2)(k_1^2 + k_2^2 + \frac{1}{4L^2})}(k_1^2, k_1 k_2) \qquad (3.13)$$

and from Fig.3.6 phase velocity $|\vec{C}_p|$=586 cm/s was estimated, directed to the southwest. Since in Fig.3.11b the alongshore direction of the continental slope is parallel to k'-axis, the direction of phase propagation is almost along the slope, toward the negative k' direction, with small onshore component. The Doppler effect due to the mean flow is neglected here because the observed mean velocities in the EGC range between 9 and 21 cm/s (Strass et al., 1993), which constitutes between 1.5% and 3.5% of the phase speed.

The components of the group velocity are given by

$$\vec{C}_g = \frac{\beta}{(k_1^2 + k_2^2 + \frac{1}{4L^2})^2}\left(k_1^2 - k_2^2 - \frac{1}{4L^2}, 2k_1 k_2\right) \qquad (3.14)$$

and the group velocity is calculated to be $|\vec{C}_g|$=409 cm/s and directed to the northeast with offshore component $C_{gy'}$=103 cm/s, and alongshore component $C_{gx'}$=396 cm/s. The
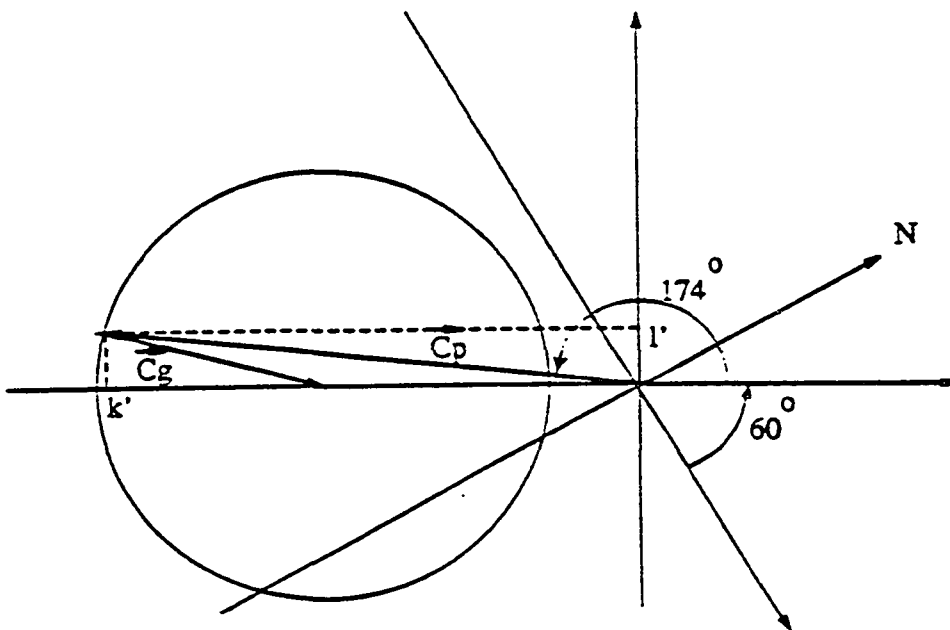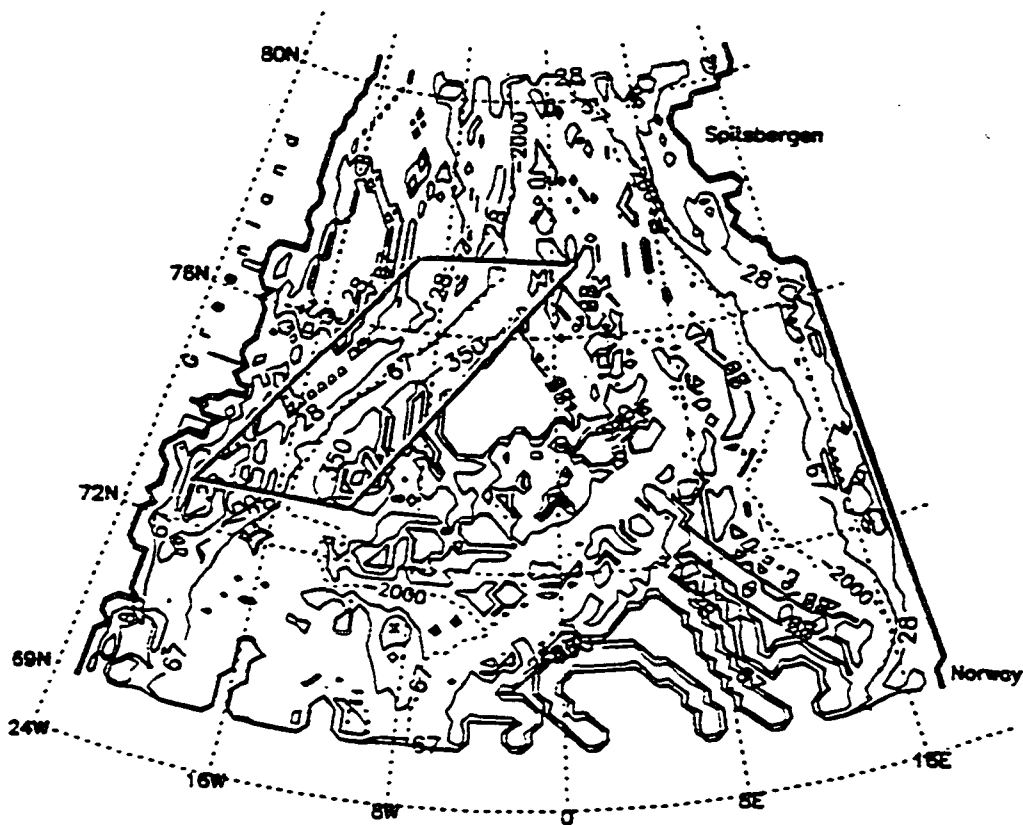
Figure 3.11 a) Topographic length scale calculated as $H_y/H=-1/L$ from the depth data used in the model, b) The slowness circle in rotated coordinates (x',y')

direction of the group velocity vector away from the continental slope agrees with the expected direction of energy propagation for waves forced at the boundary. Although the along-slope component of the group velocity implies that the bulk of energy is propagated along the shelf slope to the northeast direction, it is the offshore component of energy propagation that is of great interest.

The East Greenland Front (EGF) (Fig.1.4) located over the continental slope of Greenland results from the sharp temperature and salinity gradients between waters to the west and east of the slope. In the upper layers. cold and fresh Polar Water (PW) is advected from the Arctic Ocean within the EGC. and it occupies most of the Greenland shelf (Aagaard et al., 1985).. This water mass meets with warm and saline waters of Atlantic origin. return Atlantic Water. In the deep layers. Arctic Ocean Deep Water meets Greenland Sea Deep Water in the EGC. The simulated barotropic continental shelf waves with energy propagating across shelf may provide a significant source of energy for cross-frontal mixing within the EGF, leading to formation of such deep water masses as Norwegian Sea Deep Water (NSDW) or Denmark Strait Overflow Water (DSOW), which are the main sources of North Atlantic Deep Water.

Mixing of different water masses within the EGC, leading to formation of NSDW and DSOW. has been recently reported in literature. Based on observations around 75°N, Aagaard et al. (1991) in a discussion of possible mechanisms of the Norwegian Sea Deep Water (NSDW) formation. imply diapycnal mixing (between waters of different

densities) across the continental slope of Greenland, as a major component of this water mass generation. They find no evidence of baroclinic instability over the slope, and also suggest little importance of double diffusion processes in diapycnal mixing of the deep water masses. They conclude that the AODW controls the temperature-salinity properties of the various deep basins south of Fram Strait, but no source of energy is conclusively suggested for diapycnal mixing. The amount of energy in the cross-shelf direction derived from the topographic waves simulated in this experiment could support diapycnal mixing in the deep EGC.

Strass et al. (1993), based on hydrographic and current meter data, reveal that about 50% of Denmark Strait Overflow Water (DSOW) may originate in the Greenland Sea where it forms by mixing in the EGC. As for a generation mechanism, they suggest isopycnic mixing (between waters of same density but with different T-S characteristics), which derives energy from baroclinic instabilities as observed in the measurements. An increase of the current variability starting in January 1988 is found at all depth levels at all moorings, suggesting the existence of a strong barotropic response in the EGC, hence oscillations of barotropic nature may also be in part responsible for isopycnic mixing and formation of DSOW.

Roach et al. (1993) using satellite microwave images of ice cover in conjunction with meteorological data and in situ velocity, temperature and salinity records, describe a sequence of processes beginning with preconditioning of water column, leading to

convective overturning, which brings warmer water to the surface which caused the rapid removal of sea ice cover in the central Greenland Sea gyre (75°04'N, 2°58'W) in winter of 1988–1989. Convective mixing reached at least down to 200 m, and resulted in the mixture with T-S properties centered on -1.4°C and 34.85 psu. A year earlier at a similar location (74°45'N, 0–5°W), Rudels et al. (1989) measured similar mixed water characteristics (-1.5°C, 34.86 psu) during deep convection. Water with such properties corresponds to upper Arctic Intermediate Water (Swift, 1986) and is a source of the Denmark Strait overflow (Swift et al., 1980).

Based on unfiltered hourly time series of velocity at mooring GSP-4 (75°04'N, 2°58'W), Roach et al. (1993) calculated variance-preserving spectra before and after convective overturning (Fig.8 in their paper). A tenfold increase in horizontal kinetic energy at near-inertial frequencies is observed due to a convective event. A smaller peak at frequencies smaller than 1 cpd. but significant at 95% confidence level, occurs at about 17 hrs. Its period and magnitude are very close to the 17.2 hr peak as shown in Fig.3.7. As shown in the next experiments, inertial oscillations (~12 hrs) become more important with variable wind forcing (see Fig.3.15, 3.20, 3.25, 3.33). Although the mooring location is still within a range of continental shelf waves activity, it is far enough from the shelf slope to let inertial oscillations dominate the kinetic energy distribution. Also not simulated in the model here are small scale eddies, sea ice motion and tides, which can locally concentrate kinetic energy. This may explain why continental shelf waves along the shelf slope of Greenland have not been observed yet.

In a different modeling approach, Proshutinsky and Polyakov (1991) using a two-dimensional frictionless model with real topography, calculated normal mode oscillations in the Arctic Ocean, induced by an arbitrary initial perturbation of the sea level field. For these free oscillations, they calculated spectral energy distributions at several monitoring points. In the Greenland Sea (74°N and 7°20'E), a peak of maximum energy concentration was at 17.3 hrs. which is the same as the period of simulated here continental shelf waves.

To complete this analysis, a possible generation mechanism for barotropic continental shelf waves is proposed, a mechanism classified by Mysak (1980) as generation by alongshore variations in topography. The Greenland Sea gyre, commonly defined as extending over the Greenland and Boreas Basins, is closed on the outer boundaries by the WSC at the east, the EGC at the west, the Jan Mayen Current at the south, and the westward turning branch of the WSC at the north. Quadfasel and Meincke (1987), modify this definition and suggest that there exist two separate cyclonic gyres, one in each of the deep basins, separated by the Greenland Fracture Zone (GFZ). This implies that due to topographic steering the flow is eastward on the northern side and westward on the southern side of the GFZ. Kolterman and Machochek (1985) suggested topographic steering of the barotropic flow over the GFZ as a possible explanation for the existence of the two separate gyres. Evidence for the strong barotropic mode in the EGC at 79°N is also provided by Foldvik et al. (1988) and a similar conclusion about topographic steering of the EGC over the GFZ can be made based on the results of this model

experiment. As shown in Fig.3.3, waters of the westward and then southward flow of the WSC branch in the Boreas Basin, together with the EGC, are being disturbed by the presence of a cross-slope barrier, the GFZ. The generation mechanism is consistent with the conservation of potential vorticity in the barotropic flow (Eq.3.1). The southward flow of the EGC from north of 77°N to the GFZ changes depth by more than 500 m (Fig.2.1). To conserve potential vorticity, the fluid must acquire anticyclonic relative vorticity. This means that after passing the GFZ, some anticyclonic flow produces cross-isobath flow, up the continental slope. This can be viewed as an initial disturbance, a condition equivalent to one required for generation of the topographic Rossby waves (Pedlosky, 1987). Some discussion on the generation of barotropic shelf waves by a uniform wind stress applied over a shelf region with a localized topographic feature has been provided by Martell and Allen (1979). Since the southward flow of the EGC over the GFZ occurs constantly, it provides a continuous mechanism for the generation of continental shelf waves. A disturbance, propagating over the steep and almost constant (in alongshore direction between 76°N and 73°N) Greenland shelf slopes (Fig.3.11a, 2.1), may manifest itself as a wave of distinct frequency and wavenumber, defined by the topographic length scale (L ~ constant along the slope), steepness of the continental slope, and the alongshore scale of the wave generating topographic feature (Huthnance, 1975; Mysak, 1980; Martell and Allen, 1979). Because the slope becomes too variable south of 73°N (since L varies along the slope) to support waves of a single characteristic, dispersion of the original wave results. The constant slope between 76°N and 73°N, acting as a waveguide over

the limited distance, defines the extent of measurable variabilities, as shown in Fig.3.5b.

Section 3.3 Seasonal barotropic experiment

In this section, the results from a barotropic model are used to investigate the influence of bottom topography on the ocean response to seasonal atmospheric forcing in the Greenland Sea. The same configuration as well as all the methods described in the previous experiment are adopted here. The model is restarted from the end state of the previous run and integrated for another 4 years. Each month is 30.5 days long (366 days/year), and each monthly mean wind stress is considered as observed in the middle of that month. Monthly mean stresses as specified by Hellerman and Rosenstein (1983) are used. A new wind stress is reconstructed at every timestep by linear interpolation between each pair of monthly mean values. Stream function on the southern and northern OBs is fixed in time and has the same spatial distribution as before.

3.3.1 Results and analysis

The approach of restarting the seasonal barotropic model from the end of the constant wind experiment allows a decrease in the spin up time. It takes about 50 days for the model to reach mean TKE levels (Fig.3.12). The time series of TKE is quite similar to the one of Fig.3.2, and the absolute mean of TKE (of about 4 erg/cm^3) decreased compared to the mean of the previous experiment. This should be of no surprise, since the constant, strong January mean wind stress yields strong circulation, while the seasonal wind fields consist of weaker monthly means through summer, and drive weaker currents. The similarity of the two time series (Fig.3.2, 3.12) is surprising because there is almost
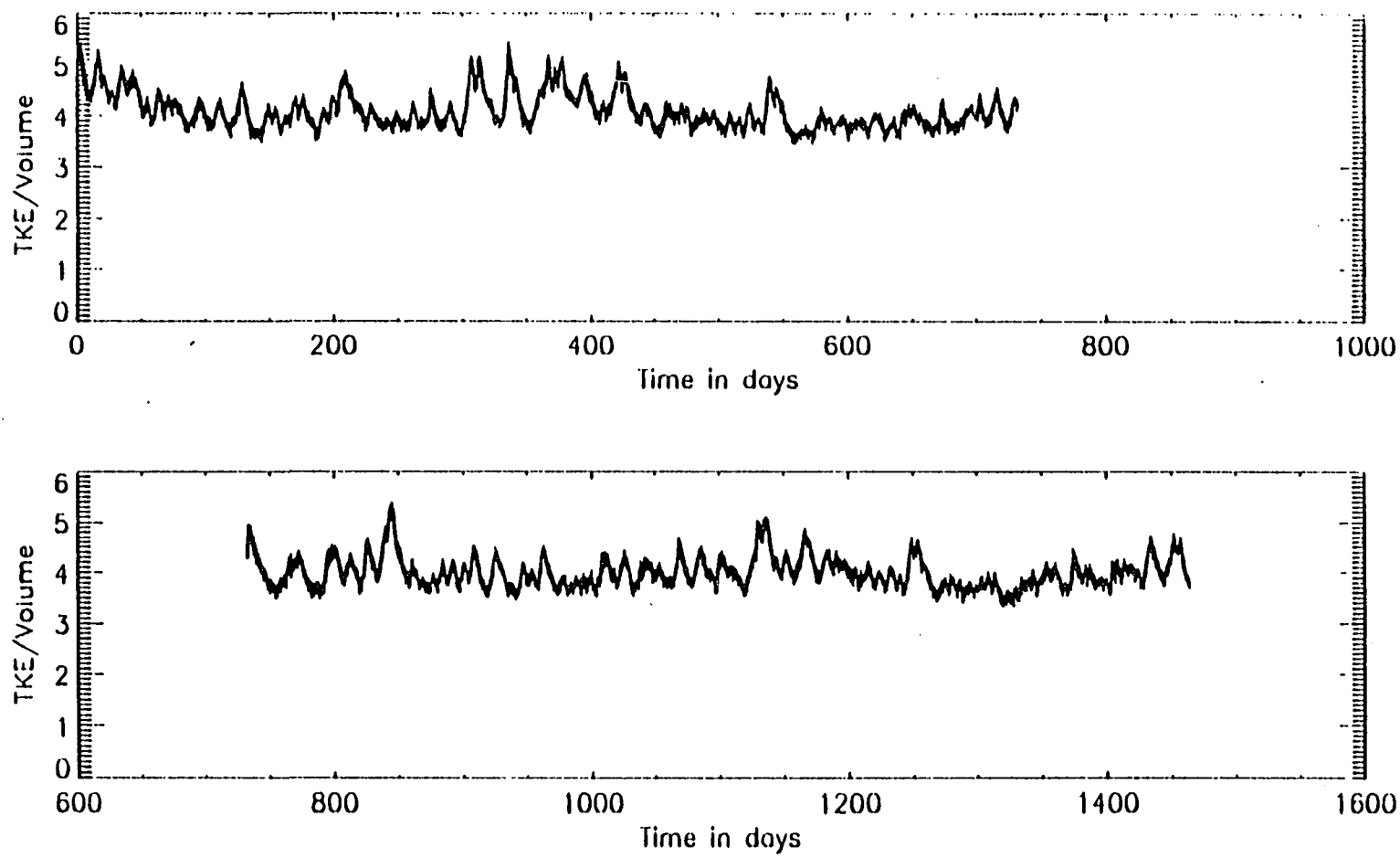
Figure 3.12 Time series of TKE (in erg/cm^3) - experiment #2.

no signature of the expected seasonal cycle in Fig.3.12. The time series of this experiment shows some fluctuations of variable magnitude and frequency but it is rather difficult to conclude about the presence of annual oscillations.

In Fig.3.13–3.14 the seasonal: spring, summer, fall, winter mean circulations are shown. They reveal overall generally weak circulation. Even the winter mean, forced by the strongest winds, reaches a maximum of ~ 7 Sv in the Greenland Sea gyre, which is less than half of 15 Sv simulated in the previous experiment. This suggests that the monthly mean atmospheric forcing is inadequate. To investigate circulation forced with much stronger winds, another barotropic experiment is performed, and discussed shortly in next section. For now, the results of this experiment are analyzed, and an issue of different wind forcing will be addressed later.

Seasonal circulations, shown in Fig.3.13, with the exception of the strength of the Greenland Sea gyre, are not much different from the one in Fig.3.3. The topographically trapped eddy in the vicinity of the Molloy Deep is still resolved and permanently present. An important change to notice is the stream function on the northern OB. Since the circulation is generally weak, even in winter and spring, the volume exchange prescribed at the north is too high, and an excess of mass entering from the north recirculates back into the Arctic Ocean. The constant stream function on the northern OB can still simulate temporal variabilities of the WSC flow through Fram Strait, if sensibly "overprescribed". From the prescribed southward flow of 4.2 Sv through the boundary, only ~3 Sv in
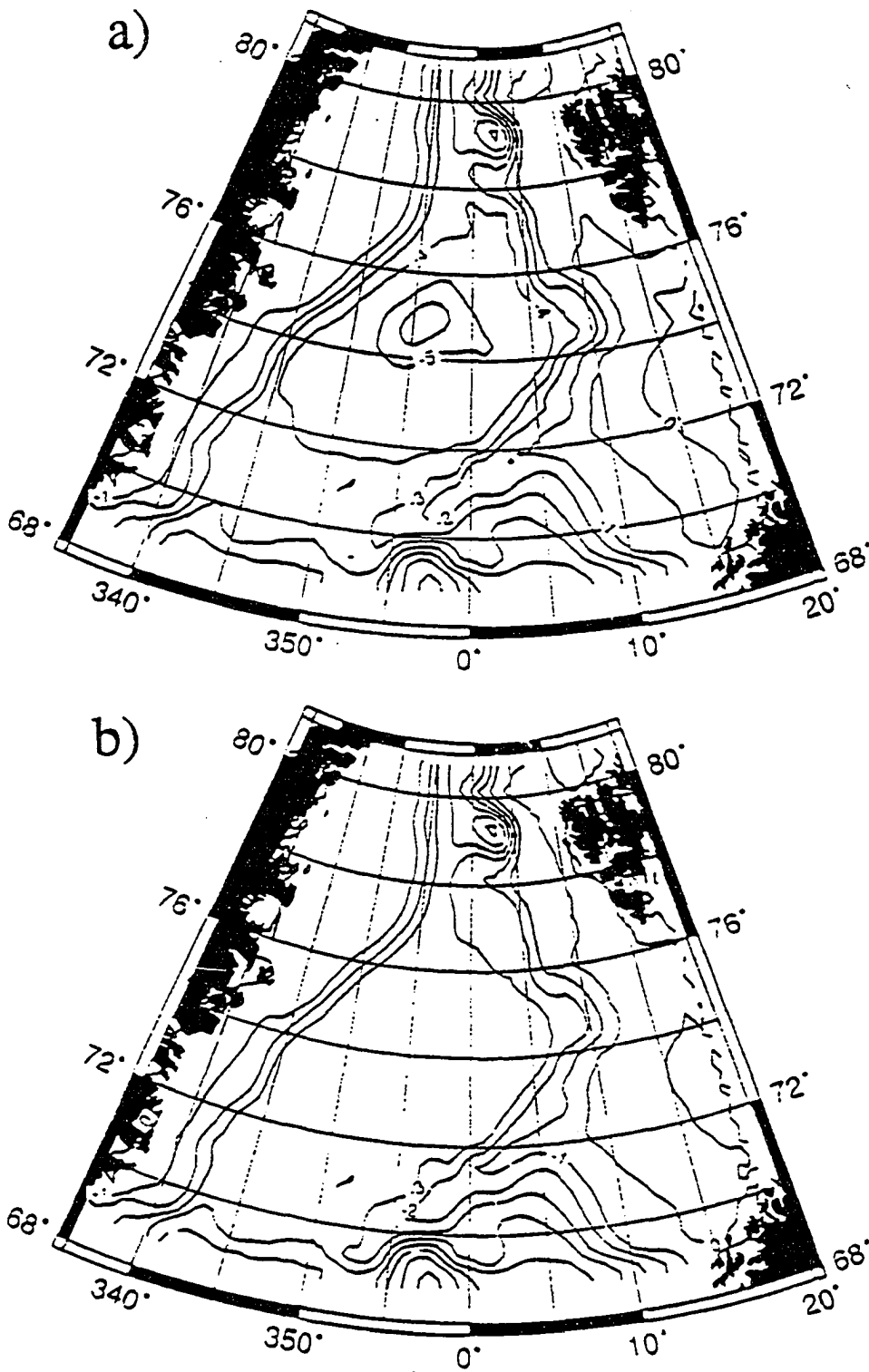
Figure 3.13 Seasonal mean circulations (contour interval is 1 Sv): a) spring (21 March - 20 June), b) summer (21 June - 20 September)

a)

b)
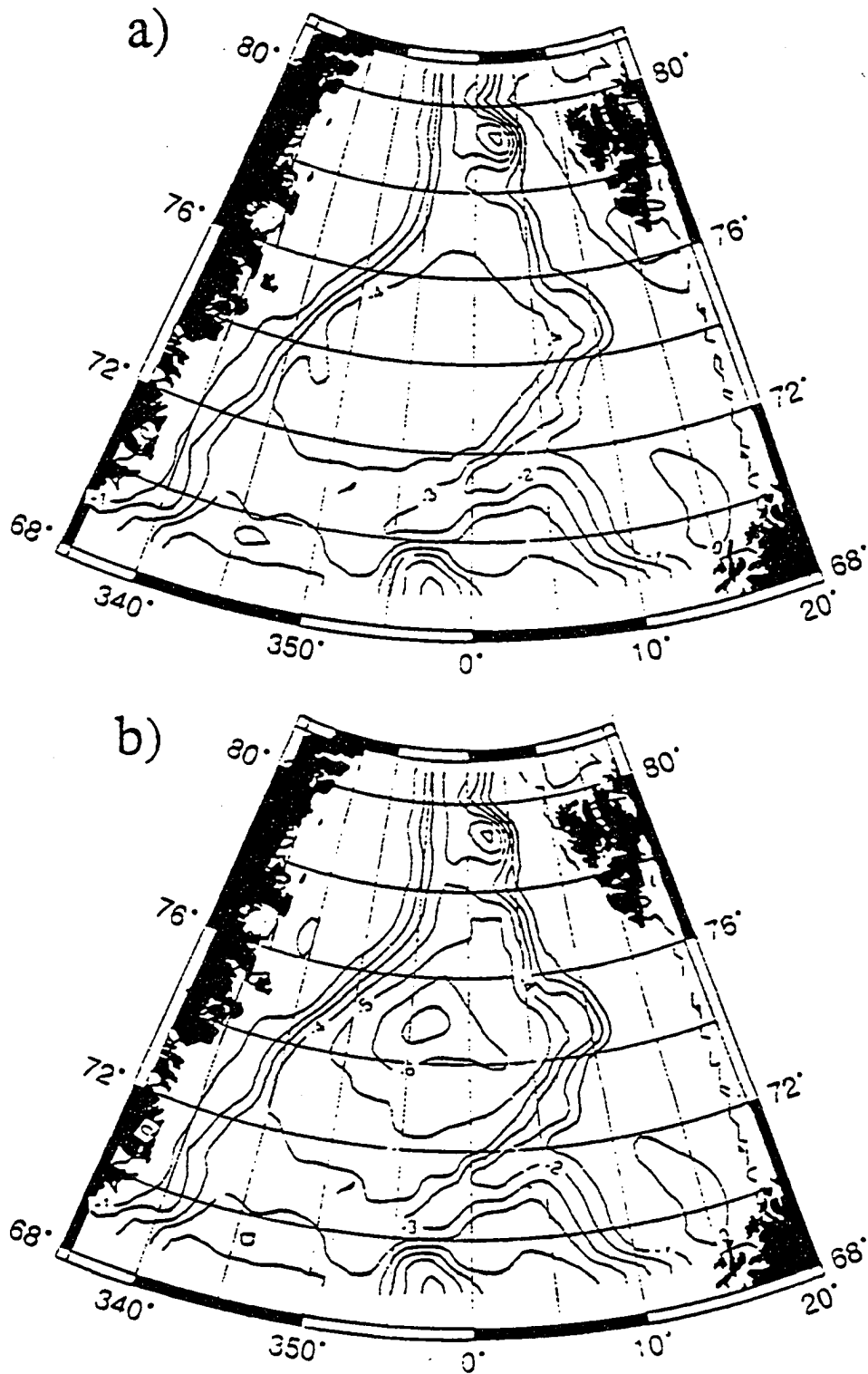
Figure 3.14 As Fig.3.13 but: a) fall (21 September -
20 December), b) winter (21 December - 20 March)

summer, and less than 4 Sv in winter, continues further south, and the rest recirculates back north within Fram Strait. This way the resultant flow from the Arctic Ocean into the Greenland Sea varies in time with an amplitude of ~1 Sv.

The previously discussed topographic planetary waves are still present. Their behavior has not changed due to variable winds, supporting the suggestion that they originate from topographically initiated disturbances due to the EGC flow over the GFZ. If the atmospheric forcing would be involved in the generation process, variable in time and space wind stress, and wind stress curl fields would introduce temporal and spatial variabilities in waves propagation as well.

Spectral analysis of TKE per unit volume of the 4 year long time series from the seasonal experiment (Fig.3.15), shows an annual peak, but, as expected, it is not significant at 95% level. The most prominent peak in the PSD is still the one at 17.2 hrs, but there appear new peaks that are significant at 95% level. One of the new peaks is a broad peak to the right of 17.2 hrs, centered between 12 and 13 hrs, identified as an inertial frequency peak. The inertial period ($2\pi/f$) at 69°N is 12.82 hrs, and at 80°N it is 12.15 hrs. With strongly variable seasonal winds, as it is the case in the Greenland Sea, inertial oscillations are present because the momentum flux from the atmosphere into the ocean is variable in time.

To determine the distribution of variance of circulation, EOF analysis performed on stream function results of a 40 day of integration, sampled every 3 hrs, is shown in Fig.3.16–3.17. The first two EOF modes, accounting respectively for 44% and 38.4% of

a)

b)
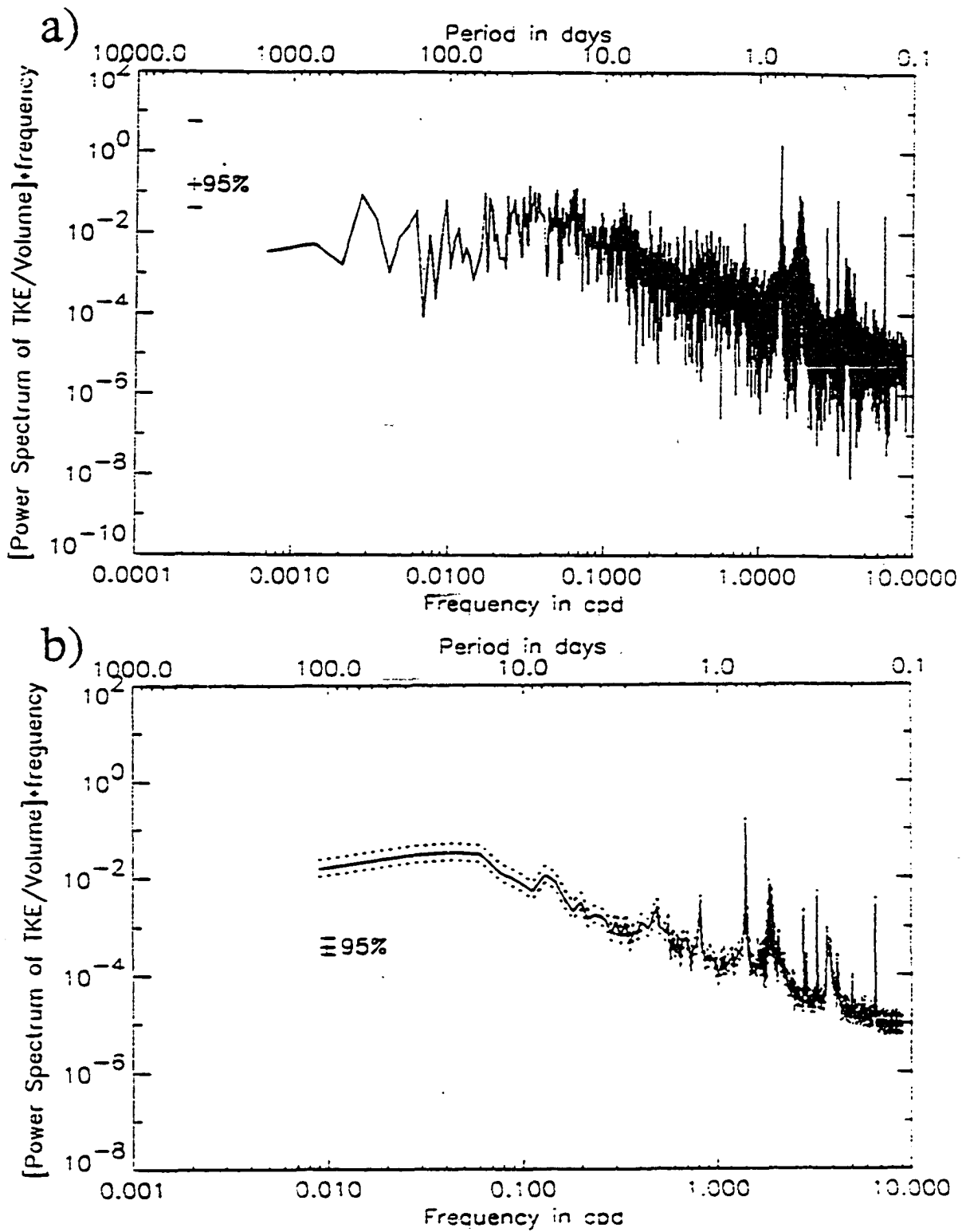
Figure 3.15 Variance preserving PSD of TKE/Volume (f>0.5f_N not plotted): a) "raw" with dof=2, b) box average with dof=50.

a)

b)
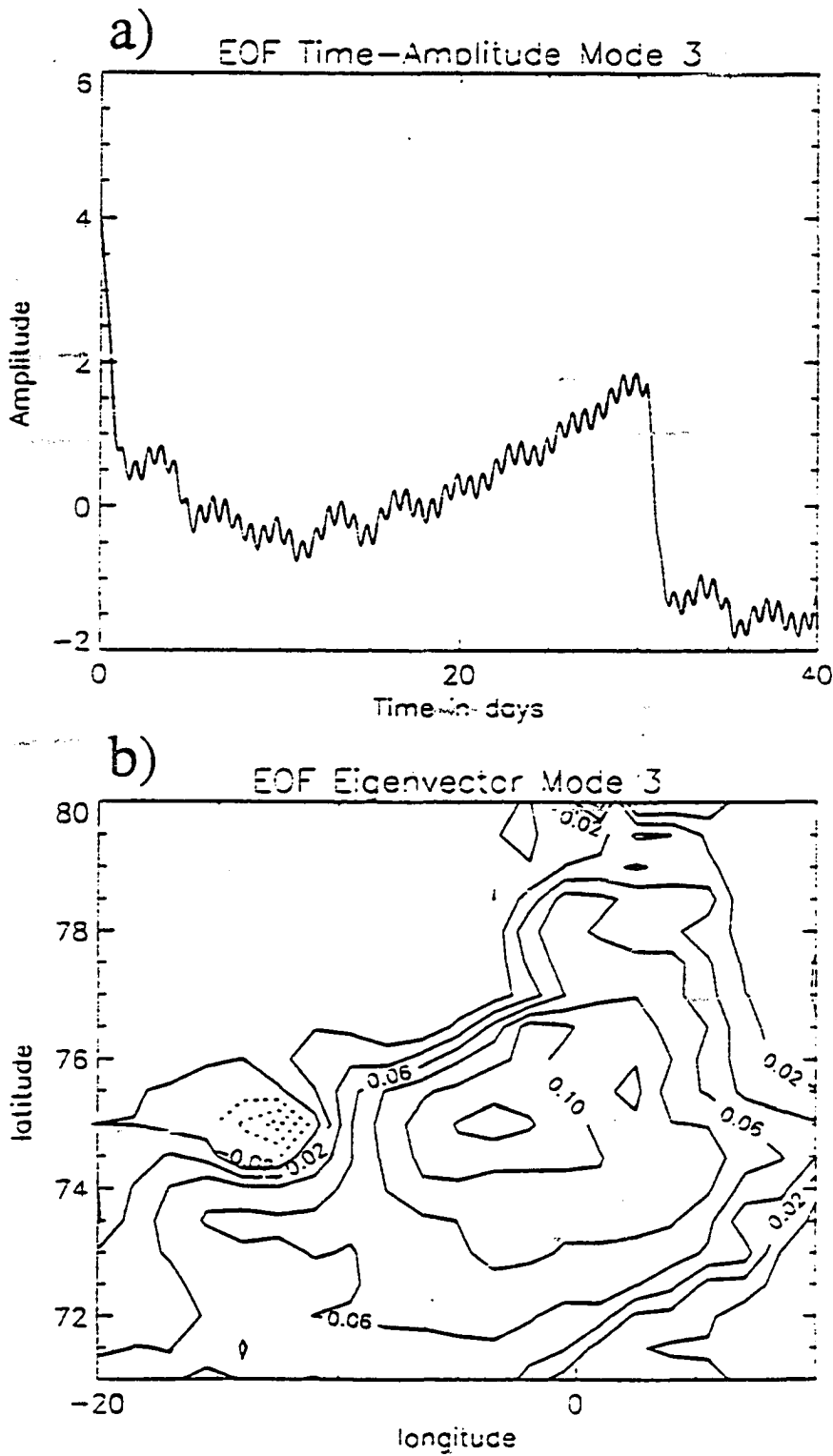
Figure 3.16 EOF mode 3 TAF (top - units are 10^6 m^3/s) and eigenvector (bottom - CI=0.02 dimensionless units) of stream function.

a)

EOF Time-Amplitude Mode 4

b)

EOF Eigenvector Mode 4
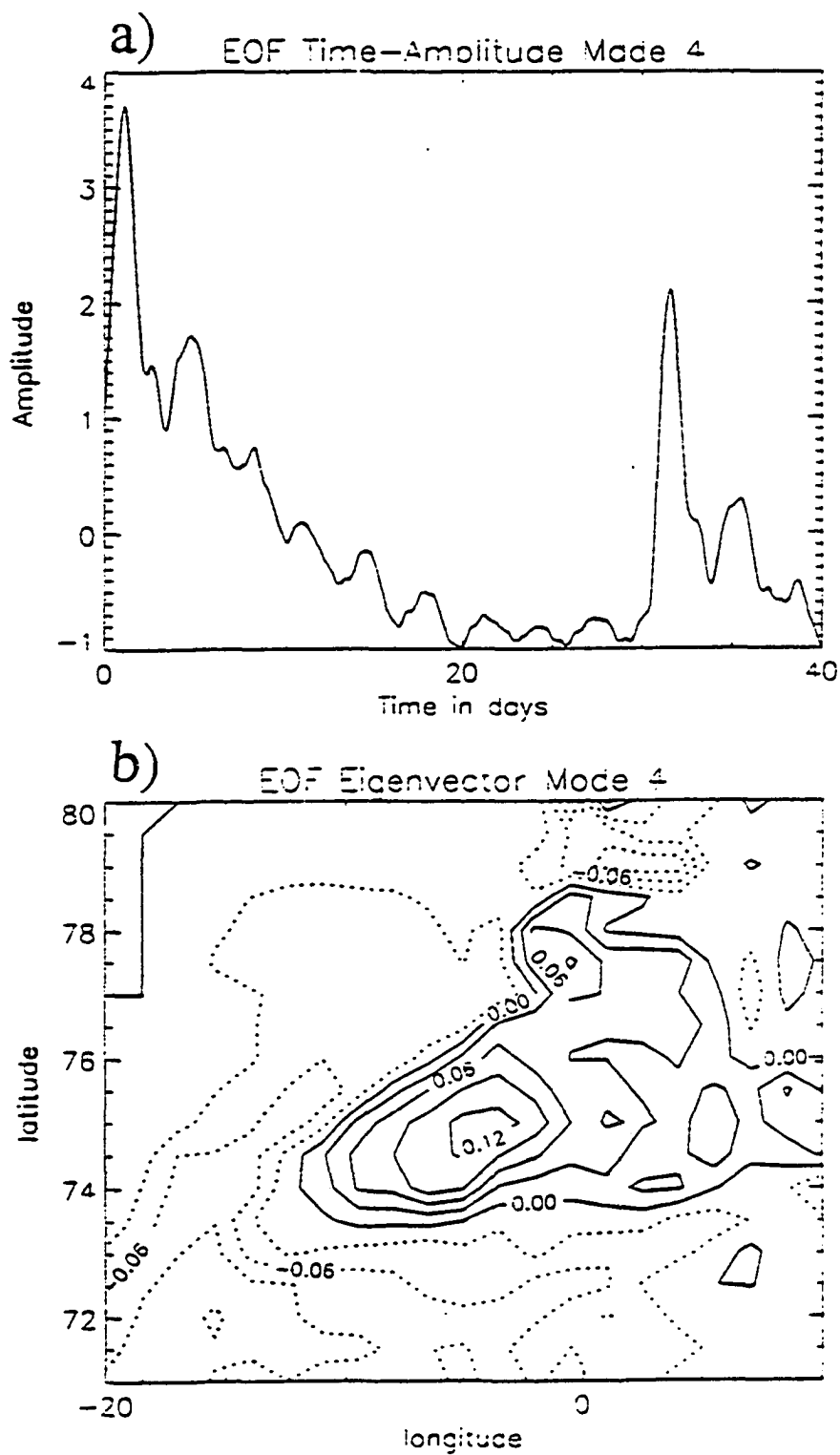
Figure 3.17 EOF mode 4, as in Fig.3.16

the total variance, are not shown because they are exactly the same as in the previous experiment (Fig.3.8–3.9). This is in agreement with the spectral energy distribution of Fig.3.15, where the peak at 17.2 hrs still dominates all others by more than an order of magnitude. The third EOF mode (Fig.3.16), accounting for 11% of the variance, shows basin-wide oscillations with a period of about 30 days in TAF. A 30 day period can be deduced from the time series of TKE (Fig.3.12). PSD (Fig.3.15) also shows a broad banded energy peak centered at ∼30 days.

This low frequency oscillation is identified as a westward propagating quasi-geostrophic normal mode, or the Rossby basin mode, defined after Pedlosky (1987). The normal mode in a closed rectangular barotropic basin has a frequency given by:

$$\sigma_{mn} = -\frac{\beta}{2\pi\left\{\left(\frac{m^2}{x_0^2} + \frac{n^2}{y_0^2}\right)\right\}^{\frac{1}{2}}} , \quad m = 1, 2, 3, \dots, \quad n = 1, 2, 3, \dots \qquad (3.15)$$

where x_0 and y_0 are lengths of the basin in x (zonal) and y (meridional) directions, respectively. In the model with open boundaries in y-direction, y_0 is assumed to be much greater than x_0 ($1/y_0^2 \ll 1/x_0^2$), and the period of the lowest mode (m=1) is 66 days, with x_0=1180 km and β at 75°N. This period is too large compared to the observed period of 30 days. The higher modes have also longer periods. A decrease in x_0, to account for shorter oscillations in x-direction, as shown in Fig.3.16, would only increase the period. An increase of β due to the effects of bottom topography will decrease the period calculated from Eq.3.15. As already discussed, topography is a dominating component of β in the Greenland Sea. It requires a relatively small input of topographic

effect into total β (from 5.9×10^{-14} to 1.3×10^{-13}), to decrease the period from 66 to 30 days. The deep and almost flat Greenland, Boreas, and Lofoten Basins can provide such small topographic effects. As shown in Fig.3.16, these basins are the area of major activity of variabilities with the resultant period of 30 days. This means that this EOF mode describes the combined effect of many subdomains, each with its own mode of oscillation.

The fourth EOF mode, with only 2.6% of the variance, which is still above the level of noise according to a significance test of Overland and Preisendorfer (1982), clearly shows (Fig.3.17) that the basin-wide oscillations consist of many regional modes of similar frequencies as in EOF mode 3. The eigenvector distribution of Fig.3.17 shows separate gyre circulations in the Boreas and Greenland Basins, which supports the earlier conclusions of Quadfasel and Meincke (1987), and Kolterman and Machochek (1985) about existence of such two separate gyres. The percentage of the total variance explained by the higher modes is too small though, to make any further conclusions.

It is expected that additional information about the circulation in the Greenland Sea can be obtained from experiments with increased atmospheric forcing, which is addressed next.

Section 3.4 Seasonal strong wind barotropic experiment

3.4.1 Introduction

This experiment is different from the seasonal barotropic experiment in the strength of the wind forcing. The main reasons for performing additional barotropic simulations was the absence of an annual cycle in the previous computations, using original variable wind forcing. This experiment was restarted from the end state of the previous one and integrated again for four years. The model configuration and all the methods are as before, except that only the wind stresses are doubled.

To calculate their wind stresses, Hellerman and Rosenstein (1983) (hereafter referred to as HR83) used the quadratic bulk aerodynamic formulations

$$\tau^x = \rho C_D u (u^2 + v^2)^{\frac{1}{2}}$$

$$\tau^y = \rho C_D v (u^2 + v^2)^{\frac{1}{2}}$$

(3.16)

where τ^x and τ^y are exchanges between the atmosphere and ocean of zonal and meridional momentum, ρ is air density, C_D is the exchange coefficient for momentum, the so-called drag coefficient, u and v are the eastward and northward components of wind velocity. The wind speed and stability dependent drag coefficient of Bunker (1976) was used in their analysis.

In spite of the large amount of work done, the value of C_D is not known exactly. According to Bunker (1976) the general variation in the drag coefficient is from 1×10^{-3} for low wind speeds, to 4×10^{-3} for hurricane winds. For the same wind speed range, for example between 10 and 15 m/s, C_D changes due to different 'air minus sea temperature

class', from 1.4×10^{-3} for temperature class $>5°C$, to 2.1×10^{-3} for temperature class $<-5°C$. The air minus sea temperature in the Greenland Sea in winter is often $<-15°C$ (Glavnoe Upravlenie po Navigacii i Okeanografii, 1985), which even further increases the drag coefficient, in a given wind speed range. HR83 supplemented the sparse data sample at the subpolar Arctic with 1957–58 wind-rose data from the Arctic (Oceanographic Atlases of the Polar Seas of the U.S. Navy Hydrographic Office, 1957–1958), where a neutral stability was assumed. They indicated that, there may be a bias toward lower stresses in polar regions of their data, when the unstable stratification occurs (i.e., the air is colder than the underlying leads and ice). In the Greenland Sea, in winter, Atlantic Water located to the south and east of the Polar Front (Fig.1.5) has an average surface temperature between +3 and +4°C (Fig.1.4), while at the same time, usually northerly winds bring very cold air from the Arctic Ocean.

Recently, Guest and Davidson (1991) specified the median neutral surface drag coefficient C_{Dn} for ice-free regions within 100 km of sea ice regions to be 1.8×10^{-3}, with maximum of 3×10^{-3}, for speed ranging between 4 and 12 m/s. This is above the range 1×10^{-3} to 1.4×10^{-3} generally accepted for open ocean C_{Dn} values at these wind speeds. According to Bunker (1976) and HR83, these values would increase further in unstable atmospheres (negative air minus sea temperature classes).

Bakun (1973) in order to partially offset the effect of using monthly mean atmospheric pressure data in calculating coastal upwelling indices along the west coast of North

America, used a value of the drag coefficient 2.6×10^{-3}, which is twice the value commonly used in such computations. Also, Salmon (1992) in his analysis of the monthly mean atmospheric data of the North Pacific and the Bering Sea, used $C_D=2.6\times10^{-3}$ in calculations of wind stresses.

Based on the results of the previous experiment, where no clear seasonal signal was present, and on the discussion above, the drag coefficients of HR83 are increased here by 2, so the wind stress components of Eq.3.28 are doubled. Since the sea ice effect on momentum transfer, which increases the rate of momentum transfer, is not accounted for here, doubled wind stress should not produce unrealistically high circulation. The results discussed in the next sections in this chapter, rather indicate, that the commonly used drag coefficients for ice-free polar regions, may underestimate the atmospheric forcing effect on the oceanic circulation in the regions under consideration here.

3.4.2 Results and analysis

There is a very clear seasonal oscillation signal in the time series of TKE (Fig.3.18). Although winter months are quite energetic, summer months are roughly at the same energy levels as in Fig.3.12, and the absolute mean of 4.5 erg/cm^3 is not extremely high - it is still below the mean value of the experiment with constant January winds. The ocean response to doubled wind stresses may be locally much stronger in a baroclinic model, where motions are not so strongly coupled in the vertical direction, as in a barotropic model.
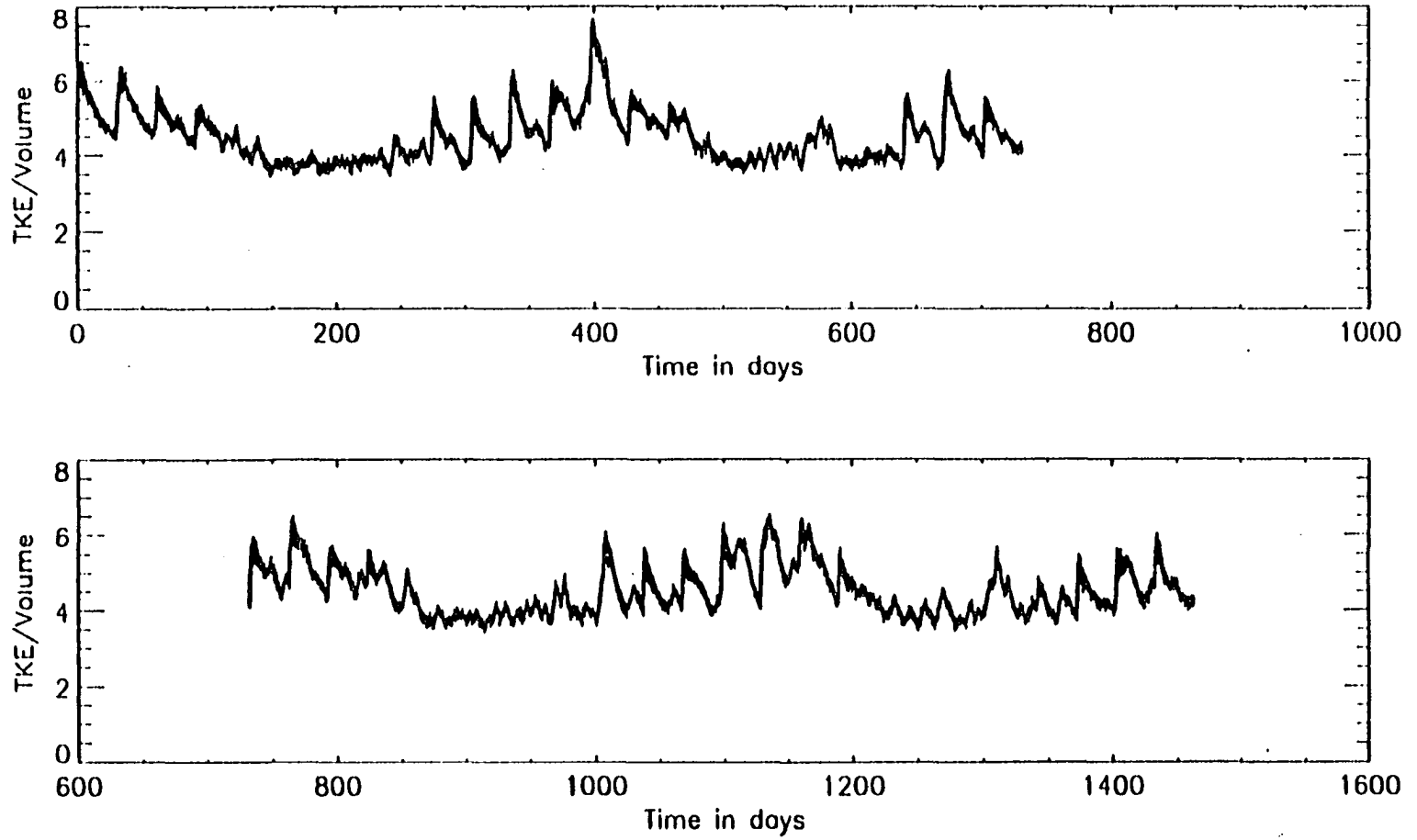
Figure 3.18 Time series of TKE (in erg/cm^3) - experiment #3.

The mean winter circulation. as shown in Fig 3.19a increased significantly, with the Greenland Sea gyre strength above 11 Sv. The mean summer circulation (Fig.3.19b) has not changed much in response to increasing winds (see Fig.3.13b for comparison). The increase in the strength of the Greenland Sea gyre following the increase in wind forcing, suggests that the circulation in this area strongly depends on the atmospheric forcing.

Due to the explicitly prescribed stream function solution on the OB. it is rather difficult to make similar conclusion about the boundary currents. Jonsson (1989) in analyzing the 6–hourly wind Hindcast data base from January 1955 to May 1987 of the Norwegian Meteorological Institute. found that the wind field is the main energy source for the mesoscale motion in the Greenland Sea. especially to the east of the East Greenland Polar Front (see Fig.1.5). Using a primitive equation model of the Greenland and Norwegian Sea. Legutke (1991a) suggests that on the shelves the predominately barotropic circulation due to wave-like motions. is highly correlated with the wind stress component parallel to the coast.

The power spectral density of TKE (Fig.3.20) shows a distinct peak at one year period. which is significant at the 95% level. The peak at 17.2 hrs still dominates the variance. but the inertial frequency broad peak centered at ~ 12.5 hrs. is almost equal to it. This can be explained as before: strongly variable seasonal winds yield variable in time momentum transfers. So doubled wind stress forcing introduces even stronger variabilities in momentum transfer. hence inertial oscillations become stronger.
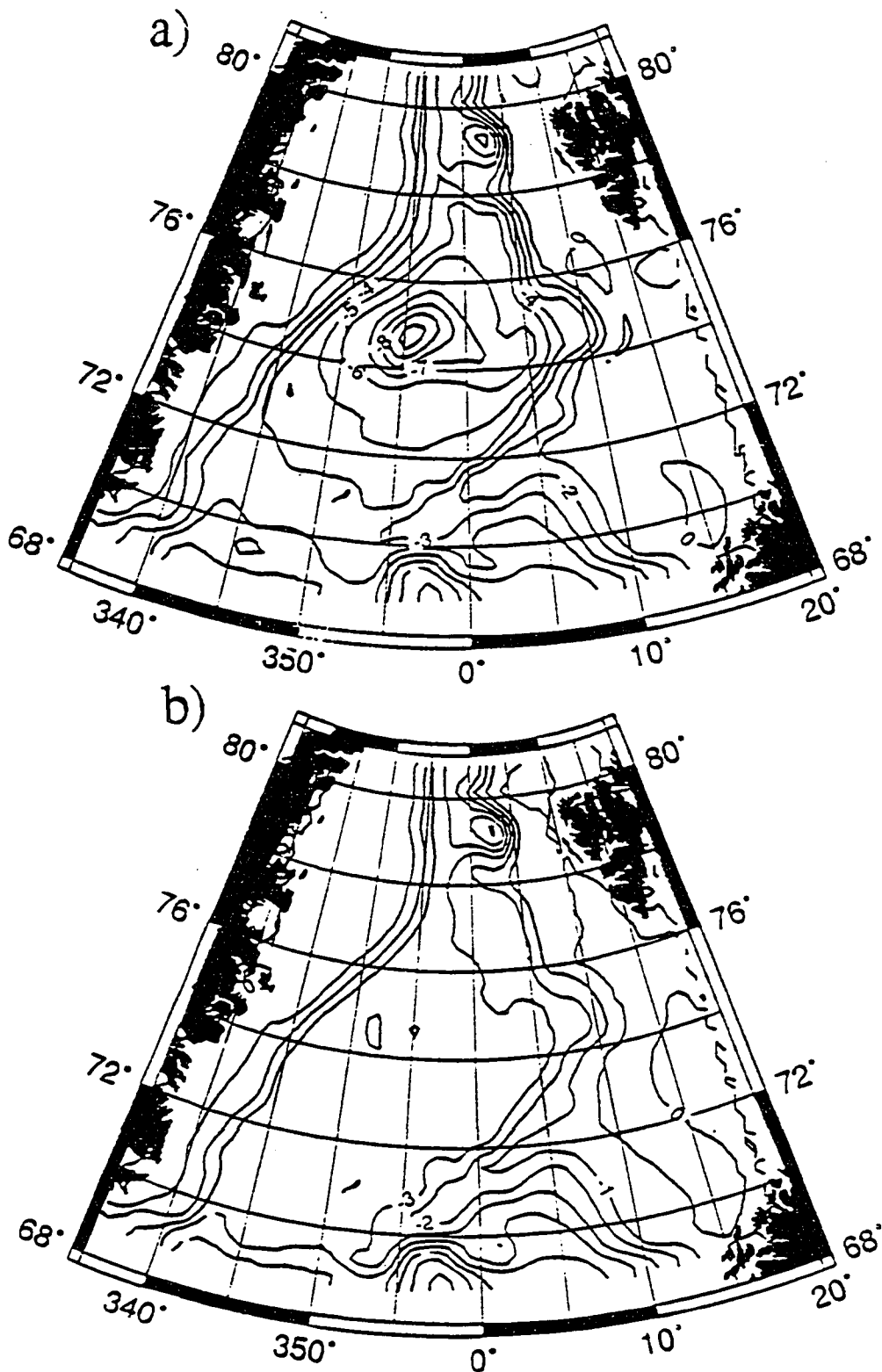
Figure 3.19 The mean circulation (in Sv) as forced by a doubled wind stress: a) winter (21 December — 20 March). b) summer (21 June — 20 September)
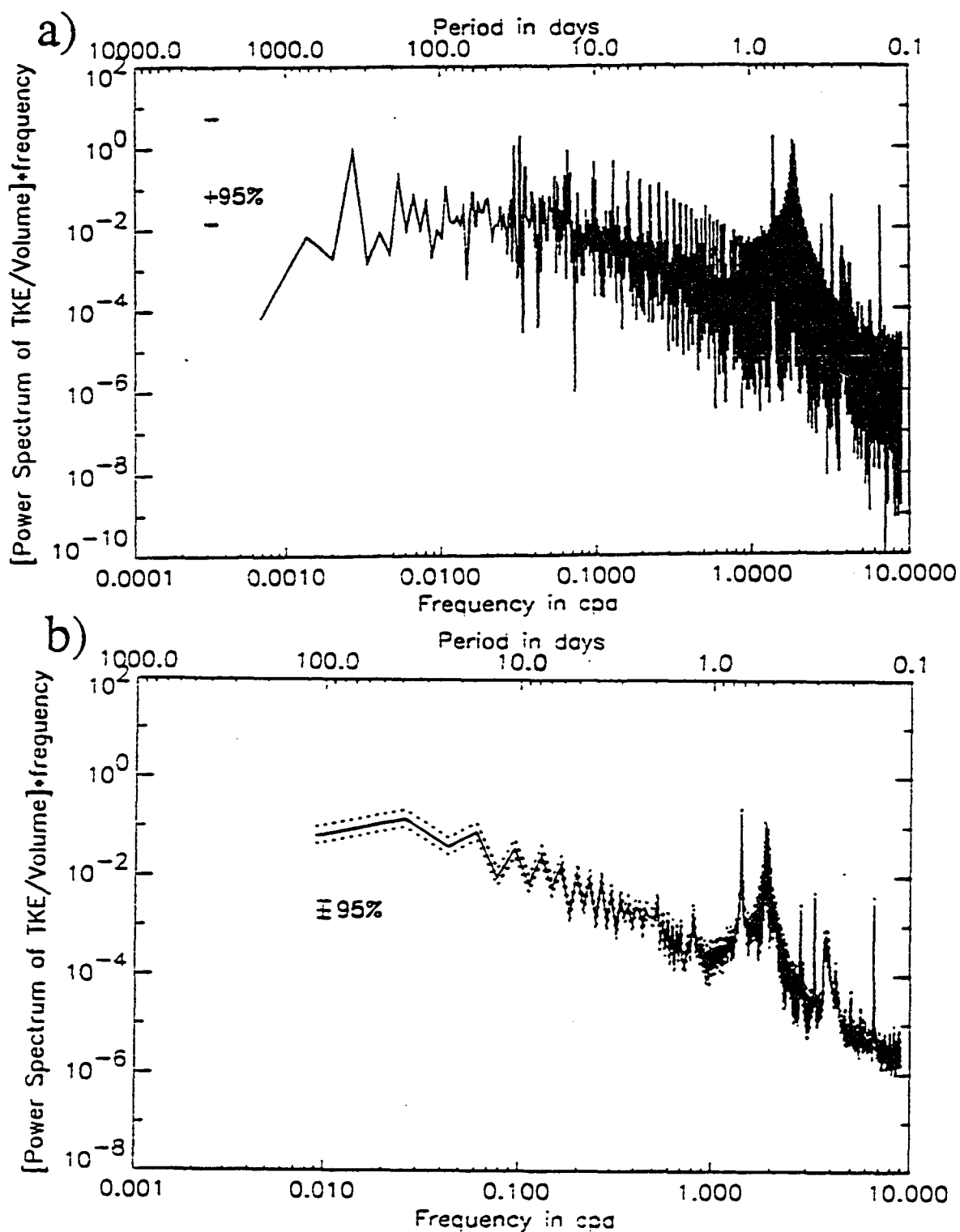
Figure 3.20 Variance preserving PSD of TKE/Volume — experiment #3 (f>0.5f_N not plotted): a) "raw" with dof=2, b) bax average with dof=50.

a) EOF Time-Amplitude Mode 1

b) EOF Eigenvector Mode 1
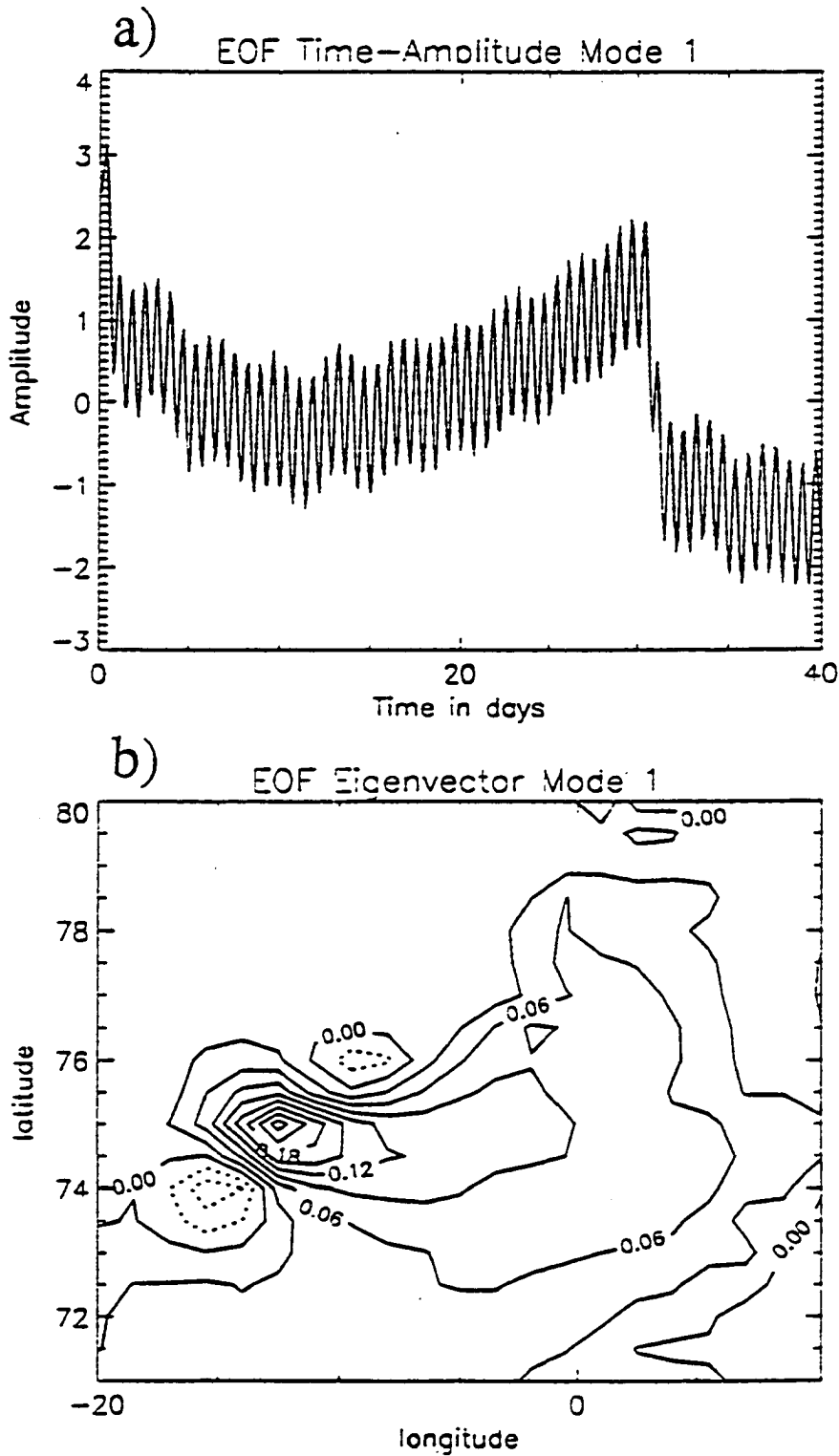
Figure 3.21 The EOF mode 1 TAF (top - units are 10^6 m^3/s) and the eigenvector (bottom - CI=0.02 dimensionless units) of the stream function — experiment #3.

Quasigeostrophic normal modes, as revealed by EOF analysis, also become more significant. The first EOF mode (Fig.3.21), explaining 33% of the total variance, shows both in eigenvector distribution and in TAF, combined influence of topographic waves with the period of 17.2 hrs, and normal modes, with the period of 30 days. It is similar to the third EOF mode of the previous experiment (Fig.3.16), but in Fig.3.21 the signature of topographic waves is more pronounced. The next two EOF modes, 2 and 3 (not shown), are the same as modes 1 and 2 of the two previous experiments, but now they account, respectively for ~27% and 24% of the total variance, which is much less than before. Also the fourth EOF mode (not shown) is the same (see Fig.3.17), but it explains now 7.25% of the total variance. Higher EOF modes, explaining very little of the total variance, show localized oscillations in a frequency range between ~0.4 to 0.033 cpd. All of them could be explained as quasigeostrophic normal modes, with the topographic β-effect appropriately scaled at a given region of oscillations. Since these higher EOF modes account for a very small portion of the total variance, their analysis is neglected.

Section 3.5 Seasonal baroclinic experiment

3.5.1 Introduction

The model resolution of 18.5 km meridionally, and varying from ~20 km at 69°N to ~9 km at 80°30'N zonally, is sufficient to take into account mesoscale topographic structures, which according to observations and model results (Legutke, 1991a), have a large influence on the distribution of hydrographic variables and generally on the dynamics of the GIN Sea. For numerical simulations to fully account for the physical realism of a basin circulations. model gridsize should be as small as the internal radius of deformation there. The internal radius of deformation r_i ($r_i = NH_i/f$, where $N^2 = -\frac{g}{\rho}\frac{\partial \rho}{\partial z}$ is the $Brunt - V\ddot{a}is\ddot{a}la$ frequency. and H_i is the local scale height of the stratification), is about 5–10 km in the GIN Sea (Johannessen et al.. 1983. Hunkins, 1975: Guest and Davidson. 1991: Strass et al.. 1993). Hence while in modeling of other oceans (where $r_i \geq 20$ km), the resolution of this model would be an eddy-resolving, it is not in the GIN Sea.

Some justification of the choice of horizontal grid spacing in the model has already been provided. Problems with prescribing boundary conditions at the southern open boundary, and computational limitations were the main reasons given so far. Another important argument against increasing resolution in the model is the quality of available temperature and salinity data on the model boundaries in the Greenland Sea. The data of Levitus (1982) used here. which are in fact the only readily available data for modeling,

are highly interpolated, smoothed, and of low resolution (1°x1°) in the Greenland Sea. Increasing resolution of the model while still using these data for forcing, would not improve the simulation results. As the most recent data from the GIN Sea become readily available for modeling purposes, improvements in model resolution will follow.

In this experiment another component of complexity is added, mainly the thermo-haline forcing. This type of forcing is at least as important as wind forcing, since both influence the dynamics of the Greenland Sea. The weak stratification in the region and its northern position combined with large topographic gradients ($\beta << f/H$) suggest a priori that a dominant part of the variabilities simulated in this baroclinic experiment will still be depth independent. In the GIN Sea the bottom relief strongly influences the distribution of currents and hydrographic variables. This is also suggested by observations. In light of the theory of Anderson and Corry (1985), the response of the ocean at high latitudes to the seasonal forcing is mainly barotropic, which is strongly controlled by topography.

Before analyzing results of this run, the methods are explained, since use of a new type of forcing requires additional treatment in the model, especially on the boundaries.

3.5.2 Methods

The series of simulations presented in this chapter has been designed so that the results of experiments can be compared to each other to determine the dynamical significance of each forcing component. In this case the influence of thermohaline forcing added to seasonal barotropic experiment is investigated. So in addition to the methods used in the

previous case, boundary conditions for temperature and salinity at the surface and on the open vertical boundaries must be specified.

Some information about vertical velocity profiles at open lateral boundaries can be obtained from the thermal wind equation. Assuming a reference level at the bottom of each water column, baroclinic transports may be estimated. In the case of boundary currents with appreciable barotropic flow entering or leaving the domain, such estimates provide only part of the necessary information (J. Wilkin, personal communication, 1993). Retaining the depth varying structure that is consistent with the thermal wind equation, and adding on the necessary barotropic velocity from observations and model results with a larger domain, provides an approach to the fundamentally ill-posed open boundary problem. Generally this approach is used here.

At the surface, T and S are relaxed to the prescribed values based on seasonal fields (Levitus, 1982), with a relaxation time scale of 30 days. The same relaxation time of 30 days is used on the northern OB. Due to earlier discussed problems on the southern OB, T and S are held constant in time, and the monthly means of January are used there. Use of the bottom friction sponge layer, close to the southern OB, prevents creation of instabilities and unrealistic currents, but T and S constant in time may influence the adjacent fully prognostic results of the interior. Hence, a 'buffer zone' is introduced in the vicinity of the southern OB. Within the buffer zone, over 2° of latitude between 71°N and 69°N, prognostic solutions of the interior T and S change linearly to the prescribed

constant in time boundary solutions. This approach produces non-seasonal results within the buffer zone of the southern OB, and fully prognostic solution in the interior. Only results north of 71°N are analyzed in baroclinic simulations.

As with wind stresses, monthly means of temperature and salinity are linearly reconstructed at each time step to provide instantaneous variable forcing at the surface and on the northern OB. The model is started from no motion, and is then integrated for 30 days, using the January mean three dimensional density field as initial data. The restoring robust diagnostic term is retained only in the surface layer and on the northern OB. After the 30 day initialization, the restoring fields at these two locations change on each time step continuously simulating seasonal forcing. The rest of the model configuration and all the parameters are the same as in the seasonal barotropic experiment.

3.5.3 Results and analysis

The model was restarted from the end of the 30–day—long initialization run and was integrated for 8 years. The timeseries of TKE, in which the absolute mean is 5 erg/cm^3, is shown in Fig.3.22. Compared to the timeseries of the seasonal barotropic experiment (Fig.3.12), the absolute mean increased by 25%, and it is the highest of any barotropic run. Thermohaline forcing introduces an additional source of both potential and kinetic energy, so increased energy levels should be expected.

An important feature of Fig 3.22 compared to Fig.3.12 is a presence of an annual oscillations, but still TKE in summer is only little lower (about 15%) than in winter. The
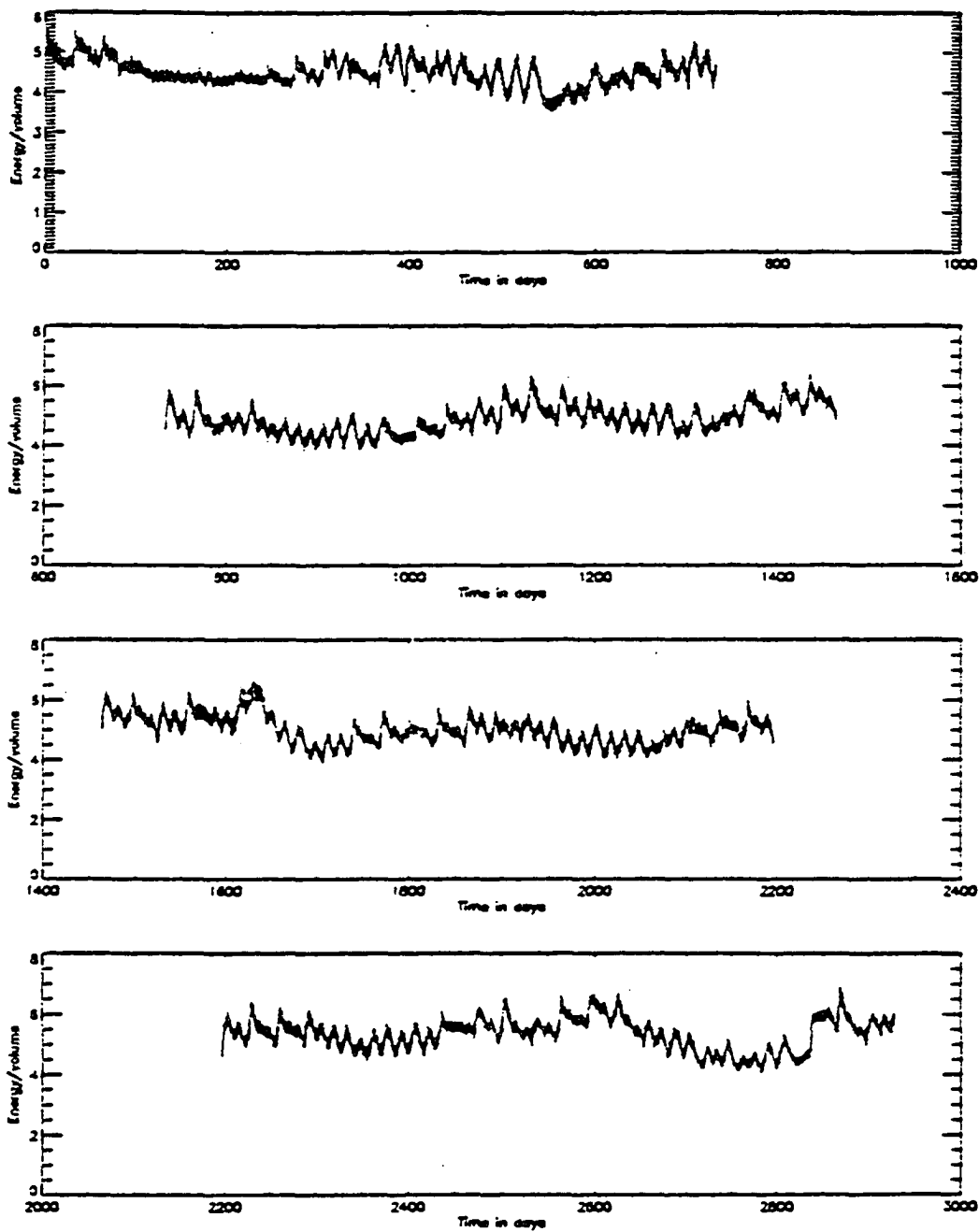
Figure 3.22 Time series of TKE per unit volume
(in erg/cm³) for the seasonal baroclinic experiment.
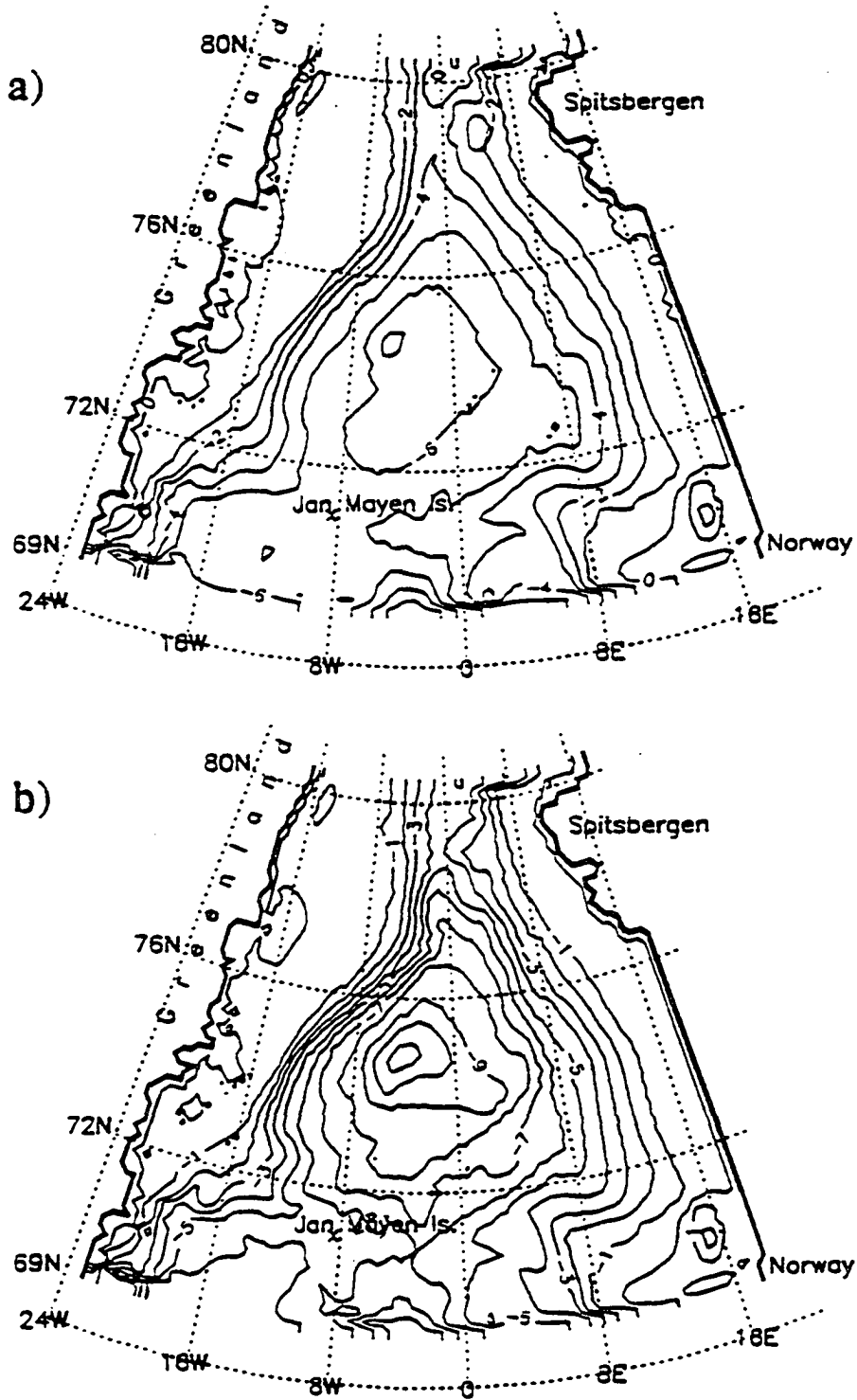
Figure 3.23 a) Summer and b) winter mean circulations of seasonal baroclinic experiment. Contour interval is 1 Sv.

mean vertically integrated summer circulation, as shown in Fig.3.23a, with the Greenland Sea gyre strength of 7 Sv is as energetic as the mean winter circulation of the seasonal barotropic simulations (Fig.3.14b).

The volume exchange on the northern OB is close to 3 Sv in summer, with the excess of inflow recirculating back north. In Fig.3.23b of the mean winter circulation, all prescribed inflow on this boundary is carried farther south, suggesting that in winter (and also in fall) there is more mass being exchanged through Fram Strait between the Greenland Sea and the Arctic Ocean. This is in agreement with observations (Timofeyev, 1962; Hanzlick, 1983; Jonsson, 1989) indicating late fall and winter as a maximum flow of the WSC through Fram Strait. The amplitude of seasonal variability of mass transport through Fram Strait is greater than 1 Sv. The mean strength of the Greenland Sea gyre in winter is greater than 11 Sv, resulting in greater than 4 Sv amplitude of seasonal variations. Dependence of these variations on the strength of winds in all the previous barotropic runs, suggests that the main driving force of the circulation in the Greenland Sea gyre are local winds.

Another way to look at the variability of the currents, is to calculate the range of maximum amplitude variations in the flow. This is shown in Fig.3.24. The main variabilities are still confined to the shelf slope of Greenland, between 73°N and 76°N (compare with Fig.3.5b), but fluctuations of smaller amplitudes are present in most of the area and provide information about the circulation. It can be seen, that greater than

1 Sv variations in the flow through northern boundary is in direct connection with the mass transport from and to the south. Eddy-like variabilities of the order of 2 Sv in Fram Strait indicate the existence of the topographically trapped eddy. which could not be seen in any of the mean seasonal circulation figures. Fig.3.24 also shows that this eddy may depend on the strength of the WSC south of Fram Strait. in the Boreas Basin and over the Knipovich Ridge and continental slope of Spitsbergen.
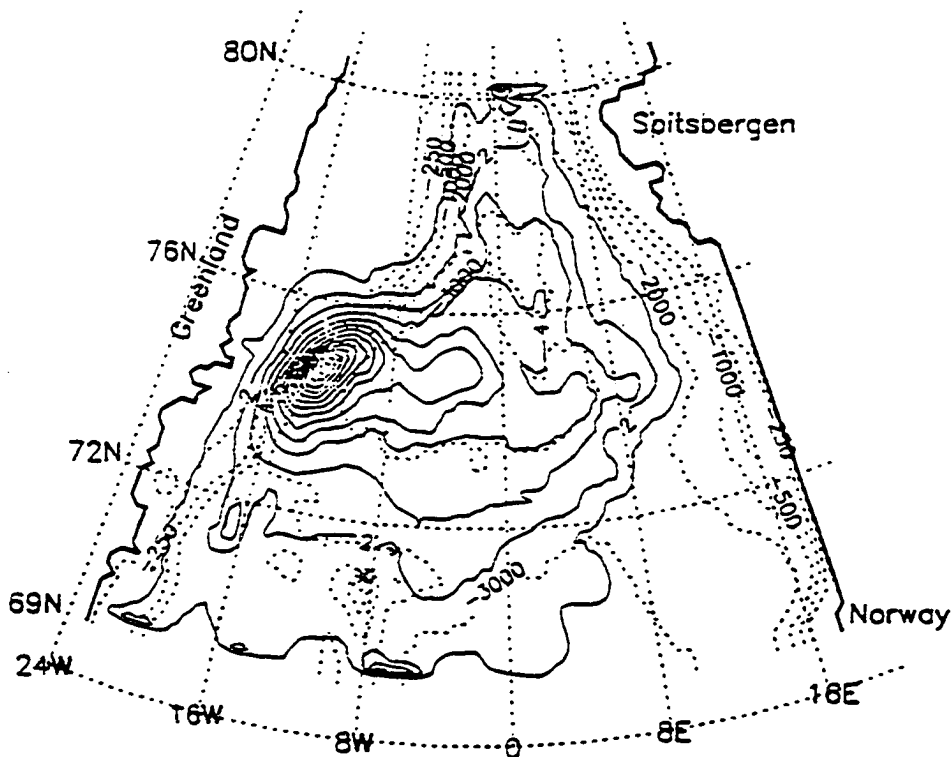
Figure 3.24 Maximum amplitude variabilities of stream function (solid line. CI=1 Sv)

Further information about the temporal and spatial distribution of energy in the region is presented by means of spectral and EOF analysis results. In Fig.3.25 PSD of TKE shows very little difference from the seasonal barotropic experiment (Fig.3.15). The

peak at 17.2 hrs is still dominating the spectrum. The inertial oscillations peak is much stronger now, probably due to additional baroclinic response. Its magnitude is like that of the seasonal barotropic run with doubled wind stresses. The quasigeostrophic normal modes of 30 and 15 day periods are two peaks next in terms of energy concentration, as shown by PSD distribution. EOF analysis (not shown) in the first four EOF modes is identical in eigenvector distributions and TAFs to those of seasonal barotropic experiment (Fig.3.8–3.9 and Fig.3.16–3.17). The difference is in the percentage of the total variance explained, which is now respectively, 41, 36.4, 16 and 3%, accounting together for about 96.5%. Both spectral and EOF analysis results suggest that there is very little influence of baroclinicity in the overall distribution of kinetic energy in the basin. The major part of variabilities carrying the energy is still depth independent, which is in agreement with both observations and the theory on the response of the high latitude oceans to the seasonal forcing (Anderson and Corry, 1985).

Analysis of velocity fields at different layers of the baroclinic model reveals important details of the distribution of currents not apparent from the stream function fields. As an example, the instantaneous circulation as simulated at the end of January of the seventh year of integration is presented at four chosen layers. At the surface (Fig.3.26), mainly wind driven Ekman transport is represented, showing the instantaneous ocean response to the changing wind forcing. The main feature of Fig.3.26 is the well-defined strong EGC with velocities between 10 and 20 cm/s, locally reaching up to 40 cm/s. These speeds agree reasonably with the recent measurements in the EGC around 75°N (Strass
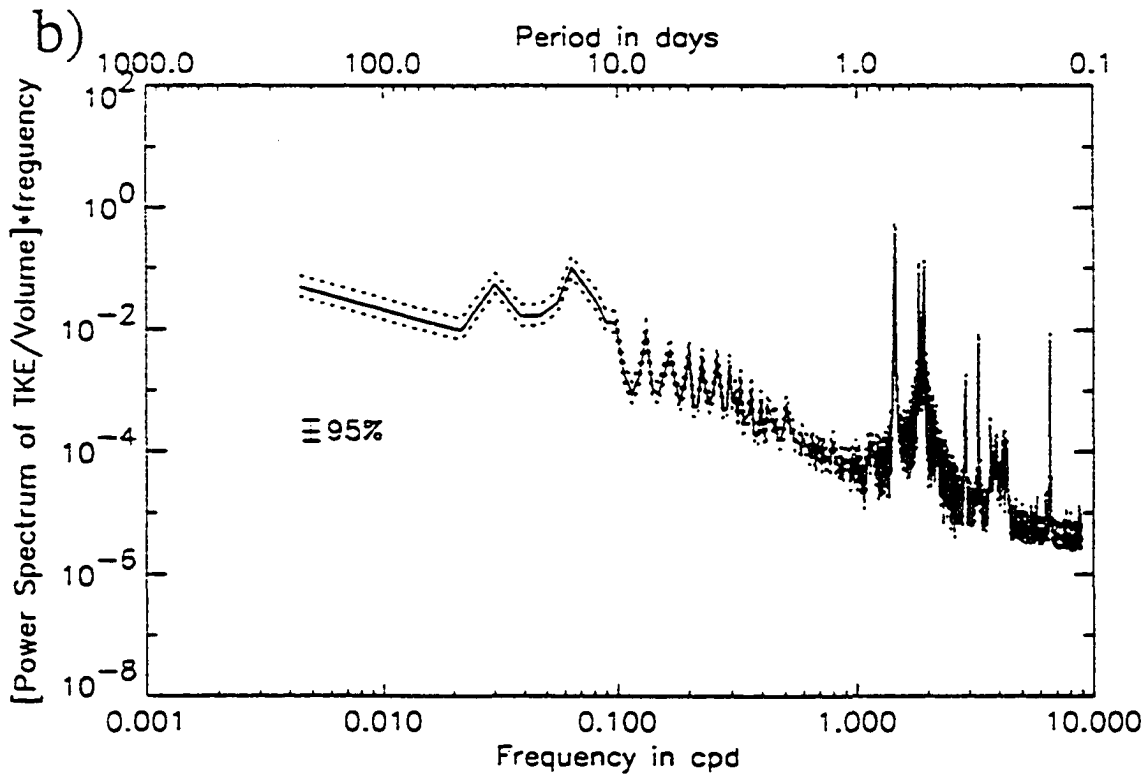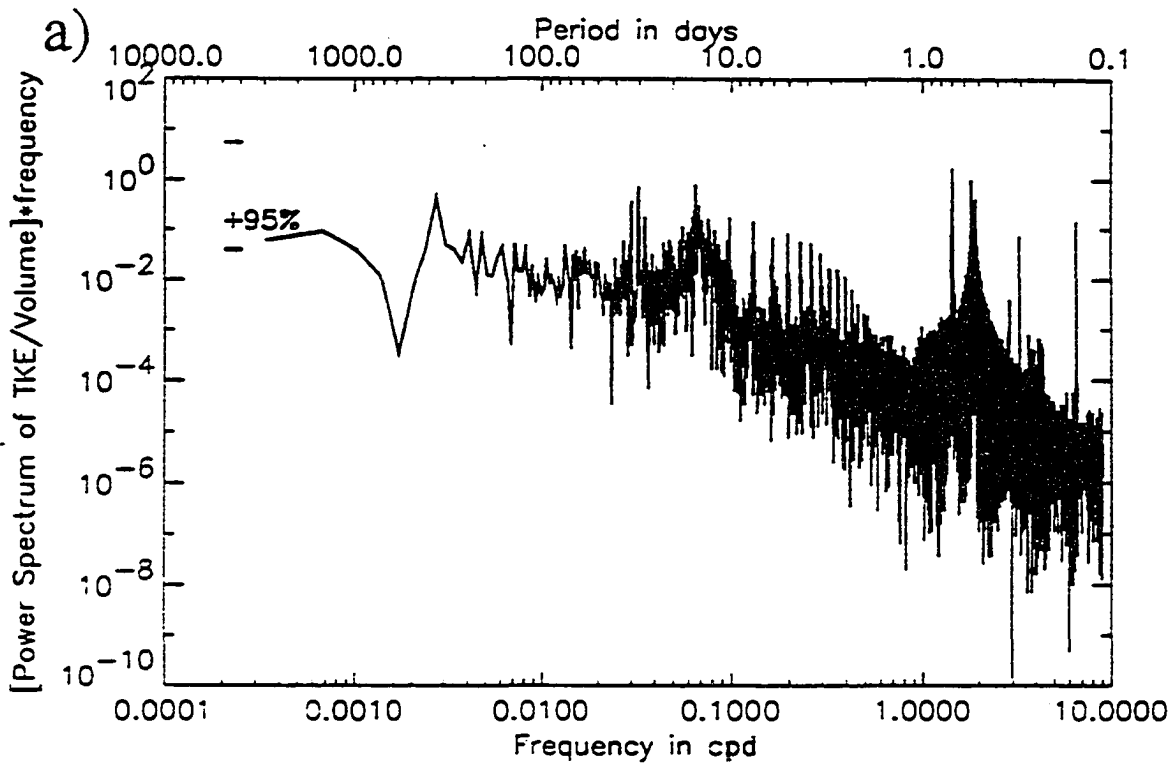
Figure 3.25 Variance preserving power spectral density of
TKE/Volume of seasonal baroclinic experiment: a) dof=2. b) dof=50.

et al., 1993) that give an annual average of ~21 cm/s close to the surface.

On the western side, the WSC is a broad and relatively slow flow to the north with velocities from 5 to locally above 10 cm/s. Measured at 79°N by Hanzlick (1983) average velocities in the WSC range between 5 to 15 cm/s. Also Aagaard et al. (1988) measured velocities of ~15 cm/s at mooring located at 79°N and 8°E, at depth of 80 m. Recirculation of this flow to the west starts south of 75°N and continues up to Fram Strait. where outflow takes place to the east of 0° meridian. and inflow to the west of it. Despite the fact that wind forcing based on the monthly means may not be quite representative of real instantaneous atmospheric fields. simulated ocean speeds compare quite well with observations.

At an intermediate depth of 300m (Fig.3.27) the circulation is not only wind but also thermohaline driven. The Greenland Sea gyre is well defined at this depth, with a separate gyre developed in the Boreas Basin. The core of the EGC has velocities from 5 to above 10 cm/s. and it strongly confined to the continental slope. The jet-like structure of the current agrees with the conclusion of Gascard et al. (1988) stating that the EGC is a narrow and stable (at least in the northern part) current. Between 76°N and 73°N strong cross-isobath currents are observed. indicating topographic wave activity. As a part of such down-slope flow, the Jan Mayen Current branches off to the east at about 73°N. Part of this flow continues further east thus closing the Greenland Sea gyre on the south. but part of it. as a wide meander in the EGC. flows further south into the Iceland Sea. This pattern closely follows the description of Bourke et al. (1992) who suggest that
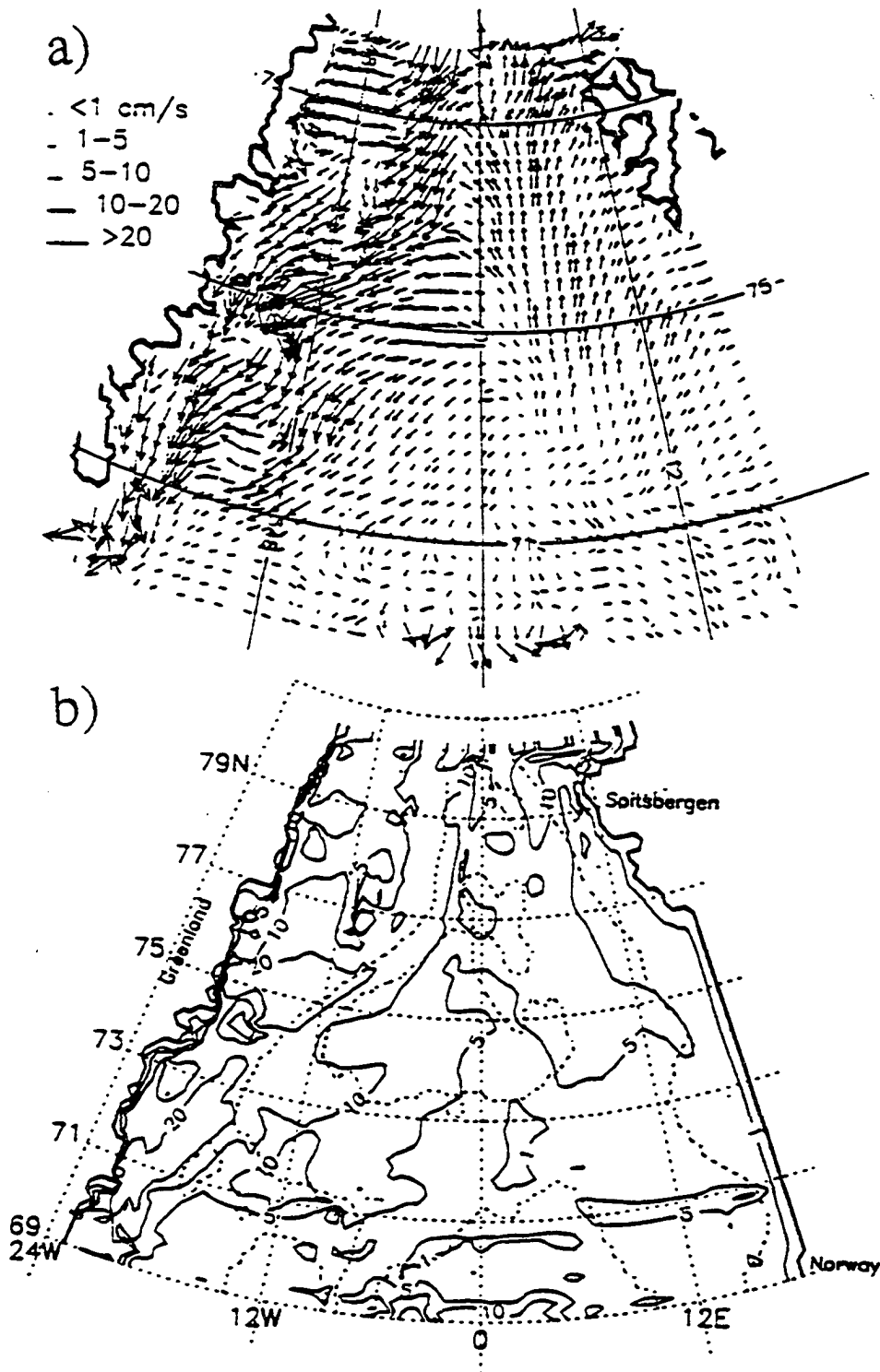
Figure 3.26 Surface horizontal velocity field in January (layer 1, 0–20 m): a) vector field (every 4th point plotted), b) contours of 1, 5, 10, 20 cm/s of velocity magnitude (solid lines) and 1500, 3000 m depths (dotted lines).

a)

. <1 cm/s
- 1-5
- 5-10
— 10-20
— >20

b)

79N

77

75

73

71

69
24W

Greenland

Spitsbergen

Norway

12W

0

12E
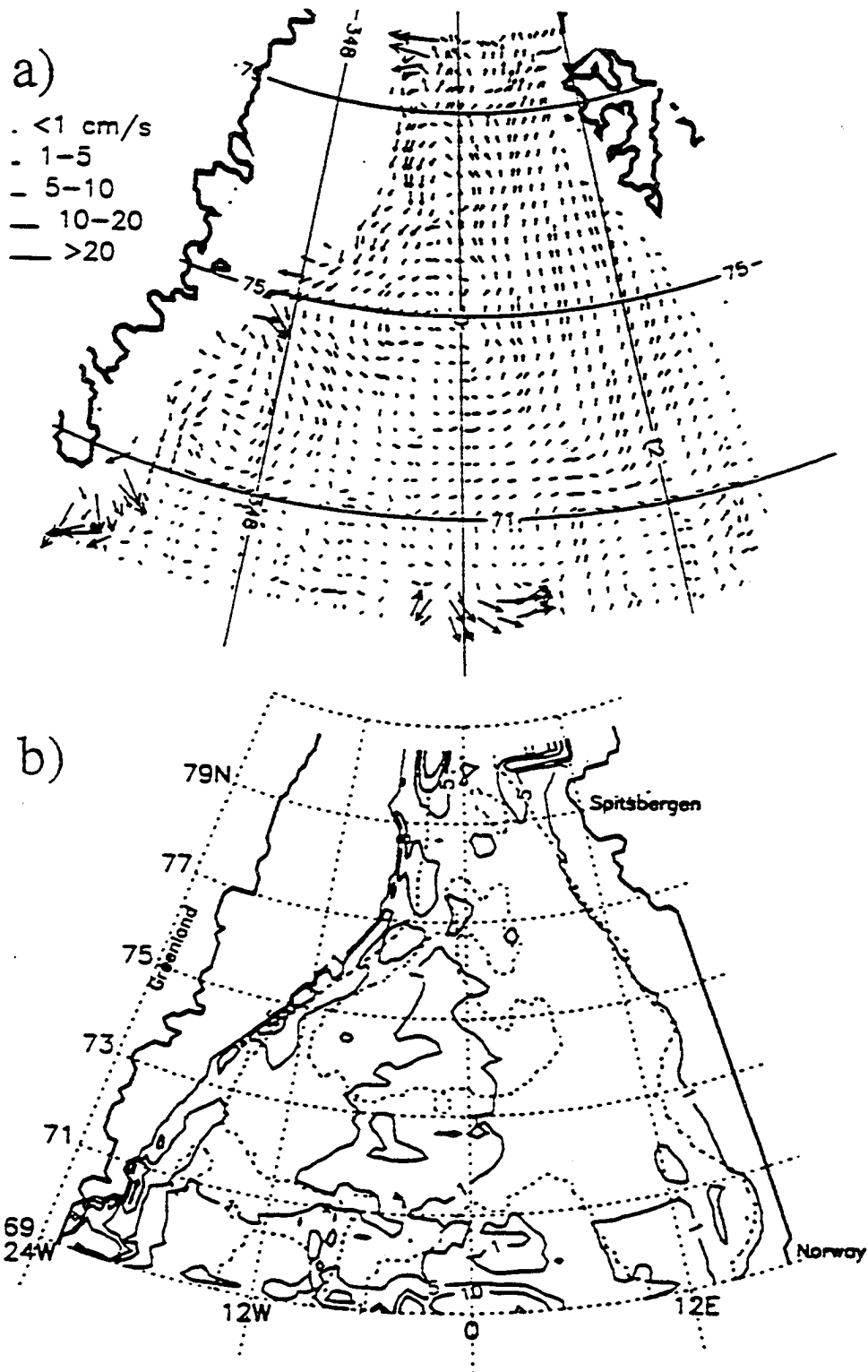
Figure 3.27 As Fig.3.26 but intermediate horizontal velocity field (layer 5. 240–360 m)

in the upper layer baroclinic flow (<100m) about half of the JMC joins the EGC further south, and another half closes the cyclonic gyre in the Greenland Sea. Cross-isobath flow along the Greenland slope can be seen also north of 78°N, but no topographic waves are observed there, suggesting that such waves can develop only in a topographically 'right' environment, i.e., along constant slopes. In Fram Strait, most of the flow is into the Arctic Ocean now, with the inflow pushed against the slope. The western side of the basin is still dominated by the slow northward flow of AW within the WSC. Velocities there are ranging from 1 to 5 cm/s within Fram Strait. At these depths, Aagaard et al. (1985b, 1988) report current speeds between 1.5 and 13 cm/s at moorings located around 79°N across the southern Fram Strait.

Increasing the depth to 1200 m (Fig.3.28) further decreases the magnitude of the currents, but the general pattern of circulation does not change dramatically. The core of the EGC, confined between the 1500 and 3000 m isobaths, has speeds greater then 1 cm/s but only locally exceeds 5 cm/s. A strong topographic steering of the southward flow is present above the GFZ at 77°N. Downstream of this location the EGC develops wave-like cross-isobath motions along the slope. Since no waves are observed north of 77°N, this supports the earlier conclusion about the GFZ producing initial disturbances in the EGC, a mechanism of continental shelf wave generation (Mysak, 1980). Between 75°N and 76°N along the slope, Aagaard et al. (1991) measured velocities, which time-weighted mean value at depths 1200–1300 m was about 12 cm/s. In Fram Strait velocities are between 1 and 5 cm/s, and they are close to those measured by Aagaard et al. (1985b,
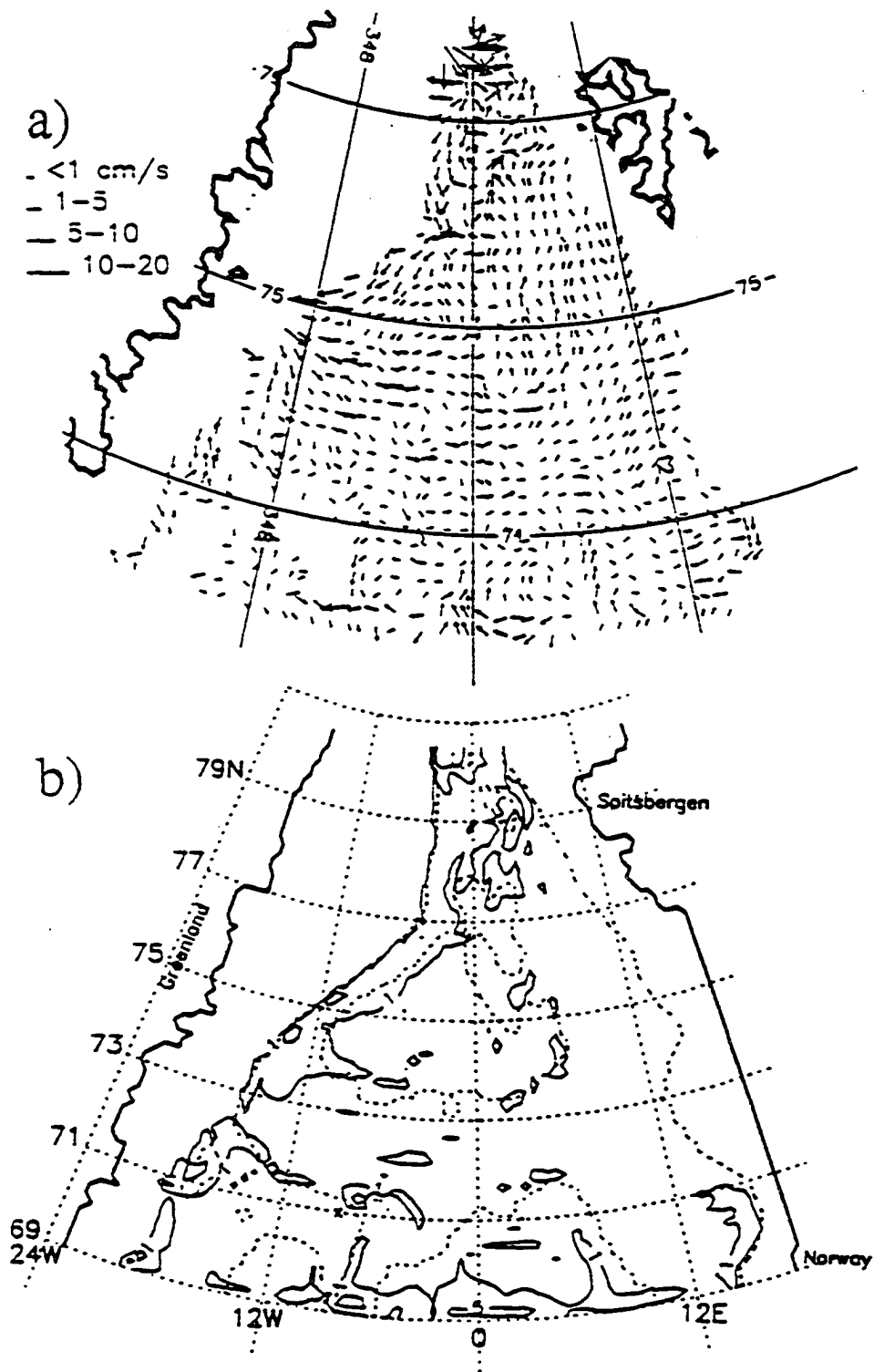
Figure 3.28 As Fig.3.26 but deep horizontal velocity field (layer 10, 1100–1300 m)

1988) at similar depths there. Better agreement of simulated current speeds in Fram Strait, where they are forced by the prescribed stream function on the OB, and much less agreement in the interior, where they depend more on wind stress, may be due to problems in the derived monthly mean wind forcing. The next baroclinic experiment will address this issue.

Deep circulation at 2000 m, which is quite similar to that at 1200 m is shown mainly to illustrate the simulated deep overflow of water from the Greenland Sea into the Norwegian Sea. Bourke et al. (1993) suggest a passage through Mohn's Ridge near 72°N and 2°W as likely route of newly formed NSDW, the mixture of AODW with GSDW. They report that the flow, after reaching the east side of the ridge, reversed and returned to the Greenland Sea with the mean generally northward flow of AW. Just such a picture is closely simulated by the velocity distribution at this and also at the 1200 m depth layers.

a)

<1 cm/s
1-5
5-10
10-20

b)

79N

Spitsbergen

77

Greenland

75

73

71

69
24W

Norway

12W

12E

0
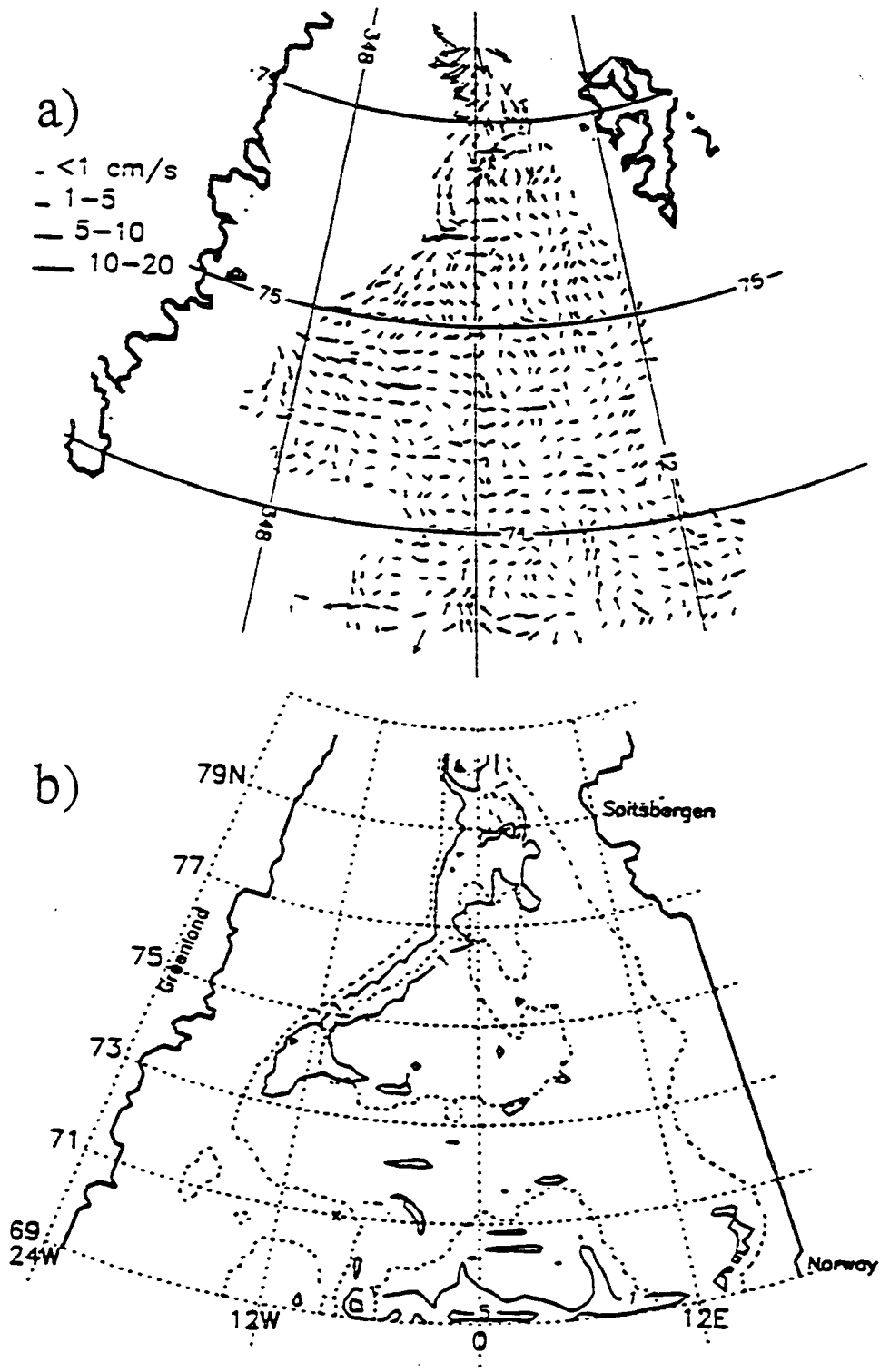
Figure 3.29 As Fig.3.28 but (layer 14, 1900-2100 m)

Section 3.6 Seasonal strong wind baroclinic experiment

3.6.1 Introduction

As in the case of barotropic experiments, the ocean response to strong wind forcing is investigated also by the baroclinic model. Although some seasonal oscillations are present in the seasonal baroclinic case, velocity fields. especially in the interior were still below observed values. so the wind stresses are doubled in this experiment. The arguments supporting such an approach were discussed in section 3.4. Simulation results with doubled wind stresses. by comparison with the previous experiment. will also identify regions in the Greenland Sea that strongly depend on the local wind forcing.

The methods discussed in the first baroclinic run. the model configuration and all the parameters are the same as before. except for wind stress which is doubled here.

3.6.2 Results and analysis

The model was restarted from the end state of the seasonal baroclinic case and run for another 10 years. The seasonal cycle. as shown in Fig.3.30. has a strong clearly pronounced signal. The absolute mean of this stationary timeseries of TKE is 6 erg/cm^3 and it reaches well above 9 erg/cm^3 in winter. Such energy levels do not depart much from the other experiments. suggesting that doubling of wind stresses may still produce quite realistic results.

In summer. the mean vertically integrated circulation (Fig.3.31a) has not changed compared to the run with original winds (Fig.3.23a). It is still quite weak with the
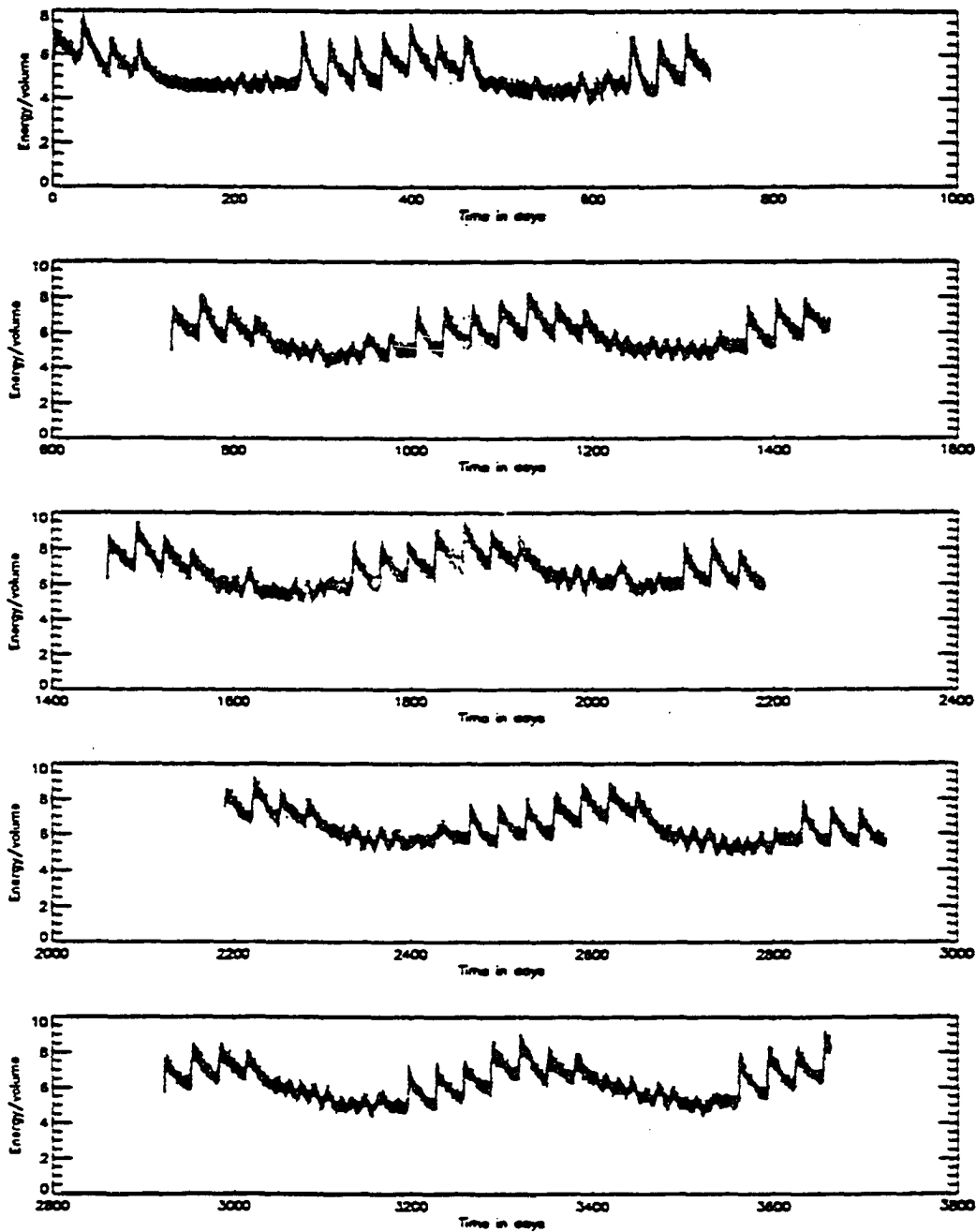
Figure 3.30 The timeseries of TKE per unit volume
from the seasonal strong wind baroclinic experiment.
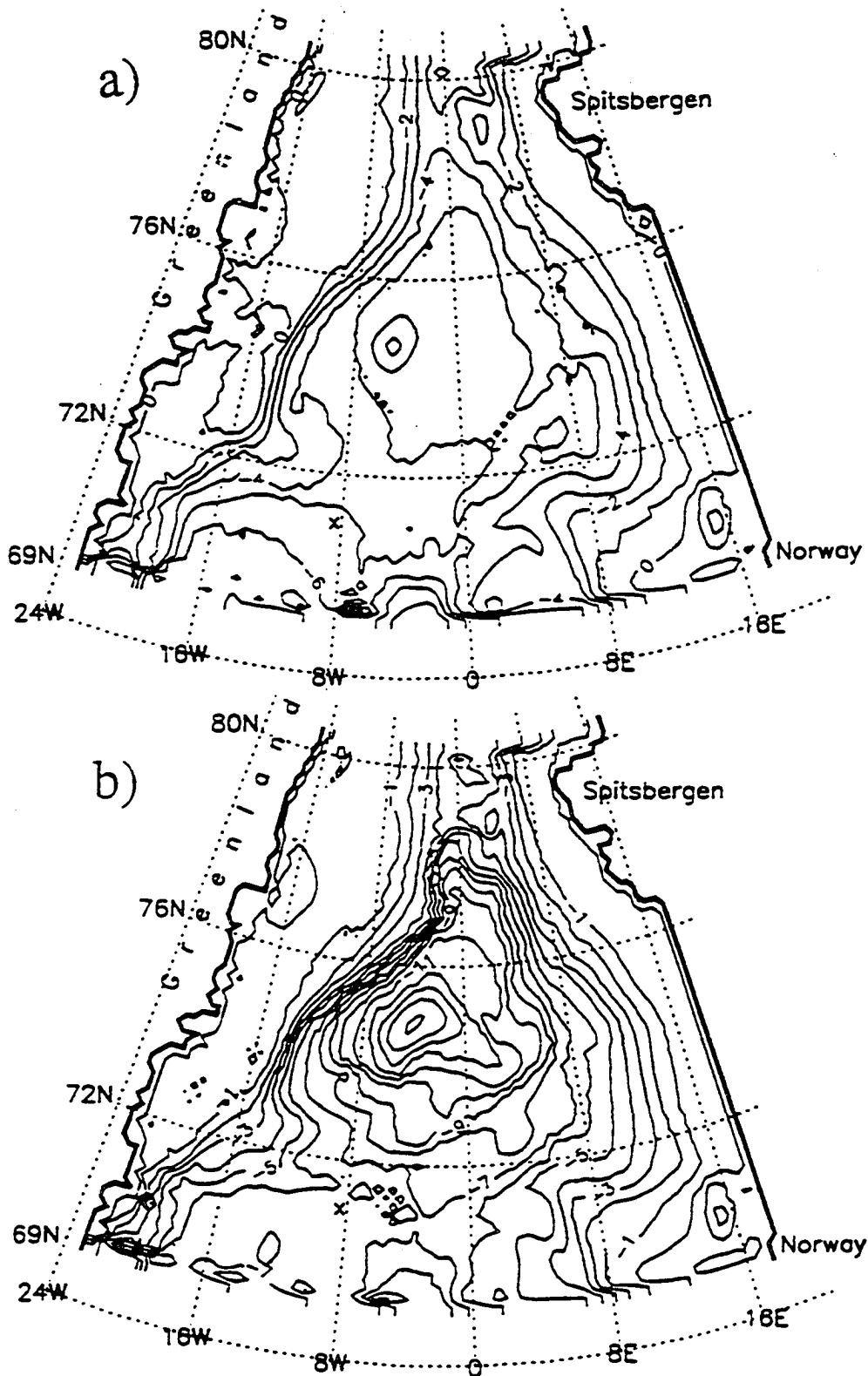
Figure 3.31 a) Summer and b) winter mean circulations of seasonal strong wind baroclinic experiment. Contour interval is 1 Sv.

Greenland Sea gyre strength of 6–7 Sv. As before, part of the inflow on the northern OB recirculates back, indicating that in summer less than 4 Sv of water takes part in the mass exchange process between the Arctic Ocean and the GIN Sea. The presence of the Lena Trough in the northern part of Fram Strait, combined with the topographic steering can in reality produce recirculation there, especially during weak winds.

Another interesting feature in Fram Strait, already apparent in Fig.3.23a, is an anticyclonic eddy a little south of the Molloy Deep. The recirculation of the inflow on the boundary and the westward flow in the northern Boreas Basin and over the Hovgard Fracture Zone, sets the right conditions for an anticyclonic eddy in between. As depicted in the mean winter circulation figure (Fig.3.31b), such an eddy may still exist even when there is a cyclonic eddy present slightly to the northwest of the Molloy Deep. The latter eddy has been analyzed in the previous experiments and has been reported in literature (Bourke et al., 1987: Smith et al., 1984: Vinje, 1977: Wadhams and Squire, 1983). The dynamics of Fram Strait seem to be strongly influenced by the basin-wide oscillation of the 30 days, which will be discussed further in the EOF analysis.

A plot of maximum amplitude current variabilities (Fig.3.32a) shows two maxima, one related to topographic wave activity over the Greenland shelf slope, and other even stronger, with amplitude of 15 Sv, located in the Greenland Basin. Increased winds influence the circulation of the Greenland Sea gyre which controls the flow through Fram Strait. The amplitude of the mass flow through the strait can vary over a year by

more than 2 Sv, which is in agreement with recent estimate (Jonsson, 1989) of 3±1 Sv. Since the stream function is explicitly prescribed on the northern OB, it is difficult to decide how much winds influence the WSC and EGC north of the Boreas Basin, but they definitively do. Doubled wind stress increased variability of the flow through Fram Strait by more than 1 Sv, from the seasonal baroclinic experiment with original winds (compare Fig.3.32a and Fig.3.24). In the central Greenland Sea at the same time, amplitudes have risen from 6 Sv to 15 Sv. Such big amplitudes are obtained with both strong winter and weak summer circulations.

Fig.3.32b shows instantaneous vertically integrated flow at the end of February of the ninth year of integration. The Greenland Sea gyre strength of 20 Sv, although higher than in any other experiment, it is still below the mean integrated Sverdrup transport estimated by Aagaard (1970) and Jonsson (1989) at about 35 Sv. Even during a period of strong winter winds, the gyre strength can change by 3–5 Sv over a time scale of several to tens of days. The results presented here suggested that circulation in the region is not directly related to wind forcing, but it is rather controlled by basin-wide and regional scale the Rossby normal modes, that are excited by variable winds but undergo their own dynamics. Normal mode oscillations can possibly be generated in the Greenland Sea by frequent severe storms passing through (Fig.1.9b). The Icelandic Low together with the Aleutian Low in winter are the most powerful in the northern hemisphere (Hellerman and Rosenstein, 1983; Jonsson, 1989). Some support for existence of quasigeostrophic normal modes in the modeled region has been provided in the previous experiments. The
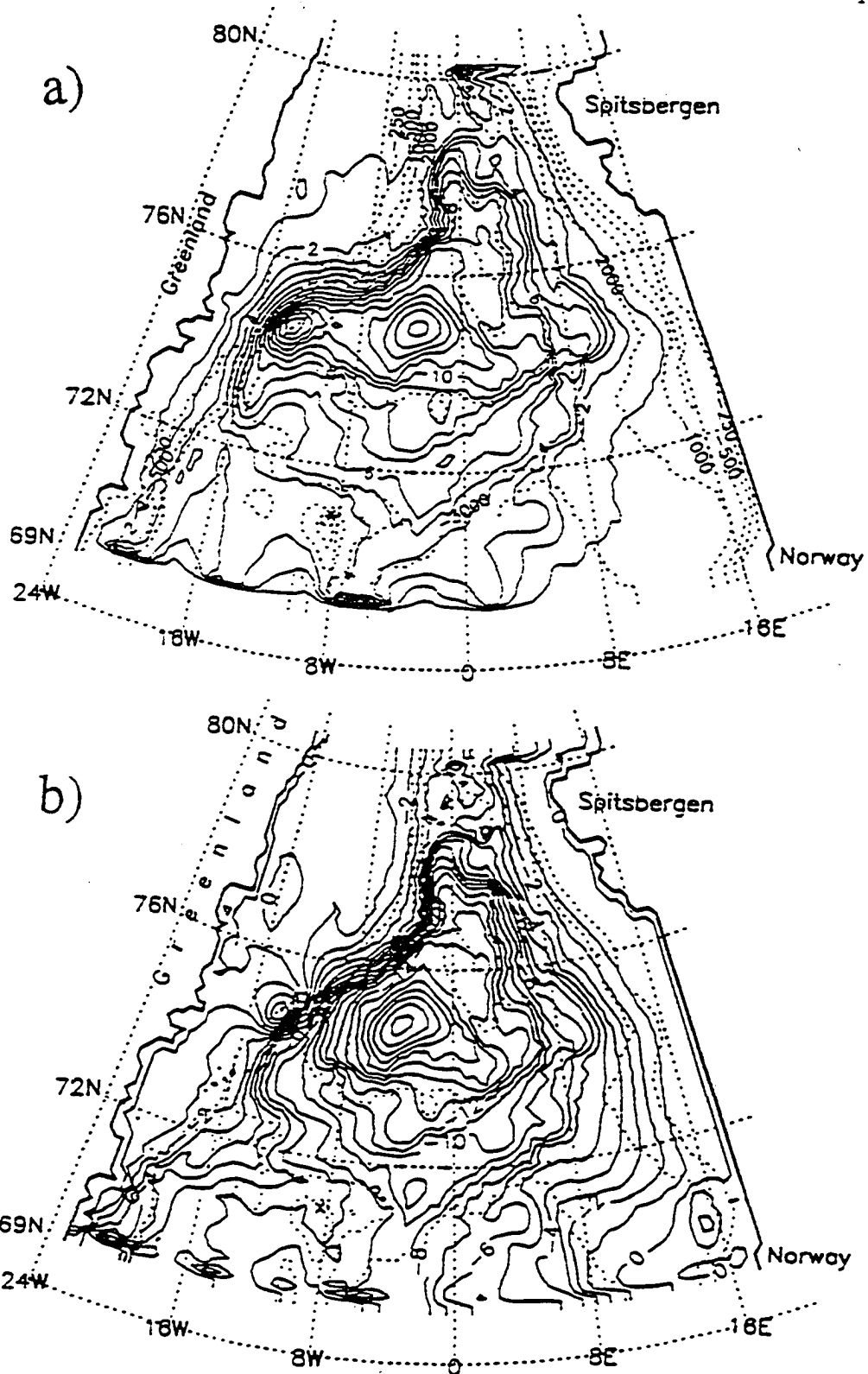
Figure 3.32 a) Maximum amplitude current variabilities and b) instantaneous (day 2972) vertically integrated circulation of seasonal strong wind baroclinic case.

following spectral and EOF analysis will shed more light on this issue.

As shown earlier, there exist few major peaks in PSD (Fig.3.33) of the TKE timeseries. There is an annual peak related to the variable annual wind forcing. The 17.2 hrs peak, explained by propagation of topographic planetary waves along the Greenland slope was extensively analyzed in section 3.2. At about 12.5 hrs period, the inertial oscillations peak has been identified. In the seasonal strong wind barotropic experiment, peaks in range of frequency between 0.4 to 0.033 cpd. with a leading peak at 30 day period (0.033 cpd) has been explained as basin and smaller scale normal modes. All these peaks are present in this experiment with only differences in their magnitude. Thus their existence. unlike magnitude. is not dependent on the stratification.

EOF analysis of the 60 day-long time series of the stream function sampled every third point in space and every 2 hours in time is presented in Fig.3.34. The first EOF mode. explaining 45.3% of the total variance. shows basin-wide oscillations with the period of 30 days. Such oscillations. especially in winter, are readily seen in the timeseries of TKE. Fig.3.30. All the current fluctuations to the east of the EGF, including the Greenland Sea gyre and the flow through Fram Strait are explained by this mode. This same mode explained only 16% in the seasonal baroclinic run. and 33% in the seasonal strong wind barotropic case. Both wind forcing and stratification seem to influence the level of current variabilities in this EOF mode.

The next two EOF modes. 2 and 3, accounting respectively for 20.4% and 18.3% of the total variance. are confined above the shelf slope in the EGC. between 77°N and 73°N.
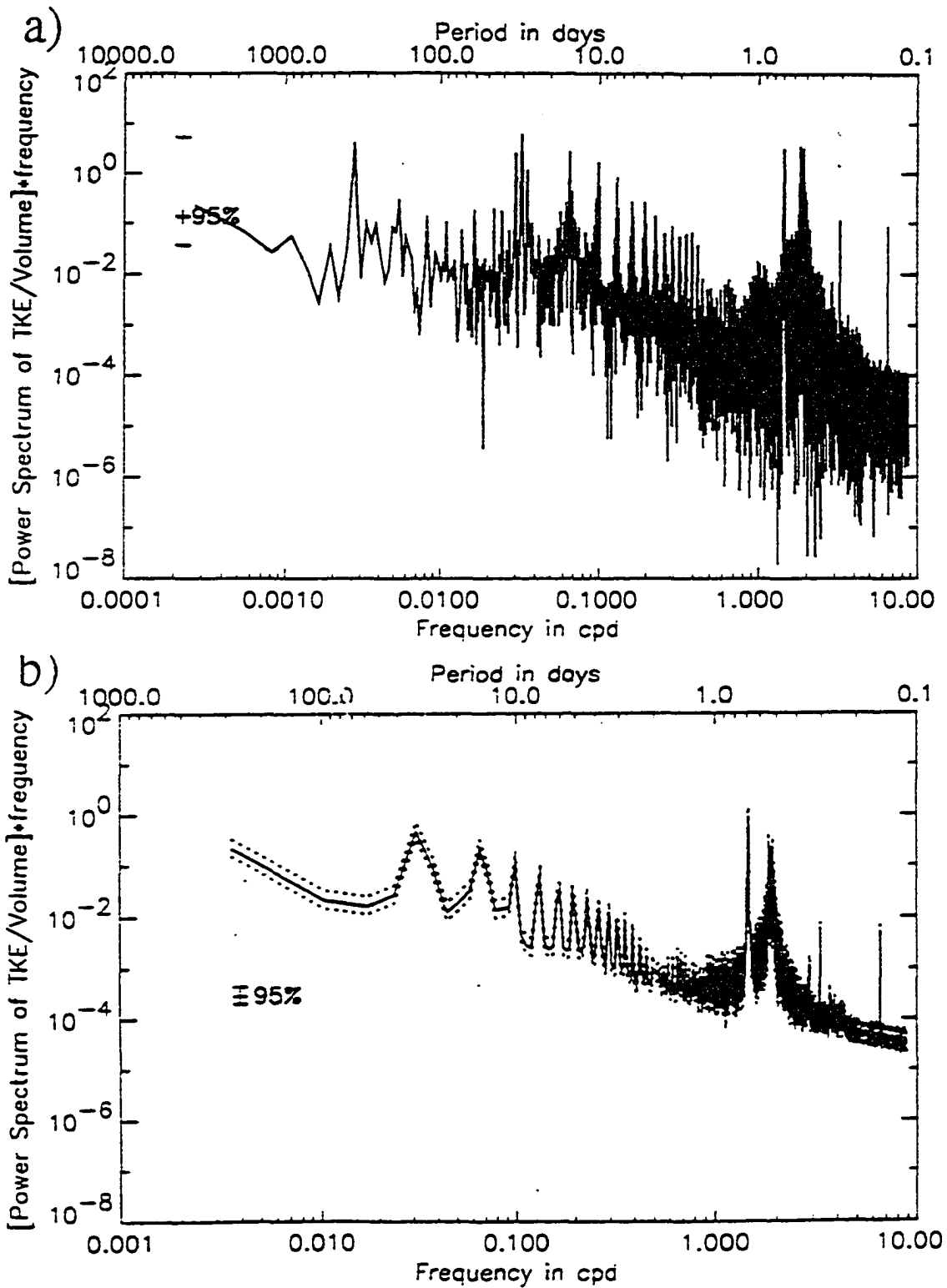
Figure 3.33 Variance preserving power spectral density of the TKE/Volume of seasonal strong wind baroclinic experiment: a) dof=2. b) dof=50.

These two modes although orthogonal to each other. since both are of similar variance. the period of 17.2 hrs. and very similar eigenvector distribution, are part of the same statistical propagating process (North et al., 1982; White and Tabata, 1987), as illustrated earlier by Fig.3.4 and Fig.3.6 of section 3.2.The phase, propagating southward along the slope as shown in the eigenvector distributions, describes continental shelf wave activity.

The fourth EOF mode. which explains 7.5% of variance, has periods similar to those of the first EOF mode. but its eigenvector divides the modeled region into two parts: one in the center and the second adjacent to the boundary. The first part consists of two separate gyres. one in the Greenland Basin. and one. connected to the EGC inflow from the north. in the Boreas Basin. These two areas. although in phase, are separated by the GFZ which is responsible for separation of circulation in the two deep basins due to topographic steering, and the generation of the initial disturbance in the southward flow of the EGC. The first four EOF modes together account for 91.5% of the total variance. and they define two main periods of oscillation: the period of 30 days of quasigeostrophic normal mode. and the 17.2 hrs period of the topographic planetary waves.

For comparison of the modeled and observed energy levels. instantaneous velocity fields at day 2943 (January 30) at two chosen levels are shown. At the surface (Fig.3.35) the EGC south of $77°N$ has speeds greater than 20 cm/s. and further south they often exceed 30 cm/s. Sellmann et al. (1992) and Strass et al. (1993) report the mean velocities ranging from 6.5 to 21 cm/s. from moorings located in the upper layer between

75°N and 76°N across the slope. The maximum measured values are above 60 cm/s and generally they are decreasing seaward off the slope. Paquette et al. (1985), for a narrow frontal jet associated with the EGF within the EGC, obtain velocities greater than 80 cm/s. The maximum surface velocity of the EGC in this experiment is above 40 cm/s. A scale of the order of 5 km suggested by Paquette et al., necessary to resolve frontal jet structure is much beyond the model resolution, though. Model velocities in the Greenland Sea decrease from above 20 cm/s within the Greenland slope to below 5 cm/s in the southeastern Greenland Basin, and a similar decreasing trend can be deduced from the observations.

In the WSC speeds generally increase going to the north, from below 5 cm/s south of 74°N to 10–20 cm/s north of 77°N, and locally are higher than 20 cm/s at locations above the shelf slope in Fram Strait. Hanzlick (1983) and Aagaard et al. (1985b, 1988), report average velocities in the WSC at 79°N range from 5 to 15 cm/s. The mean velocity of 15.4 cm/s at a depth of 79 m is reported from the mooring located at ∼79°N and 8°E and it also compares well with the value of about 20 cm/s obtained at a similar location in the stronger-than-annual-mean model winter circulation presented here. The results of the surface velocity field in this last experiment, representing wind driven Ekman transport, are in much better agreement with the observations than those of the seasonal baroclinic experiment, suggesting that doubled wind stresses better represent real wind forcing than the original monthly means of Hellerman and Rosenstein (1983).

To complete this analysis, energy levels of deep circulation at 1200 m (Fig.3.36) are
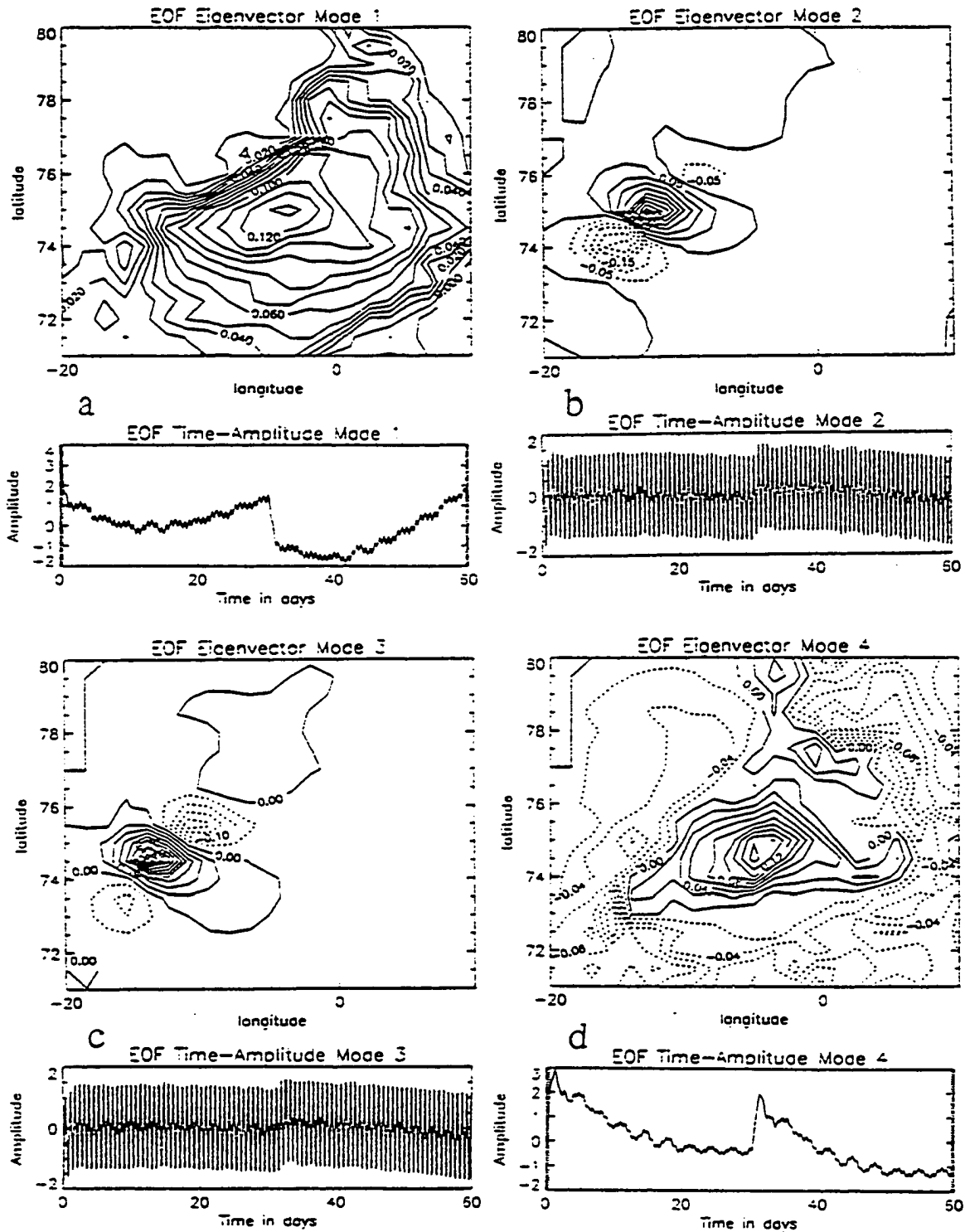
Figure 3.34 EOF time-amplitude function and eigenvector of mode:
a) 1. b) 2. c) 3. d) 4 of seasonal strong wind baroclinic experiment.
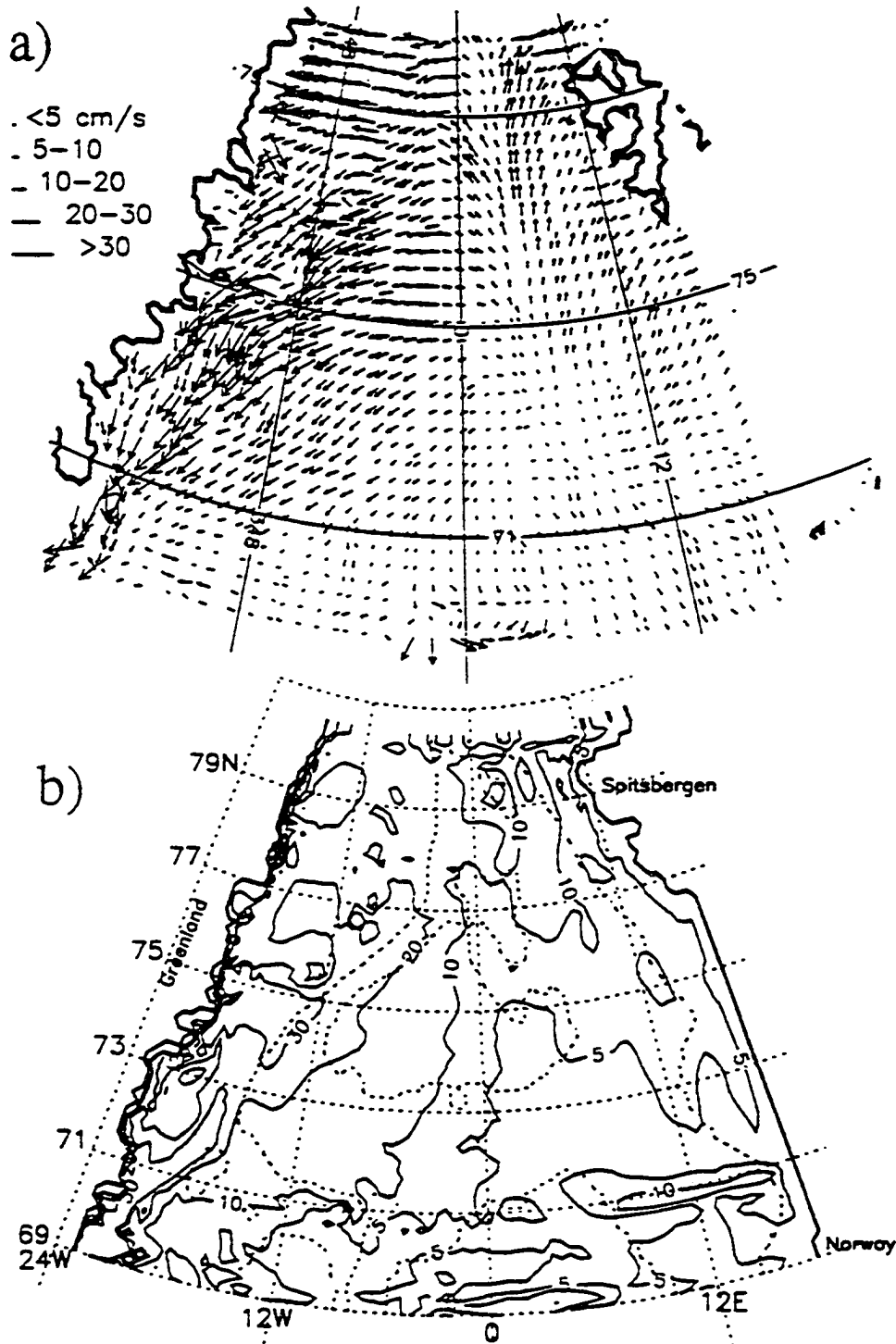
Figure 3.35 Surface horizontal velocity field of seasonal strong wind baroclinic experiment (day 2943. layer 1. 0–20 m): a) vector field (every 4th point plotted). b) contours of 5. 10. 20. 30 cm/s of velocity magnitude (solid) and 1500. 3000 m depths (dotted).

a)

- <1 cm/s
- 1-5
— 5-10
— >10

b)

79N

Spitsbergen

77

75

Greenland

73

71

69
24W

12W

0

12E

Norway
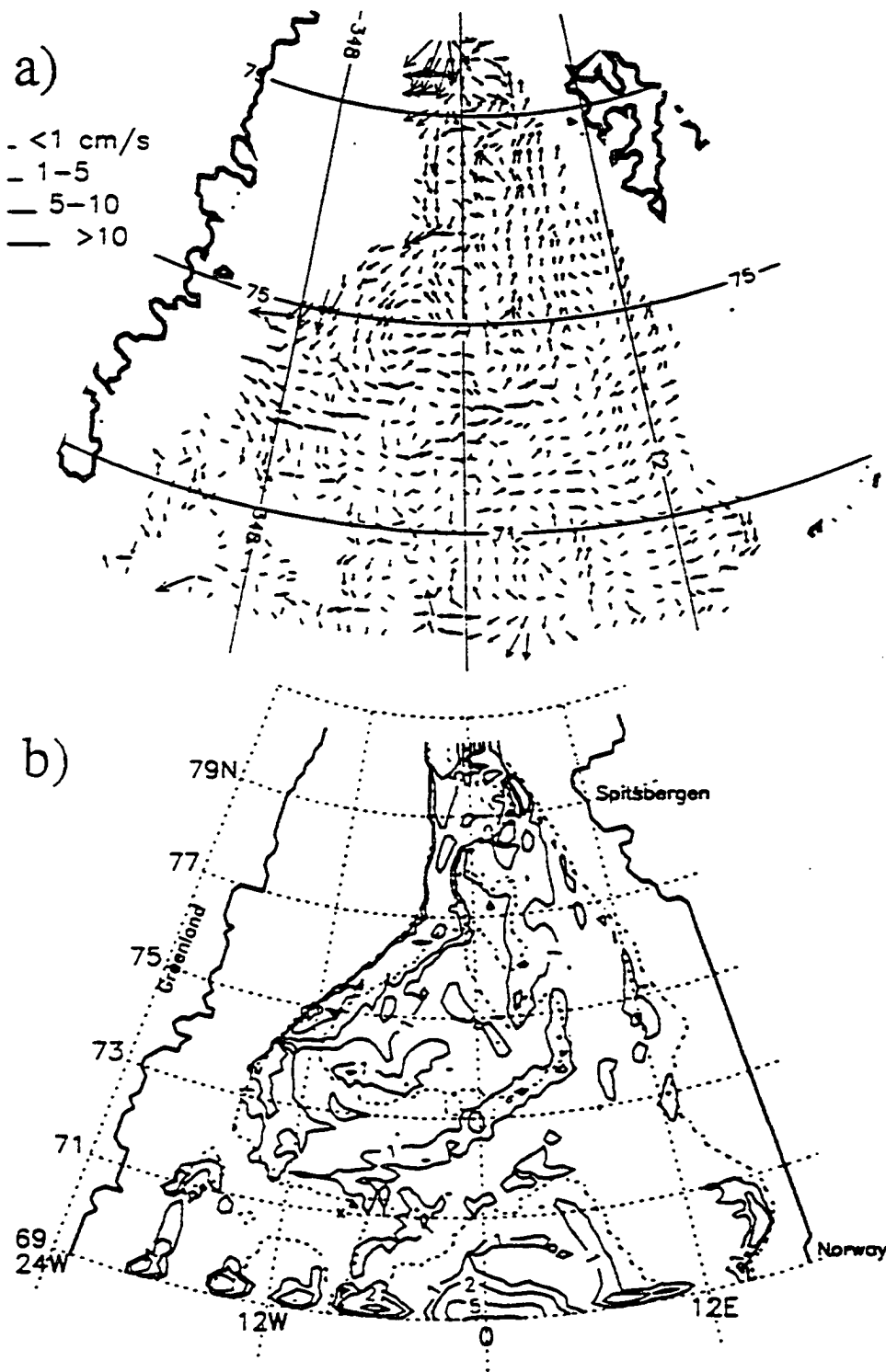
Figure 3.36 As Fig.3.35 but deep horizontal velocity field (layer 10. 1100–1300 m).

compared with available field measurements. At 75°N simulated velocities over the slope are between 5 and 10 cm/s. Most of the EGC has the speeds in the range of 2–5 cm/s. At this location and depth, observed mean velocities (Strass et al., 1993; Sellmann et al., 1992) range from 9 to 14 cm/s. In the WSC at this depths at 79°N, Aagaard et al. (1985b, 1988) report velocities around 2 cm/s, and this is about the same as simulated here.

Section 3.7 <u>Conclusions</u>

A series of numerical experiments described and discussed in this chapter provides information on the importance of wind and thermohaline forcing on the Greenland Sea circulation. A major outcome of this approach is the simulation of topographic planetary wave propagation along the shelf slope of Greenland between 77°N and 72°N. Analysis of the results. including spectral and EOF analysis. showed a period of 17.2 hrs. a wavelength of 363 km. and a phase speed of 586 cm/s. The southward flow of the EGC together with recirculating AW in the Boreas Basin. is disturbed by the presence of the GFZ. By means of conservation of the potential vorticity. flow over a variable bottom translates into an initial disturbance of the quasigeostrophic flow. traveling as a topographic planetary wave along the relatively constant Greenland shelf slope between 77°N and 73°N. Downstream. where slopes in the along-slope direction become much more variable. these waves are dispersed. Most of energy related with wave activity, propagates back along the slope. to the northeast. with the group velocity $C_{gy'}=396$ cm/s. However some energy propagates in the offshore direction. with group velocity $C_{gx'}=103$ cm/s. The latter component of the group velocity may provide energy for cross-frontal mixing in the EGC. The process of isopycnal mixing across the EGF results in formation of DSOW. and diapycnal mixing of AODW with GSDW across the slope below 2000 m governs formation of NSDW. Both water masses are the main source of NADW. which has been suggested to drive the global ocean conveyor belt circulation.

Simulation with different wind forcing schemes suggest strong dependence of the Greenland Sea gyre circulation on the variations with time of the local wind stress curl. Between the original wind stress experiment and doubled wind stress forcing, the mean winter gyre strength changes from 7 to 11 Sv in the barotropic experiments, and from 11 to 15 Sv in the seasonal baroclinic experiments. The maximum instantaneous strength of the Greenland Sea gyre in the seasonal strong wind baroclinic experiment reaches 20 Sv.

Results obtained in the experiments with doubled wind stress are in better agreement with observations than are the experiments that used the original monthly mean wind stress. Smoothing due to time averaging, interpolation due to scarce data in the region, and small values of the drag coefficient used in wind stress calculations, are the probable factors resulting in an underestimate of wind forcing in the model.

Overall, results of the baroclinic experiments are more energetic than barotropic ones, because the thermohaline forcing introduces an additional source of kinetic energy. Also vertical decoupling of horizontal currents allows for more energetic motions. The influence of wind and thermohaline forcing on the levels of energy in each experiment is shown by means of spectral analysis. Annual, inertial and quasigeostrophic normal mode oscillations show peaks of increasing energy concentrations with stronger winds and stratification. Also the absolute mean TKE per unit volume indicates increasing energy when increased winds or baroclinicity are introduced.

As expected in a high latitude region with weak stratification, major part of variabil-

ities (as shown by spectral and EOF analysis) carrying most of the energy is barotropic hence also depth independent. The mainly barotropic ocean response to seasonal forcing, implies a strong topographic control in the distribution of currents and hydrographic variables.

A cyclonic eddy topographically trapped on the depression depicted by the 3000 m isobath in Fram Strait north of 79°N, is a typical example of such topographic control. Its presence is explained in term of the potential vorticity conservation in the northward flow of the WSC. EOF analysis shows the direct dependence of this eddy on the large scale dynamics, resulting in the northward mass transport of the WSC. By trapping some of the WSC flow, the eddy eventually acts to control a net flow of the WSC into the Arctic Ocean.

Another example of topographic steering is the Greenland Sea gyre separation into two gyres, one in the Greenland Basin and one smaller in the Boreas Basin. The GFZ between the deep basins strongly influences the southward flow of the EGC. Also the westward turning branch of the WSC in the Boreas Basin as well as the EGC are closely correlated to local topography. The EGF (Fig.1.5), which is strongly correlated with the Greenland shelf break, separates fresh and cold waters to the west from the warm and saline waters to the east, exemplifying the role of topography in the distribution of hydrographic variables. Velocity fields analyzed at different depths, compare reasonably well with observations, especially in the seasonal strong wind baroclinic experiment.

From the numerical point of view, results on the northern OB suggest the possibility of variable-in-time simulations of mass, heat and salt transport across the boundary. An open boundary, if chosen in an area where flow is not too complicated and is well measured, may allow for a satisfactory treatment of the time dependent solution of this ill-posed problem.

Chapter 4 THE SALINITY ANOMALY SIGNAL IN THE GREENLAND SEA GYRE

Section 4.1 Introduction

Deep water formation is the most important climatic feature of the Arctic Ocean and its adjacent seas (Broecker. 1991). A path of the deep flow from the central basins of the Arctic Ocean overflowing the Greenland-Iceland-Scotland Ridge system into the Atlantic Ocean can be summarized as follows. In the Arctic Ocean. a saline and relatively warm deep water (AODW), which most probably originates in the surrounding shelf seas (Aagaard. 1981: Aagaard et al.. 1985a: Swift et al.. 1983), enters the Greenland Sea through Fram Strait (Aagaard et al.. 1985a. 1991: Smethie et al.. 1988: Swift and Koltermann. 1988). Near the center of the Greenland and Boreas Basins. much colder and fresher GSDW is formed by convection (Bogorodskii et al.. 1987: Johannessen et al.. 1991: Roach et al.. 1993; Rudels et al., 1989; Rudels. 1990), which by mixing with AODW forms Norwegian Sea Deep Water (NSDW) (Aagaard et al.. 1985. 1991: Bourke et al.. 1993: Rudels. 1986: Swift and Koltermann. 1988). This water overflows the Iceland-Scotland Ridge becoming one of the two major sources of NADW. The other source. Denmark Strait Overflow Water (DSOW) is formed at intermediate depths of the EGC (Roach et al.. 1993: Strass et al.. 1993) and in the Iceland Sea (Swift et al.. 1980: Swift and Aagaard. 1981). and overflows Denmark Strait between Greenland and Iceland.

152

Deep waters formed in the northern North Atlantic and at various sites on the continental shelf of Antarctica. drive the thermohaline or the conveyor-belt circulation. i.e., a global-scale transport of heat and fresh water between the high-latitude North Atlantic and the Pacific Ocean (Fig.1.8). Alternation in the supply of these waters. especially NADW, establishes their controlling role on the thermohaline circulation which in turn. defines their importance in global climate change.

Some very cold periods in the past might be the result of a temporary shutdown of the conveyor. known as halocline catastrophes. and are proposed for past deglaciations (Broecker. 1987. 1991). Analysis of paleoclimatic data and model simulations (Bryan. 1986) suggest that the strength and pattern of the thermohaline circulation have changed significantly between glacial and interglacial periods. A common element of such theories is the interaction between the thermohaline circulation and the salinity distribution. Salinity variations dominate the buoyancy distribution at low temperatures. i.e.. at high latitudes. where deep water forms.

The Great Salinity Anomaly (GSA) of the late 1960s and 1970s (Dickson et al.. 1988), as manifested by salinity decreases of 0.1-0.2 psu (Fig.4.1) due to anomalously large sea ice and fresh water outflow from the Arctic. may be considered as a small-scale analog of the halocline catastrophes. The effect of the GSA in the Greenland Sea is by now well understood (Aagaard et al.. 1991; Clarke et al.. 1990: Schlosser et al.. 1991: Rhein. 1991). Beginning in the late 1970s through 1980s. the formation of GSDW was reduced by about 80%. A capping of the convection in the Greenland Sea combined with

continuous flow of AODW, resulted in a markedly warmer, slightly more saline. and less

dense deep regime in both the Greenland and Norwegian Seas.

Modeling of the GSA (Hakkinen. 1993 – hereafter referred to as H93) supports the

sea ice advection hypothesis of Aagaard and Carmack (1989) as the anomaly origin. but

the study also suggests a salinity minimum in the upper water column of the Greenland

Sea occurred in 1968. i.e.. the year when maximum sea ice outflow from the Arctic Ocean

through Fram Strait is simulated. However. according to multitracer measurements of
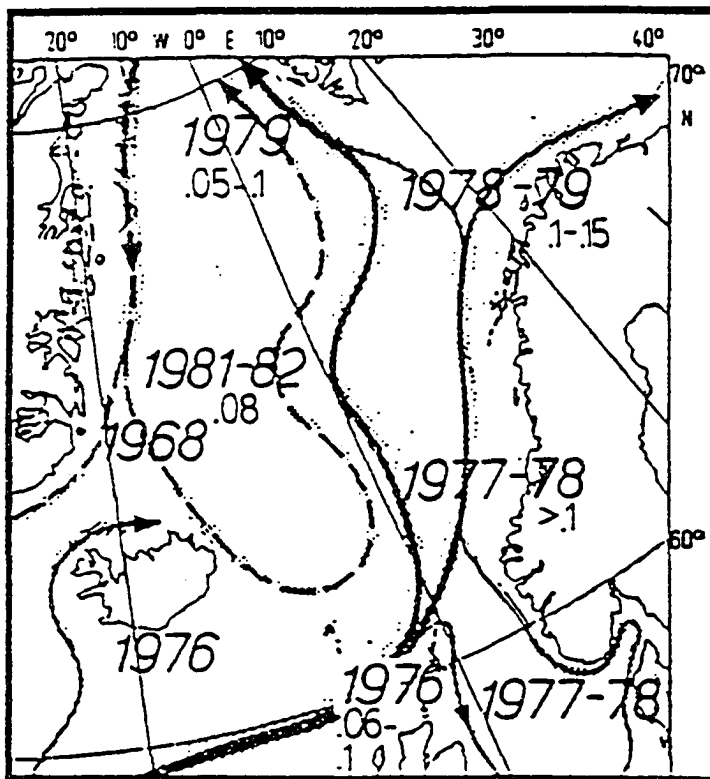
Figure 4.1 Years (big numbers) and amplitudes (numbers below. in psu)
of observations of the GSA in the GIN Sea (adopted from Dickson et al.. 1988).

Schlosser et al. (1991), there is no evidence of a significant decrease of convection during that time, i.e., through the 1960s and 1970s. The reduction of open ocean convection began between 1978 and 1982, coinciding with the reappearance of the salinity anomaly in the WSC, after recirculation in the northern North Atlantic. This suggests that convective system of the Greenland Sea is not that sensitive to variations of fresh water and sea ice volume carried out from the Arctic Ocean by the EGC, but rather it depends on the fresh water content, heat loss and moisture transported into the atmosphere from the WSC. The absence of a fresh water signal in the Greenland Sea gyre as it circulated south during the late 1960s and 1970s, implies a strong separating role of the EGF along the shelf slope, preventing mixing of fresh waters of the Arctic Ocean origin to the west of the front, with recirculating Atlantic Water to the east.

To investigate possible mechanisms for mixing of fresh water signal across the EGF (Fig.1.5), as it propagated south within the EGC, and across the Polar Front (PF), as it recirculated later north in the WSC, two experiments designed to simulate such events are presented in this chapter. First, for verification with available data (Dickson et al., 1988) and for comparison with model results of Legutke (1991), the propagation of the salinity anomaly to the north in the WSC, as it reappeared in the late 1970s, is analyzed. The following experiment has the salinity anomaly entering from the Arctic Ocean, as it took place in the late 1960s. In this chapter, the term negative amplitude salinity anomaly, i.e., decreased compared to climatological salinities, is referred to as an anomaly. Positive anomalies whenever discussed, will be explicitly referred to as positive.

Section 4.2 <u>Salinity</u> <u>Anomaly</u> <u>in</u> <u>the</u> <u>WSC</u>

The results presented in this and next sections, exemplify the usefulness of ocean modeling, providing the shortcomings of the model are carefully taken into consideration. At first, by comparison with the actual measurements, results are qualitatively and quantitatively verified. Then in a second step, the results provide additional information about an earlier or later part of the process that has little or no data coverage.

The early stage of the GSA propagation, i.e., its advection to the south with the EGC is not well documented by observations. Indirect, multitracer measurements in the region (Schlosser et al., 1991, Rhein, 1991) indicate no significant reduction of convection at that time. This implies that the fresh water signal advected in the EGC was either not mixed at all or not significantly mixed with the upper waters of the Greenland Sea gyre, to affect convection there.

To address some aspects of fresh water spreading in the Greenland Sea this experiment simulates the salinity anomaly entering from the south, an equivalence of the GSA reappearance in the GIN Sea in the late 1970s. As shown in Fig.4.1 the negative anomaly signal reached 69°N sometime in 1978 and its absolute amplitude was greater than 0.1 psu (Dickson et al., 1988). In the vertical the anomaly penetrated to at least 500 m depth. Walsh and Chapman (1990), who correlated the Icelandic sea ice index with the mean pressure field for the previous 12 months, conclude that prior to the GSA the high-latitude atmospheric circulation was in an anomalous state that would have favored

ice export through Fram Strait. The atmospheric circulation reached its maximum at the time of the GSA.

Such conditions define the methods to be used in this experiment. The model configuration and parameters, including strong wind forcing as suggested from the observations, are as in section 3.6 of the seasonal baroclinic strong wind experiment. To study spreading of the salinity anomaly entering from the south, two model integrations, which differed only in the salinities specified on the southern OB are compared. The first reference run used January monthly mean salinity data on the boundary, as in the previous experiments. In the second run. salinities specified at inflow points (east of 2°W) on the southern OB were reduced by maximum of 0.125 psu in the upper 5 layers (0–360 m). and no reduction was prescribed below 1000 m. Such freshening is close to that observed in the area during 1976–1979. For example. at Ocean Weather Station Metro (66°N. 2°E) the anomaly represented a deviation of 0.1–0.15 psu below the long-term mean. and extended to ∼500 m depth (Dickson et al.. 1988). The other boundary conditions as well as the forcing and initial fields were identical. Both simulations were restarted in mid January of the ninth year of the integration of the seasonal baroclinic strong wind experiment. and ran for two years.

4.2.1 Results and analysis

To analyze the spreading of a salinity anomaly with the subsurface core of Atlantic Water. while on its way north. as well as to eliminate direct wind driven effects in the

salinity distribution at the surface, results at a depth of 300 m are discussed here. In Fig.4.2a, the salinity distribution in January at the end of the eighth year of the model integration, as described in section 3.6, is presented. As prescribed after Levitus (1982), the January mean salinity maximum of entering AW is above 35.175 psu. The outflow through the northern OB. which allows some degree of variability is above 35.05 psu. In the Boreas Basin and the northern and eastern part of the Greenland Basin, recirculating AW supports salinities above 35.00 psu. The central Greenland Basin has a salinity between 34.95 and 35.00 psu. and only its southwestern part is below 34.95 psu.

After two years of anomaly propagation. salinities drop below 34.975 all over the Greenland Sea gyre (Fig.4.2b). Especially the northern parts of the gyre show significant changes. indicating the direction from which the signal is coming. Recirculation of AW in the Greenland Sea is well known. and it is simulated here as a mechanism of spreading of a salinity anomaly into the gyre circulation.

A better way to look at fresh water spreading in this region. is to compare the results of the two runs. with and without the salinity reduction specified on the southern OB. Salinity anomalies obtained as a difference between the original and reduced run values are presented in Fig 4.3. After one year of integration (Fig.4.3a), the anomaly maximum reaches mid-latitudes of the region (72–75°N) and locally it is even stronger than originally prescribed (-0.125 psu). Downstream 'sharpening' of the anomaly signal is also suggested from the observations (Dickson et al.. 1988).
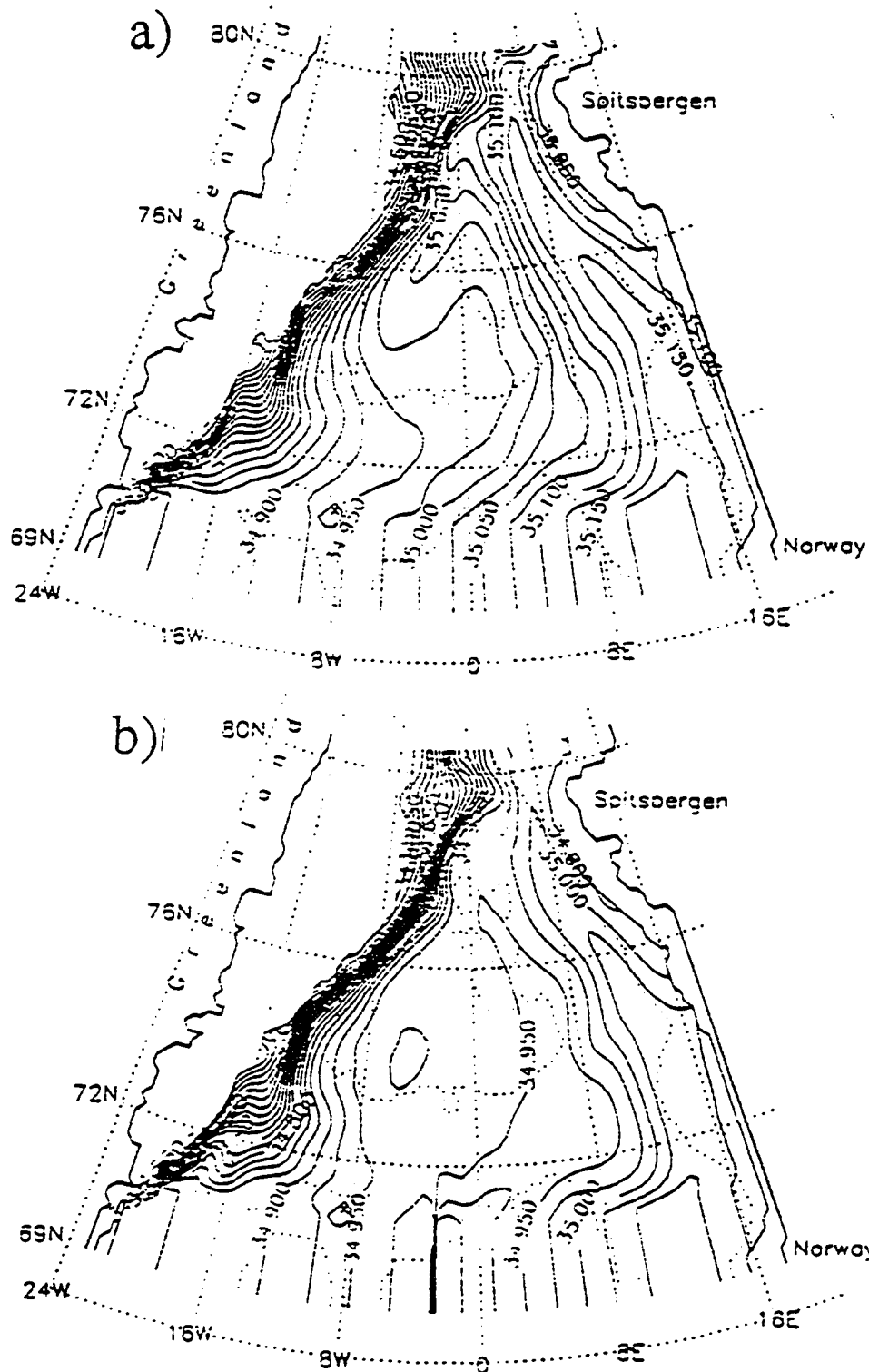
Figure 4.2 The salinity distribution at depth 300 m a) before prescribing the salinity anomaly (day 2928 – see Fig.3.30), and b) after two years of anomaly spreading with the WSC.

a)

b)
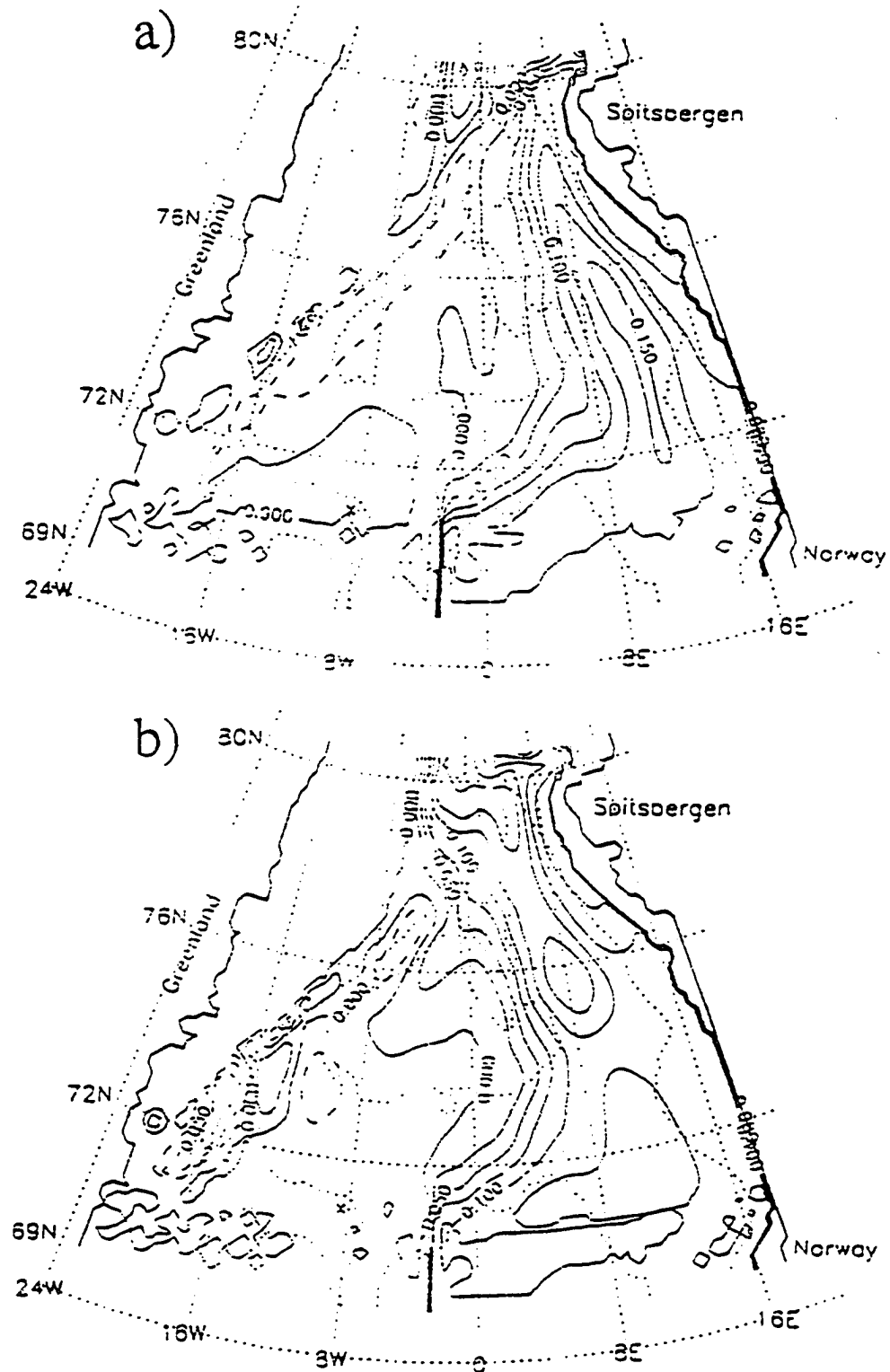
Figure 4.3 Salinity anomaly advection with the WSC at 300 m after a) 1 year. and b) 2 years of integration (negative anomalies are denoted by solid. and positive by dashed lines).

Amplitudes of the simulated anomaly are in agreement with the observations. In the Bear Island - Fugløy (Norway) section, upper ocean maximum deviations reached –0.15 psu in 1978, and in the Sørkapp section (south of Spitsbergen along 76°30'N, across the WSC) about one year later, deviations were still below –0.1 psu (Dickson et al., 1988), which is close to the model results presented in Fig.4.3.

Dickson et al. (1988) speculate that the anomaly recirculated into the Greenland Sea gyre sometime in 1981–1982. i.e., about 3–4 years later as it passed 69°N. Simulation results at the end of the second year of integration show salinity anomalies between –0.05 and –0.1 psu in the Boreas Basin and there is a clear indication of this signal being advected into the Greenland Basin. Assuming the start time of this experiment as January 1978. Fig.4.3b reveals that significant amounts of fresh water would reach the Boreas Basin as early as January 1980. and that their volume maximum has not been reached yet.

This arrival time falls in the middle of the Schlosser et al. (1991) estimate of about 80% reduction of GSDW formation beginning between 1978 and 1982. Gradual warming of GSDW. an indication of no renewal of deep waters between 1982 and 1989 has been confirmed by measurements (Clarke et al., 1990: Meincke et al., 1990: Aagaard et al., 1991). Freshening in the upper layers resulted in a markedly warmer. slightly more saline and less dense deep regime in the Greenland Sea. NSDW, as a mixture of GSDW and AODW that overflows the Iceland-Scotland Ridge to eventually become NADW, is directly affected by such variability.

Section 4.3 <u>Salinity</u> <u>Anomaly</u> <u>in</u> <u>the</u> <u>EGC</u>

After verification of some model results with observations. done in the previous section. the experiment described below simulates the early stage of the GSA propagation. as it entered Fram Strait from the Arctic Ocean. So far the only modeling effort addressing this phase of the GSA is the work by H93, where the anomaly as forced by daily wind fields. is simulated as an advective event resulting in an anomalous outflow of sea ice and fresh water from the Arctic Ocean. Such a result agrees with earlier hypothesis. based on the observations about the advective nature of the GSA (Aagaard and Carmack. 1989: Dickson et al.. 1988). In her study, Hakkinen also suggests that a fresh water signal (between -0.25 and -0.75 psu in the upper 30 m) would spread all over the Greenland Sea during the year (i.e.. 1968–1969) of the anomaly passage through Fram Strait.

Such strong freshening persisting over 2–4 years (1968–1971) could decrease the surface salinity below the critical value of 34.7 psu. Below this value the surface layers can not reach high enough density, even at the freezing point. to mix with the underlaying warmer and more saline waters (Dickson et al.. 1988). The resulting stable stratification would therefore suppress convection. However. the observed multitracer concentrations (Schlosser et al.. 1991. Rhein. 1991) clearly demonstrate that intensive deep water renewal must have taken place between the mid-1960s and the early 1970s. which implies no significant freshening in the upper layers of the Greenland Sea gyre during that time. contradictory to results by H93

To address this controversy, in this experiment a salinity anomaly is prescribed as entering through the northern OB from the Arctic Ocean. Salinities were reduced by 0.125 psu in the upper 5 layers (0–360 m) at inflow points (west of 0°), while no reduction was prescribed below 600 m. The same model configuration and parameters as in the previous experiment are used. As before, this experiment was restarted at the end of the eighth year of integration of the seasonal baroclinic strong wind experiment, and it was run for two years. The reference run results of the previous experiment were used in computations of salinity anomalies. The results simulating a southward propagation of an anomaly are presented and analyzed below.

4.3.1 Results and Analysis

The GSA passing through Fram Strait was defined as a sea ice and fresh water anomaly, hence a maximum of freshening is expected at the surface. Salinity distributions at 10 m depth both before the salinity anomaly was prescribed and after two years of anomaly spreading, are shown in Fig.4.4. As stated in section 2.4, the Levitus (1982) data are highly smoothed and interpolated, hence salinity differences are given most of the attention here. Although there are some minor differences on the Greenland shelf and in the WSC, salinities in the Greenland Sea gyre (Fig.4.4) have not changed much. The EGF efficiently separates surface waters across the slope. Since reduced salinity waters inflowing from the Arctic Ocean are still confined mostly to the shelf and slope off Greenland (Fig.4.4b) and the recirculation of AW in the central basins is unaltered, across-slope density gradients might be stronger than before, thus making cross-frontal
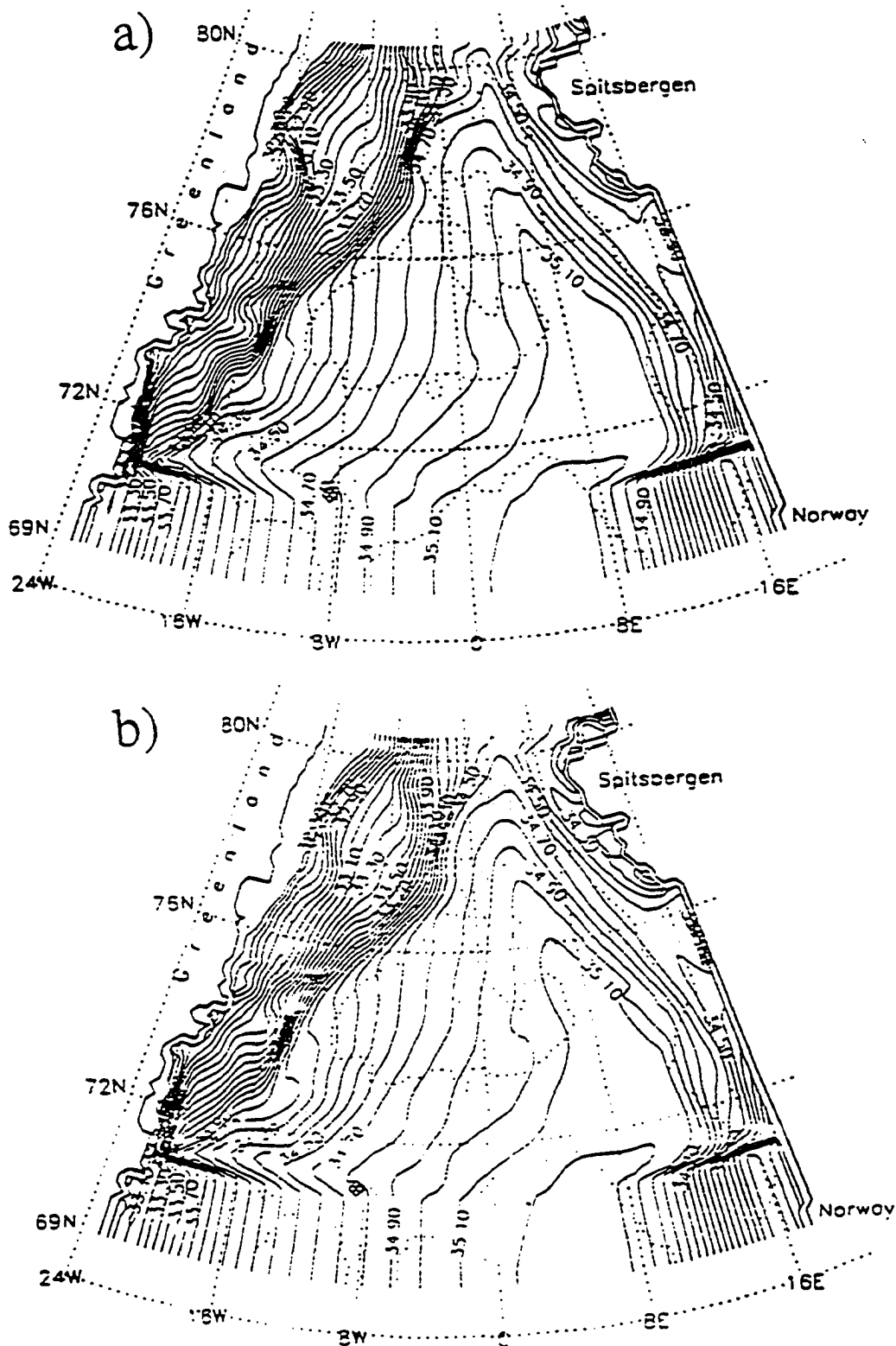
Figure 4.4 The salinity distribution at depth 10 m a) before prescribing the salinity anomaly (day 2928 – see Fig.3.30). and b) after two years of anomaly spreading with the EGC.

mixing even more difficult. Some energy for such mixing can be derived from continental shelf waves propagating along the slope, but apparently there is not enough energy to destroy the frontal structure at the surface.

Salinity anomalies calculated at depth of 10 m as a difference between the reference and anomaly run results, are shown in Fig.4.5. After one year of integration an anomaly reached the latitudes of the central Greenland Sea, but it did not enter the gyre (Fig.4.5a). Its easternmost extension is strongly correlated with the shelf slope, with the anomaly contour of 0.0 located between isobaths 1500 and 3000 m (dotted lines in the figures). The deep Boreas and Greenland Basins do not show any significant changes from the reference run results. Further south, at about 73°N, some positive anomalies are observed (i.e., with salinities greater than in the reference run), whose presence can be explained as a local effect of continental shelf wave activity, which supports mixing in the across-shelf direction.

After two years of spreading, distribution of salinity anomalies on the Greenland shelf is much more complex (Fig.4.5b), mostly due to the shelf wave activity, west of the EGF. To the east of the shelf slope in the Greenland Sea gyre, no changes are observed. The maximum amplitude signal has already reached the Iceland Plateau and it is still heading south. Hence if the fresh water signal were to spread into the Greenland Sea gyre it would have done so by that time. The wind driven simulation results at 10 m depth, show that during a salinity anomaly passage from Fram Strait to Denmark Strait,
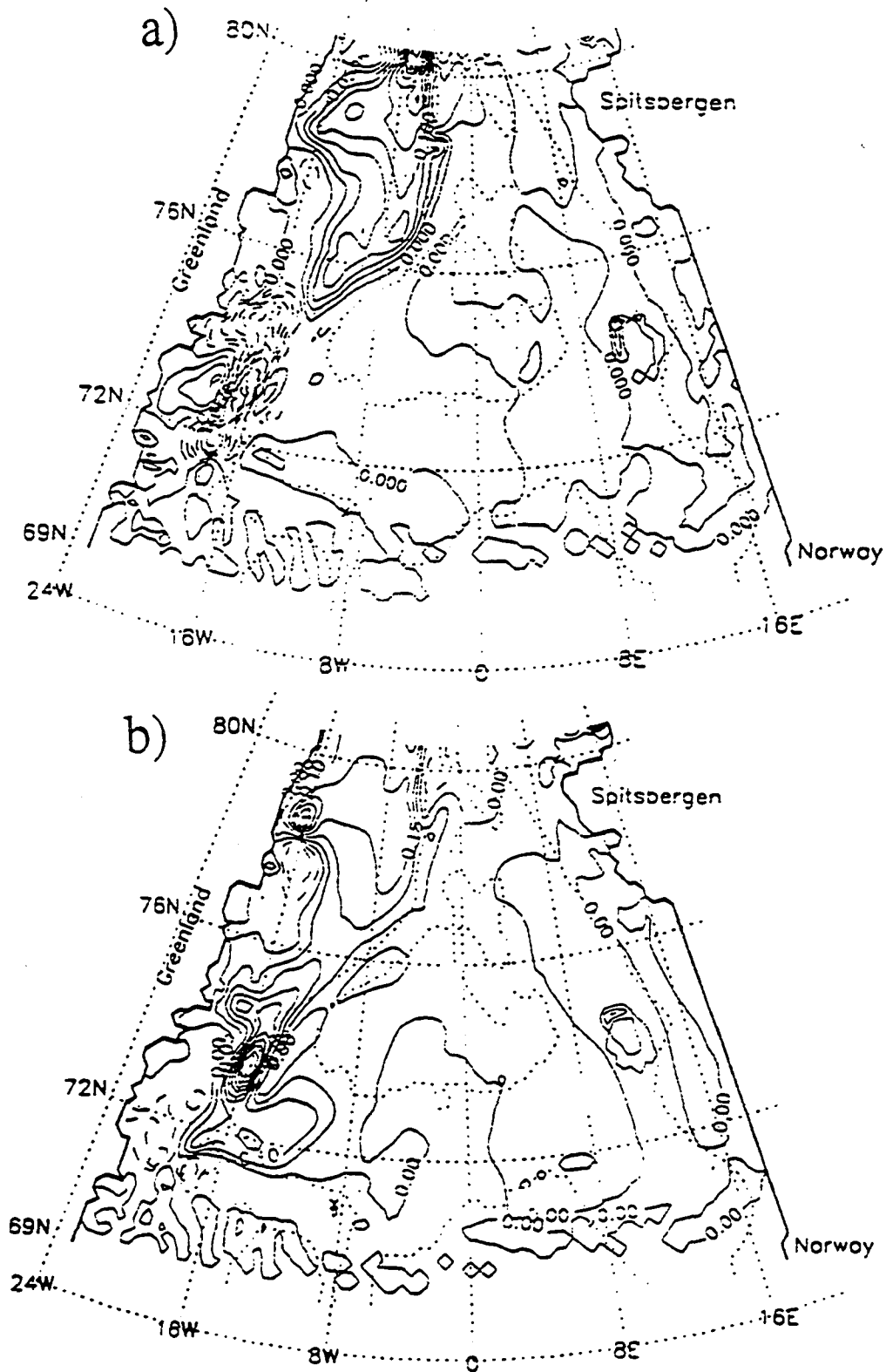
Figure 4.5 The salinity anomaly distribution at depth 10 m after
a) one, and b) two years of anomaly spreading with the EGC.

not enough significant freshening with the ability to alter the formation of GSDW, occurs in the central Greenland Sea.

An anomaly propagation below the Ekman layer at 300 m depth, where the core of recirculating AW can be expected (Strass et al., 1993), is shown in Fig.4.6–4.7. At this depth, the anomaly distribution after one year of integration is still defined mainly above the slope of Greenland, but a weak fresh water signal between 0.0 and -0.02 psu, is observed in the western part of the Greenland Basin (Fig.4.6a). Since no other mechanism has been identified there in the simulations discussed in this study, this freshening is attributed to cross-frontal mixing resulting from the barotropic continental shelf waves. The amount of fresh water spreading along the western margin of the Greenland Basin is too small and too far from the center of the gyre to influence convection there.

Four months later, the southward propagation of an anomaly maximum has reached the Iceland Plateau as seen in Fig.4.6b. A similar weak fresh water signal is now located along the southwestern part of the Greenland Basin. Two months later, at day 549 (Fig.4.7a), another small (between 0.0 and –0.02 psu) injection of fresh water on the western side of the basin occurs, and six months later (Fig4.7b), only the southwestern edge of the Greenland Sea gyre shows weak freshening, similar to Fig.4.6b. Freshening, varying in time and place, but limited to the southwestern edge of the Greenland Basin, describes a dynamically changing balance between the two major components defining the EGF: a cross-frontal mixing due to the propagation of continental shelf waves and a salt flux into the interior due to the recirculation of warmer and more saline AW, or
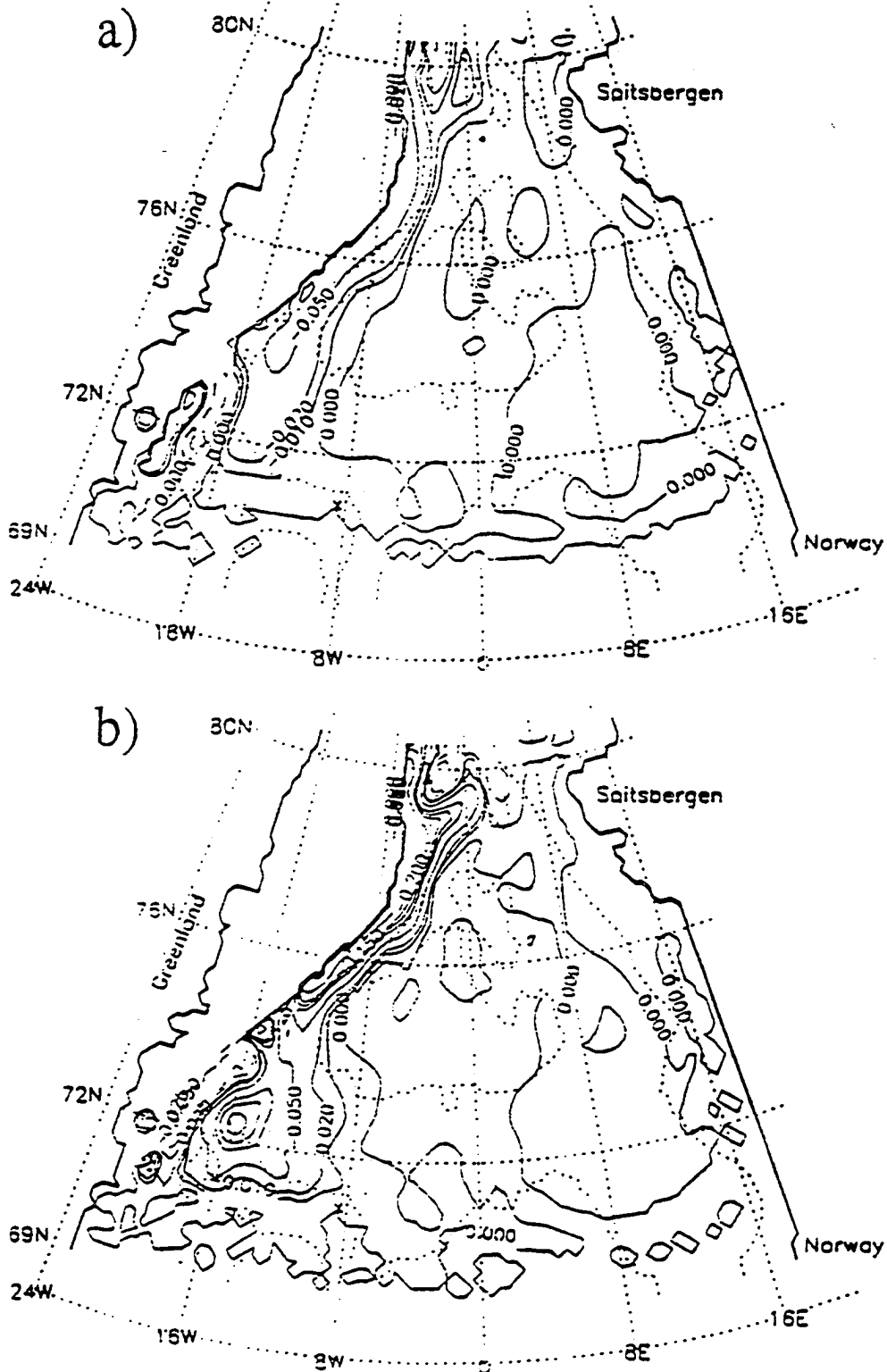
Figure 4.6 The salinity anomaly distribution at depth 300 m at
day a) 366. and b) 488 of anomaly spreading with the EGC.

a)

b)
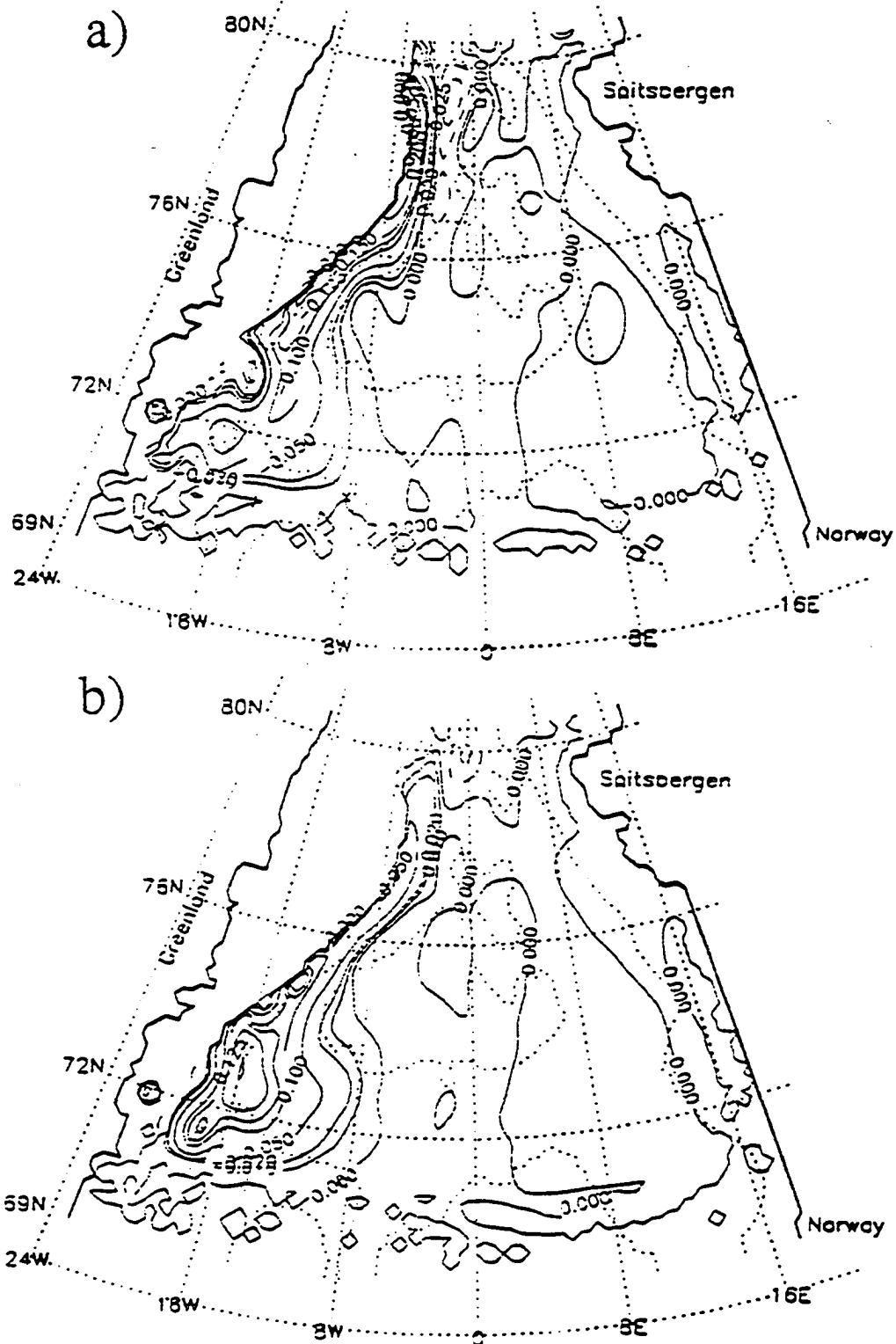
Figure 4.7 As Fig.4.6 but days a) 549. and b) 732.

lower AIW with the core at depths of about 100 to 800 m (Strass et al., 1993). The latter component, clearly dominates in such a balance.

The simulated vertically integrated mean winter circulation of the Greenland Sea gyre with strong wind forcing, as occurred during the GSA (Walsh and Chapman, 1990), is about 15 Sv (Fig.3.31b). Out of this transport only about 3 Sv are accounted for by waters of the Arctic Ocean origin (Foldvik, 1988), and only a small part of this volume is involved in mixing across the EGF. Since the recirculation of AW, unaltered during this experiment, provides a continuous salt flux into the gyre, local weak freshening (between 0.0 to –0.02 psu) along the southwestern margins of the Greenland Basin, is quickly erased and the original salinity values are reset. The Greenland Sea gyre at depth of 300 m remains in general unaffected by a salinity anomaly propagating in the EGC from Fram Strait into the Iceland Sea. This conclusion agrees with the multitracer measurements in the deep Greenland Sea by Schlosser et al. (1991) and Rhein (1991).

Based on her simulation results of the Arctic ice-ocean system, H93 suggests that the aerial average annual salinity of the Greenland Sea calculated over the upper 300 m, reaches its minimum in the fall of 1968 and winter of 1969, followed by an increase toward more normal conditions. A two-year drop, between 1967 and 1969, integrated over 300 m in the Greenland Sea is about 0.06 psu, and over the upper 100 m is about 0.14 psu. Such results compare reasonably well with the limited observations (month of June) in the Iceland Sea by Malmberg (1984). This however does not provide support for

the salinity anomaly spreading in the Greenland Sea, since in the experiment described in this section, where no significant freshening is simulated, a strong salinity anomaly reaches the Iceland Plateau (Fig.4.5b, 4.7b). Although no other direct observations are known to exist for this early stage of the GSA, the available indirect measurements (Schlosser et al., 1991; Rhein, 1991) clearly suggest the formation of GSDW during that time: a process which would not take place with a fresh water cap in the upper layers of the Greenland Sea gyre.

In the model results obtained by H93, the presence of a fresh water signal at the depths where the recirculation of AW occurs, suggests that the salt flux provided into the Greenland Sea gyre from the south by the Norwegian Atlantic Current into the Greenland Sea gyre is not strong enough to override the freshening tendency. This implies a decrease in the volume transport of the gyre, compared to the simulation results of this section, which in turn yields a weak wind forcing. However, such a conclusion contradicts the results of Walsh and Chapman (1990), who found that during the GSA the high-latitude atmospheric circulation was anomalously strong.

Based on the velocity comparisons in section 3.6, the mean winter mass transport of 15 Sv in the Greenland Sea is not overestimated by the increased wind forcing used here in the experiments with the GSA. The southward mass transport in the gyre as determined from measurements ranges from 2 to 35 Sv (Mosby, 1962; Aagaard and Coachman, 1968). In a primitive-equation model forced with historical 6–hourly wind-stress data

Legutke (1991a) obtained a mean transport of 13.6 Sv. Salinity anomalies prescribed on

the northern OB and obtained during the integration of the salinity anomalies are within

the range of values simulated by H93 values. suggesting that the fresh water signal is

not underestimated. Current measurements at 79°N (Foldvik et al., 1988), despite an

abundance of eddies. imply no significant interaction between the EGC and the interior.

thus cross-frontal mixing is not underrepresented due to horizontal resolution (i.e., the

model is not eddy resolving). On the other hand. the relatively high Laplacian lateral

viscosity of 3×10^7 cm^2/s used by H93. which is equivalent to a biharmonic coefficient

of -1.9×10^{21} cm^4/s as compared to the value of -1×10^{18} cm^4/s used here. as well as a

lower variable resolution of 28–150 km (compared to 18 km here), may be a source of

different results. As suggested by Legutke (1991a), a low resolution smooths the density

fronts and so decreases the strength of geostrophic currents related to frontal structures.

A salinity anomaly propagating slowly along a weaker density front. due to high lateral

viscosity and diffusivity can spread over a much larger area than an anomaly propagating

more quickly along a strong front in a much less viscous environment.

Since results obtained in this chapter agree with the earlier indirect measurements

(Schlosser et al.. 1991: Rhein, 1991), it is believed that the early stage of the GSA

propagation from Fram Strait to the Iceland Sea, is simulated correctly here. The fresh

water signal was not mixed into the interior circulation of the Greenland Sea gyre. and

the formation of GSDW was not altered at this stage of the anomaly spreading. As

simulated in the previous section. the process of deep convective overturn was altered

later, in the late 1970s and early 1980s, when a fresh water signal recirculated back into the Greenland Sea, and dramatically reduced deep water renewal there for about a 7 year period (Meincke et al., 1990).

Chapter 5 SUMMARY AND DISCUSSION

A primitive equation ocean general circulation model has been used to study the circulation of the Greenland Sea with special reference to its potential role in climate change. General circulation experiments have been performed and analyzed to define important dynamical processes governing the flow and water mass exchange within the Greenland Sea. In particular to understand such large scale events as the GSA, attention has been given to processes of mixing across the EGF between the EGC and the Greenland Sea gyre, and across the PF between the WSC and the central basin (Fig.1.5).

It has been found that topographic steering is one of the major mechanisms driving circulation in the region. It has also been shown that the EGC is strongly correlated with the Greenland shelf slope and that most of the recirculation of the WSC, due to topographic steering, takes places in the northern Boreas Basin. In addition, simulations have shown that the GFZ, separating the Greenland Basin from the Boreas Basin, acts as a topographic barrier in along-slope southward flow of the EGC and recirculated AW, and generates a disturbance, which propagates downstream along the constant slopes between 77°N and 72°N, as a topographic planetary wave. Most of energy in such waves propagates back along the slope to the northeast, but some of energy becomes available in the offshore direction for cross-frontal mixing. Mixing across the EGF plays a key role in processes that are important not only locally.

According to recent studies (Aagaard et al., 1985, 1991; Bourke et al., 1993; Rudels, 1986; Swift and Kolterman, 1988), it is thought that NSDW is formed by mixing of warm and saline deep water from the Arctic Ocean (AODW) with much colder and fresher GSDW. While significant NSDW production occurs in northern Fram Strait, there is also a clear evidence of this production taking place over the Greenland slope between 75 and 76°N at depths below 2000 m. No source of energy has been identified for diapycnal mixing resulting in the formation of NSDW. Both measurements (Roach et al., 1993) and model results (Proshutinsky and Polyakov, 1991) have indicated a concentration of energy at periods of about 17 hrs. in the central Greenland Sea. Since the topographic planetary waves simulated here have a very similar period of 17.2 hrs. it is suggested that these waves are a likely source of the energy for diapycnal mixing that results in the formation of NSDW.

At similar locations (around 75°N) but at intermediate depths (around 200 m), DSOW is formed by the isopycnic mixing of warm and salty recirculated AW (lower AIW) with cold and fresh upper AIW (Strass et al., 1993). According to observations, substantial DSOW formation occurs when the necessary conditions for baroclinic instability are satisfied, but the depth independent barotropic nature of current variabilities measured in the EGC suggests that additional energy for the production of DSOW may be derived from topographic planetary wave activities. Also Raoch et al. (1993) and Rudels et al. (1989) report the convective formation of waters (-1.5°C, 34.86 psu) in the central Greenland Sea, that feeds the Denmark Strait overflow.

NSDW and DSOW are the two major water masses that overflow the Greenland-Iceland-Scotland Ridge into the deep North Atlantic basins. With a total transport of ~5.6 Sv (Dickson et al., 1990), these waters produce NADW, which drives the ocean conveyor belt circulation. It is believed to control the global-scale transport of heat and fresh water between the high-latitude North Atlantic and the Pacific. This circulation is important in maintaining the Arctic sea ice cover and it also affects the atmospheric radiation balance through the ice albedo. Especially DSOW, which has a residence time of only 3 to 4 years (Swift et al., 1980), provides an exceptionally fast transfer of atmospheric and upper layer oceanic signals to the deep ocean. Variability in NADW has been shown (Charles and Fairbanks, 1992) as an important factor that promotes a rapid global reorganization of the climate system to an interglacial mode of operation. The poleward heat transport is believed to maintain anomalously warm winters in northern Europe Some very cold periods in the past might be the result of a temporary shutdown of the conveyor, an event also known as the halocline catastrophe. The GSA is considered to be a small scale analog of the halocline catastrophes, although it did not require dramatic increases in fresh water flux nor did it depend on deglaciation.

According to Mysak (1991) the GSA can be explained by a sequence of atmospheric, hydrologic, oceanic and sea ice events, a multi-component feedback loop that would result in interdecadal climate oscillations in the Arctic Ocean. The positive anomaly in fresh water output (negative in salinity output) from the Arctic Ocean led to the suppression of convection in the Northwest Atlantic which, in turn was responsible for deep water

formation in that area. A feedback loop, with a possible cycle of about 20 years, could work as a sequence of dependent events, starting from an increased inflow into the Arctic of warm water carried by the WSC, which is really the northernmost extension of the Gulf Stream-North Atlantic current system. This would result in an increased transfer of heat and moisture from the ocean into the atmosphere, northeast of Greenland, especially in an ice-free areas such as the so-called Whalers Bay Polynya. With the increase in heat transfer in the Arctic are also associated prolonged periods of increased cyclogenesis in the Arctic, particularly during winter, which are at least partly responsible for variations in the Arctic tropospheric circulation. Those variations may lead to an increase in precipitation. which would ultimately result in anomalous amounts of runoff. Hence the conclusion is that an increase in atmospheric heating northeast of Greenland would increase the north American runoff and sea ice formation in the western Arctic. More details concerning this hypothesis are provided by Mysak (1991).

Foldvik et al. (1988) based on measurements in the EGC at 79°N. and simulations presented here of salinity anomaly propagation from the Arctic Ocean into the Iceland Sea. imply that the EGC does not interact significantly with the interior of the Greenland Sea gyre, so the propagating southward GSA did not affect deep convection there in the late 1960s and 1970s. However it did affect process of deep water formation when the fresh water signal recirculated back into the GIN Sea and with the WSC spread over the Greenland Sea gyre. Both field measurements (Aagaard et al.. 1991: Clarke et al.. 1986: Meincke et al.. 1990); Schlosser et al.. 1991. Rhein. 1991) and numerical model results

(Legutke, 1991b: this study) agree that upper ocean freshening, due to recirculation of the GSA into the Greenland Sea beginning in the late 1970s and early 1980s, effectively suppressed deep convective overturn there.

The main conclusion is that the system is not particularly sensitive to variations in water and sea ice characteristics carried from the Arctic Ocean by the EGC, but rather it depends on the fresh water content, heat loss and moisture transported into the atmosphere from the WSC.

Strong dependence of the global circulation system on small changes in the atmospheric flux of fresh water (e.g., evaporation) from the northern North Atlantic to the Pacific (e.g., precipitation) is suggested by Stocker and Wright (1991). This flux for the present conveyor belt circulation is estimated to be about 0.45 Sv. Using an idealized box model, Stocker and Wright show that change of this flux (e.g., decrease of evaporation) to less than 0.03 Sv would shut off the deep water formation in the North Atlantic, forcing the global thermohaline circulation to switch to a different mode with subsequent rapid climate change.

This atmospheric fresh water flux is associated with the warm WSC, which in the GIN Sea cools and sinks to form the lower AIW. If interdecadal variations of the atmosphere-sea ice-ocean system in the Arctic Ocean are strongly correlated to anomalies of heat and moisture loss to the atmosphere and fresh water content in the WSC, the first question to be answered should be: What triggers variations in the WSC waters?

To model this problem it would require the inclusion of lower latitude dynamics. especially the Gulf Stream as a source of warm and salty water for the Arctic Ocean. With the next generation of massively parallel supercomputers becoming available for scientific computations. a model of the Arctic Ocean incorporated in high resolution simulations of the world ocean circulation becomes quite realistic.

Bibliography

Aagaard. K., 1970: Wind-driven transports in the Greenland and Norwegian Seas. Deep-Sea Res.. 17. 281–291.

Aagaard. K.. 1981: On the deep circulation in the Arctic Ocean. Deep Sea Res.. 28. 251–268.

Aagaard. K.. and L.K. Coachman. 1968: The East Greenland Current north of Denmark Strait. Part I. Arctic. 21. 181–200.

Aagaard. K.. C. Darnall. and P. Greisman. 1973: Year-long current measurements in the Greenland-Spitsbergen passage. Deep-Sea Res.. 20. 743–746.

Aagaard K. and P. Greisman. 1975: Toward new mass and heat budgets for the Arctic Ocean. J. Geophys. Res.. 80. 3821–3827.

Aagaard. K.. J.H. Swift. and E.C. Carmack. 1985a: Thermohaline circulation in the Arctic Mediterranean Seas. J. Geophys. Res.. 90. 48333–4846.

Aagaard. K.. C. Darnall. A. Foldvik. and T. Tørresen. 1985b: Fram Strait current measurements. 1984–1985. University of Bergen Rep. No. 63 and University of Washington Rep. M85-9. 85 pp.

Aagaard. K.. C. Darnall. A. Foldvik. M. Steg. and T. Tørresen. 1988: Fram Strait current measurements. 1985–1986. University of Bergen Rep. No. 66 and University of Washington Contribution No. 1021. 43 pp.

Aagaard, K., and E.C. Carmack, 1989: The role of sea ice and other fresh water in the Arctic circulation. J. Geophys. Res., 94, 14,485–14,498.

Aagaard, K., E. Fahrbach, J. Meincke, and J.H. Swift, 1991: Saline outflow from the Arctic Ocean: Its contribution to the deep waters of the Greenland, Norwegian, and Iceland Seas. J. Geophys. Res., 96, 20,433–20,441.

Anderson, D.L.T., and R.A. Corry, 1985: Ocean response to low frequency wind forcing with application to the seasonal variation in the Florida Straits-Gulf Stream transport. Prog. Oceanog., 14, 7–40.

Arakawa, A., 1972: Design of the UCLA general circulation model. Numerical Simulation of Weather and Climate. Dept. of Meteorology, Univ. of California, Los Angeles. Tech. Rept. 7. 116 pp.

Bakun, A., 1973: Coastal upwelling indices, west coast of North America, 1946–71. U.S. Dept. of Commerce, NOAA, Tech. Rep. NMFS SSRF-671.

Bang, I., 1991: Numerical modeling study of the circulation in the Gulf of Alaska. Ph.D. Thesis, University of Alaska.

Bogorodskii, P.V., A.P. Makshtas, A.P. Nagurnyi, V.G. Savchenko, and B.V. Ivanov, 1987: Features of the mesoscale interaction of the ocean and atmosphere. Meteorologiya i Gidrologiya, No. 10, 69–74.

Boning, C.W., and R.G. Budich. 1992: Eddy dynamics in a primitive equation model: Sensitivity to horizontal resolution and friction. J. Phys. Oceanogr., 22, 361–381.

Bourke, R.H., J.L. Newton, R.G. Paquette, and M.D. Tunnicliffe, 1987a: Circulation and water masses of the east Greenland shelf. J. Geophys. Res., 92, 6729–6740.

Bourke, R.H., M.D. Tunnicliffe, J.L. Newton, R.G. Paquette, and T.O. Manley, 1987b: Eddy near the Molloy Deep revisited. J. Geophys. Res., 92, 6773–6776.

Bourke, R.H., A.M. Weigel, and R.G. Paquette, 1988: The westward turning branch of the West Spitsbergen Current. J. Geophys. Res. 93, 14.065–14.077.

Bourke, R.H., R.G. Paquette, and R.F. Blythe, 1992: The Jan Mayen Current of the Greenland Sea. J. Geophys. Res., 97, 7241–7250.

Bourke, R.H., R.G. Paquette, R.F. Blythe, and M.D. Stone, 1993: On the deep and bottom waters of the Greenland Sea from summer 1989 and 1990 data. J. Geophys. Res., 98, 4629–4638.

Brink, K.H., 1982: A comparison of long coastal trapped wave theory with observations off Peru. J. Phys. Oceanogr., 12, 897–913.

Broecker, W.S., 1987: Unpleasant surprises in the greenhouse? Nature, 328, 123–127.

Broecker, W.S., 1991: The Great Ocean Conveyor. Oceanography, Vol. 4, No. 2, 79–89.

Bryan, K., 1969: A numerical method for the study of the ocean circulation. J. Comput. Phys., 4, 347–376.

Bryan, F., 1986: High-latitude salinity effects and interhemispheric thermohaline circulations. Nature, 323, 301–304.

Bunker, A.F., 1976: Computations of surface energy flux and annual air-sea interaction cycles of the North Atlantic Ocean. Mon. Wea. Rev., 104, 1122–1140.

Carmack, E., and K. Aagaard, 1973: On the deep water of the Greenland Sea. Deep-Sea Res., 20, 687–715.

Clarke, R.A., J.H. Swift, J.C. Reid, and K.P. Koltermann, 1990: The formation of Greenland Sea Deep Water: double diffusion or deep convection? Deep-Sea Res., 37, 1385–1424.

Coachman, L.K., and K. Aagaard, 1974: Physical oceanography of arctic and subarctic seas. In: Arctic Geology and Oceanography, edited by H. Nelson, and Y. Herman. Springer-Verlag, 1–72.

Charles, C.D., and R.G. Fairbanks, 1992: Evidence from Southern Ocean sediments for the effect of North Atlantic deep-water flux on climate. Nature, 355, 416–419.

Creagan, A., 1976: A numerical investigation of the circulation in the Norwegian Sea. Tellus, 28, 451–459.

Dickson, R.R., 1972: Variability and continuity within the Atlantic Current of the Norwegian Sea. In: Proceedings of a symposium held in Dublin 25–27 September 1969, edited by A.J. Lee, and H. Charnock. ICES.

Dickson, R.R., J. Meincke, S-A. Malmberg, and A.J. Lee, 1988: The "Great Salinity Anomaly" in the Northern North Atlantic 1968–1982. Prog. Oceanog., 20, 103–151.

Dickson, R.R., E.M. Gmitrowicz, and A.J. Watson, 1990: Deep-water renewal in the northern North Atlantic. Nature, 344, 848–850.

Dietrich, G., 1969: Atlas of the hydrography of the northern North Atlantic Ocean. Based of the Polar survey of the International Geophysical Year, winter and summer 1958. ICES Outside Series.

Druet C., and A. Jankowski, 1991: Flow across south and east boundaries of the Norwegian Sea. Oceanologia, 30, 37–46.

Foldvik, A., K. Aagaard, T. Tørresen, 1988: On the velocity field of the East Greenland Current. Deep-Sea Res., 35, 1335–1354.

Gascard, J-C., C. Kergomard, P-F Jeannin, and M. Fily, 1988: Diagnostic study of the Fram Strait Marginal Ice Zone during summer from 1983 and 1984 Marginal Ice Zone Experiment Lagrangian Observations. J. Geophys. Res., 93, 3613–3641.

Gathman, S.G., 1986: Climatology. In: The Nordic Seas, edited by B.G. Hurdle. Springer-Verlag, 1–17.

Gill, A., 1982: Atmosphere-Ocean Dynamics. Academic Press, 662 pp.

Glavnoe Upravlenie po Navigacii i Okeanografii, 1985: Atlas Arktiki. Edited by A.F. Treshnikov (in Russian). Moscow, pp 77, 91.

Greisman, P., 1976: Current measurements in the eastern Greenland Sea. Ph.D. Thesis, University of Washington.

GSP Group, 1990: Greenland Sea Project: A venture toward improved understanding of the ocean's role in climate. EOS June 12, 750–754.

Guest, P.S., K.L. Davidson, 1991: The aerodynamic roughness of different types of sea ice. J. Geophys. Res., 96, 4709–4721.

Hakkinen, S., 1986: Coupled ice-ocean dynamics in the Marginal Ice Zones: Upwelling/downwelling and eddy generation. J. Geophys. Res., 91, 819–832.

Hakkinen, S., 1987: A coupled dynamic-thermodynamic model of an ice-ocean system in the Marginal Ice Zone. J. Geophys. Res., 92, 9469–9478.

Hakkinen, S., 1993: An Arctic source for the Great Salinity Anomaly: A simulation of the Arctic ice-ocean system for 1955–1975. J. Geophys. Res., 98, 16,397–16410.

Hakkinen, S., G.L. Mellor, and L.H. Kantha, 1992: Modeling deep convection in the Greenland Sea. J. Geophys. Res., 97, 5389–5408.

Hansen, B., and J. Meincke, 1979: Eddies and meanders in the Iceland-Faroe Ridge area. Deep-Sea Res., 26, 1067–1082.

Hanzlick, D.J., 1983: The West Spitsbergen Current: Transport, forcing, and variability. Ph.D. Thesis, University of Washington.

Heaps, N.S., 1973: Three-dimensional numerical model of the Irish Sea. Geophys. J. R. Astr. Soc., 35, 99–120.

Helland-Hansen, B., and F. Nansen, 1909: The Norwegian Sea, its physical oceanography based upon the Norwegian researchers 1900–1904, Report on Norwegian Fishery and Marine Investigations. 2, part 1, No. 2, Mallingske, Christiania (Oslo).

Hellerman, S., and M. Rosenstein, 1983: Normal monthly wind stress over world ocean with error estimates. J. Phys. Oceanogr., 13, 1093–1104.

Hermann, F., and H. Thomsen. 1946: Drift-bottle experiments in the Northern North Atlantic. Medd. Komm. Havunders., Hydrografi. 3(4).

Hibler. W.D., III, and J.E. Walsh. 1982: On modeling seasonal and interannual fluctuations of Arctic sea ice. J. Phys. Oceanogr., 12, 1514–1523.

Hibler. W.D., III, and K. Bryan. 1984: Ocean circulation: Its effects on seasonal sea-ice simulation. Science. 224. 489–492.

Hibler. W.D., III, and K. Bryan. 1987: A diagnostic ice-ocean model. J. Phys. Oceanogr., 17, 987–1015.

Hill. H.W., and A.J. Lee. 1957: The effect of the wind on water transport in the region of the Bear Islands fisheries. Proc. R. Soc. London, Ser. B. 148, 104–116.

Holland. W.R., 1978: The role of mesoscale eddies in the general circulation of the ocean — numerical experiments using a wind-driven quasi-geostrophic model. J. Phys. Oceanogr., 8, 363–392.

Hopkins, T.S., 1991: The Gin Sea — A synthesis of its physical oceanography and literature review 1972–1985. Earth-Science Reviews, 30, 175–318.

Hunkins, K.H., 1975: Subsurface eddies in the Arctic Ocean and baroclinic instability. In: Climate of the Arctic edited by G. Weller and S.A. Bowling, 24th Alaska Science Conference, August 15–17 1973, Fairbanks, Alaska.

Huthnance, J.M., 1975: On trapped waves over a continental shelf. J. Fluid Mech., 69, 689–704.

Iida, H., 1972: Edge waves on the linearly sloping coast. II, Forced waves and β-effect. Oceanogr. Mag., 24, 39–55.

Jakhelin, A., 1936: Oceanographic investigations in the East Greenland water in the summer of 1930–1932. Skr. Svalbard Ishaver. 67.

Johannessen, J.A., O.M. Johannessen, E. Svendsen, R. Shuchman, T. Manley, W.J. Campbell, E.G. Josberger, S. Sandven, J.C. Gascard, T. Olaussen, K. Davidson, and J. Van Leer, 1987: Mesoscale eddies in the Fram Strait Marginal Ice Zone during the 1983 and 1984 Marginal Ice Zone Experiment. J. Geophys. Res., 92, 6754–6772.

Johannessen, O.M., 1986: Brief overview of the physical oceanography. In: The Nordic Seas, edited by B.G. Hurdle, Springer-Verlag, 103–127.

Johannessen. O.M., J.A. Johannessen, J. Morison, B.A. Farrelly, and E.A.S. Svendsen, 1983: Oceanographic conditions in the marginal ice zone north of Svalbard in early fall 1979 with emphasis on mesoscale processes. J. Geophys. Res., 88, 2755–2769.

Johannessen, O.M., S. Sandven, and J.A. Johannessen, 1991: Eddy related winter convection in the Boreas basin. In: Deep convection and deep water formation in the ocean. edited by J. -C. Gascard, and P.C. Chu. Elsevier, E. O. Series, 87–106.

Jonsson, S., 1989: The structure and forcing of the large- and mesoscale circulation in the Nordic Seas. with special reference to the Fram Strait. Ph.D. Thesis, University of Bergen.

Killworth. P.D., 1979: On "chimney" formations in the ocean. J. Phys. Oceanogr., 9, 531–554.

Killworth. P.D., 1987: Topographic instabilities in level model OGCMs. Ocean Modeling, 75, 9–12.

Kislyakov, A.G., 1960: Fluctuations in the regime of the Spitsbergen current. In: Soviet Fisheries Investigations in the Northern European Seas. The Polar Research Institute of Marine Fisheries and Oceanography (PINRO), Moscow. (in Russian) 39–49.

Koltermann, K.P., and D. Machoczek, 1985: On the climatological mean state distribution of temperature and salinity in the Greenland Sea. ICES C.M. C. 39 (unpublished document).

Kowalik, Z., and T.S. Murty, 1993: Numerical modeling of ocean dynamics. World Scientific.

LeBlond, P.H., and L.A. Mysak, 1978: Waves in the ocean. Elsevier Scientific Publ. Co., 602 pp.

Legutke, S., 1987: The influence of boundary conditions on the circulation in the Greenland-Norwegian Sea. A numerical investigation. In: Three-dimensional models of marine and estuarine dynamics. edited by J.C.J. Nihoul. and B.M. Jamart. Elsevier Science Publishers BV. 269–284.

Legutke, S., 1991a: A numerical investigation of the circulation in the Greenland and Norwegian Sea. J. Phys. Oceanogr.. 21. 118–148.

Legutke, S., 1991b: Numerical experiments relating to the "Great Salinity Anomaly" of the seventies in the Greenland and Norwegian seas. Prog. Oceanog.. 27. 341–363.

Leonov. A.K.. 1947: Experimental quantitative computation of the transport of water. heat and salts in the Arctic Basin by the Atlantic and Pacific currents. Meteorol. Hidrol.. 5.

Levitus, S., 1982: Climatological atlas of the world ocean. NOAA Publ. 13, U.S. Dept. of Commerce, Washington D.C., 173 pp.

Louis, J.P., B.D. Petrie, and P.C. Smith, 1982: Observations of topographic Rossby waves on the continental margin off Nova Scotia. J. Phys. Oceanogr., 12, 47–55.

Malmberg, S-A., 1972: Annual and seasonal hydrographic variations in the East Icelandic Current between Iceland and Jan Mayen. In: Sea Ice. edited by T. Karlsson. National Research Council of Iceland, Reykjavik.

Mandel, S.Z., 1979: Basic features of seasonal and year-to-year variations of the inflow of Atlantic water and heat into the Arctic basin through Fram Strait. Ark. i Antark. Nauchno-Issled. Inst., Trudy (transl.), 361, 24–29.

Martell, C.M., and J.S. Allen. 1979: The generation of continental shelf waves by alongshore variations in bottom topography. J. Phys. Oceanogr., 9, 696–711.

Meincke, J., et al., Greenland Sea Project. 1990: A venture toward improved understanding of oceans' role in climate. EOS Trans. AGU, 71, No. 24, 750–751.

Mossby, H., 1962: Water, salt, and heat balance of the North Polar Sea and of the Norwegian Sea. Geofys. Publ., 24, 289–313.

Mysak, L.A., 1980: Recent advances in shelf wave dynamics. Rev. Geophys. Space Phys., 18, 211–241.

Mysak. L.A., 1991: Current and future trends in Arctic climate research: Can changes of the Arctic sea ice be used as an early indicator of global warming? C^{2}GCR Rep. No. 91–1. McGill University.

Mysak, L.A., and D.K. Manak, 1989: Arctic sea-ice extent and anomalies, 1953–1984. Atmos.-Ocean, 27, 376–369.

Niebauer, H.J., and W.O. Smith Jr., 1989: A numerical model of mesoscale physical-biological interactions in the Fram Strait Marginal Ice Zone. J. Geophys. Res.. 94, 16.151–16.175.

North. G.R.. T.L. Bell. R.F. Callahan, and F.T. Moeng, 1982: Sampling errors in the estimation of empirical orthogonal functions. Mon. Wea. Rev.. 110. 699–706.

Okkonen. S.. 1993: Circulation variability in the Bering Sea. Ph.D. Thesis. University of Alaska.

Ostlund. H.G.. and G. Hut. 1984: Arctic Ocean water mass balance from isotope data. J. Geophys. Res.. 89, 6373–6381.

Paquette. R.G.. R.H. Bourke, J.F. Newton, and W.F. Perdue. 1985: The East Greenland Polar Front in autumn. J. Geophys. Res.. 90. 4866–4882.

Peterson W.H.. and C.G.H. Rooth. 1976: Formation and exchange of deep water in the Greenland and Norwegian seas. Deep-Sea Res.. 23. 273–283.

Pedlosky, J., 1987: Geophysical Fluid Dynamics. Springer-Verlag.

Perry, R.K., 1986: Bathymetry. In: The Nordic Seas. edited by B.G. Hurdle, Springer-Verlag, 211–233.

Pond, S., and G.L. Pickard. 1983: Introductory Dynamical Oceanography. Pergamon Press.

Proshutinsky, A.Yu., and I.V. Polyakov, 1991: The Arctic Ocean eigen oscillations. In: Proceedings of a Conference held June 11–15, 1990 at the University of Alaska Fairbanks. edited by G. Weller. University of Alaska Fairbanks.

Quadfasel. D.. and J. Meincke. 1987: Note on the thermal structure of the Greenland Sea gyres. Deep-Sea Res.. 34. 1883–1888.

Quadfasel. D.. J.-C. Gascard, and K.P. Koltermann. 1987: Large-scale oceanography in Fram Strait during the 1984 Marginal Ice Zone Experiment. J. Geophys. Res.. 92. 6719–6728.

Ramming, H.G.. and Z. Kowalik. 1980: Numerical Modeling of Marine Hydrodynamics. Elsevier.

Rhein. M.. 1991: Ventilation rates of the Greenland and Norwegian Seas derived from distributions of the chlorofluoromethanes F11 and F12. Deep-Sea Res., 38. 485–503.

Rhines. P.. 1971: A note on long-period motions at Site D. Deep-Sea Res.. 18. 21–26.

Redlinger. S.H., and R.H. Preller. 1991: The development of a coupled ice-ocean model for forecasting ice conditions in the Arctic. J. Geophys. Res.. 96. 16955–16977.

Roach, A.T., K. Aagaard, and F. Carsey, 1993: Coupled ice-ocean variability in the Greenland Sea. Atmos.-Ocean. 31, 319–337.

Røed, L.P., and J.J. O'Brien, 1983: A coupled ice-ocean model of upwelling in the Marginal Ice Zone. J. Geophys. Res., 88, 2863–2872.

Ross, C.K., 1984: Temperature-salinity characteristics of the "overflow" water in Denmark Strait during "OVERFLOW '73". Rapp. P.-v. Reun. Cons. Int. Explor. Mer. 185, 111–119.

Rudels, B., 1986: On the Θ—S structure in the Northern Seas. Implications for the deep water circulation. Polar Research, 4, 133–159.

Rudels, B., 1987: On the mass balance of the Polar Ocean, with special emphasis on the Fram Strait. Norsk Polarinstitutt Skrifter, 188, 1–53.

Rudels, B., 1990: Haline convection in the Greenland Sea. Deep-Sea Res., 37, 1491–1511.

Rudels, B., D. Quadfasel, H. Friedrich, and M.N. Houssais, 1989: Greenland Sea convection in the winter of 1987–1988. J. Geophys. Res., 94, 3223–3227.

Salmon, D.K., 1992: On interannual variability and climate change in the North Pacific. Ph.D. Thesis. University of Alaska.

Sarmiento, J.L., and K. Bryan, 1982: An ocean transport model for the North Atlantic. J. Geophys. Res., 87, 394–408.

Schlosser, P., G. Bonisch, M. Rhein, and R. Bayer, 1991: Reduction of deepwater formation in the Greenland Sea during the 1980s: Evidence from tracer data. Science, 251, 1054–1056.

Sellmann, L., E. Fahrbach, G. Rohardt, V.H. Strass, and B.V. Bodungen, 1992: Moored instruments oceanographic data from the Greenland Sea 1987–1989. Alfred Wegener Institut, Report 27.

Semtner, A.J., 1974: An oceanic general circulation model with bottom topography. Tech. Rep. 9, University of California, Los Angeles, 99 pp.

Semtner, A.J., 1976: Numerical simulation of the Arctic Ocean circulation. J. Phys. Oceanogr., 6, 409–425.

Semtner, A.J., 1987: A numerical study of sea ice and ocean circulation in the Arctic. J. Phys. Oceanogr., 17, 1077–1099.

Semtner, A.J., and R.M. Chervin, 1988: A simulation of the global ocean circulation with resolved eddies. J. Geophys. Res., 93, 15502–15522.

Semtner, A.J., and Y. Mintz, 1977: Numerical simulations of the Gulf Stream and mid-ocean eddies. J. Phys. Oceanogr., 7, 208–230.

Sloss, P.W., 1986: ETOP5 5–minute Gridded World Elevation. Marine Geology and Geophysics Division of the National Geophysical Data Center.

Smethie, W.M., Jr., D.W. Chipman, J.H. Swift, and K.P. Koltermann, 1988: Chlorofluoromethanes in the arctic mediterranean sea: Evidence for formation of bottom water in the Eurasian Basin and deep-water exchange through Fram Strait. Deep-Sea Res., 35, 347–369.

Smith, D.C., IV, J.H. Morison, J.A. Johannessen, and N. Untersteiner, 1984: Topographic generation of an eddy at the edge of the East Greenland Current. J. Geophys. Res., 89, 8205–8208.

Smith, D.C., IV, A.A. Bird, W.P. Budgell, 1988: A numerical study of mesoscale ocean eddy interaction with a marginal ice zone. J. Geophys. Res., 93, 12,461–12,473.

Sommerfeld, A., 1949: Partial Differential Equations. Academic Press, 333 pp.

Stefansson, U., 1962: North Icelandic waters. Rit Fiskideildar, 3, 269 pp.

Stevens, D.P., 1990: On open boundary conditions for three dimensional primitive equation ocean circulation models. Geophys. Astrophys. Fluid Dynamics, 51, 103–133.

Stevens, D.P., 1991: A numerical ocean circulation model of the Norwegian and Greenland Seas. Prog. Oceanog., 27, 365–402.

Stigebrandt, A., 1981: A model for the thickness and salinity of the upper layer in the Arctic Ocean and the relationship between the ice thickness and some external parameters. J. Phys. Oceanogr., 11, 1407–1422.

Stocker, T.F., and D.G. Wright, 1991: Rapid transitions of the ocean's deep circulation induced by changes in surface water fluxes. Nature, 351, 729–732.

Strass, V.H., E. Fahrbach, U. Schauer, and L. Sellmann, 1993: Formation of Denmark Strait Overflow Water by mixing in the East Greenland Current. J. Geophys. Res., 98, 6907–6920.

Swift, J.H., 1984: The circulation of the Denmark Strait and Iceland-Scotland overflow in the North Atlantic. Deep-Sea Res., 31, 1339–1355.

Swift, J.H., 1986: The Arctic waters. In: The Nordic Seas, edited by B.G. Hurdle, Springer-Verlag, 129–155.

Swift, J.H., K. Aagaard, and S.A. Malmberg, 1980: The contribution of the Denmark Strait overflow to the deep North Atlantic. Deep-Sea Res., 27, 29–42.

Swift, J.H., and K. Aagaard, 1981: Seasonal transitions and water mass formation in the Iceland and Greenland seas. Deep-Sea Res., 28, 1107–1129.

Swift, J.H., T. Takahashi, and H.D. Livingston, 1983: The contributions of the Greenland and Barents Seas to the deep water of the Arctic Ocean. J. Geophys. Res., 88, 5981–5986.

Swift, J.H., and K.P. Koltermann, 1988: The origin of Norwegian Sea Deep Water. J. Geophys. Res., 93, 3563–3569.

Timofeyev, V.T., 1962: The movement of Atlantic water and heat into the Arctic Sea basin. Deep-Sea Res., 9, 358–361.

U.S. Navy Hydrographic Office, 1958: Atlas of the Polar Seas. Part I. H.O. Pub. No. 705, Washington D.C.

Vinje, T.E., 1977: Some observations from Nimbus-6 data collecting platforms in polar areas. Paper presented at the Joint IAGA/IAMAP Assembly, Seattle, Wash. Aug. 22–Sept. 3.

Vinje, T.E., and O. Finnekasa, 1986: The ice transport through the Fram Strait. Skr. Norsk Polarinst., 186, 39 pp.

Vowinckel, E., and S. Orvig, 1970: The climate of the North Polar Basin. In: Climates of the Polar Regions, edited by S. Orvig, Elsevier. 129–226.

Wadhams, P., 1986: The ice cover. In: The Nordic Seas. Springer-Verlag, 21–84 pp.

Wadhams, P., and V.A. Squire, 1983: An ice-water vortex at the edge of the East Greenland Current. J. Geophys. Res., 88, 2770–2780.

Walsh, J.E., 1992: ARCSS modeling strategies. In: ARCSS OAII Proceedings of a meeting held in Pacific Grove, California, 13–17 July, 1992. Report No. 1. 9–11.

Walsh, J.E., and W.L. Chapman, 1990: Short-term climatic variability of the Arctic. J. Clim., 3, 1462–1473.

White. W.B.. and S. Tabata. 1987: Interannual westward-propagating baroclinic long-wave activity on Line P in the eastern midlatitude North Pacific. J. Phys. Oceanogr., 17, 385–396.

Worthington, L.V., 1970: The Norwegian Sea as a mediterranean basin. Deep-Sea Res., 17, 77–84.